UNIVERSIDADE DE LISBOA

Faculdade de Medicina

The role of nuclear positioning in muscle function

Mafalda Ramos de Melo Pimentel

Orientador:

Prof. Doutor Edgar Rodrigues Almeida Gomes

Tese especialmente elaborada para obtenção do grau de Doutor em Ciências Biomédicas especialidade em Biologia Celular e Molecular

2019

UNIVERSIDADE DE LISBOA

Faculdade de Medicina

The role of nuclear positioning in muscle function

Mafalda Ramos de Melo Pimentel

Orientador: Prof. Doutor Edgar Rodrigues Almeida Gomes

Tese especialmente elaborada para obtenção do grau de Doutor em Ciências Biomédicas especialidade em Biologia Celular e Molecular

Júri: Presidente: Doutor João Eurico Cortez Cabral da Fonseca, Professor Catedrático e Vice-Presidente do Conselho Cientifico da Faculdade de Medicina da Universidade de Lisboa

Vogais: Doctor Antoine Guichet, Group Leader and Principal Investigator, Institut Jacques Monod, Université Paris Diderot;

Doutor Reto Gassmann, Group Leader and Investigador do Instituto de Biologia Molecular e Celular da Universidade do Porto;

Doutor Ramiro Daniel Carvalho de Almeida, Professor Auxiliar do Departamento de Ciências Médicas da Universidade de Aveiro;

Doutora Solveig Thorsteinsdottir, Professora Associada com Agregação da Faculdade de Ciências da Universidade de Lisboa;

Doutora Maria do Carmo Salazar Velez Roque da Fonseca, Professora Catedrática da Faculdade de Medicina da Universidade de Lisboa;

Doutor Edgar Rodrigues Almeida Gomes, Professor Associado Convidado da Faculdade de Medicina da Universidade de Lisboa;

Instituição Financiadora: Fundação para a Ciência e Tecnologia SFRH/BD/52227/2013

2019

A impressão desta tese foi aprovada pelo Conselho Científico da Faculdade de Medicina de Lisboa em reunião de 16 de Outubro de 2018.

As opiniões expressas nesta publicação são da
exclusiva respondabilidade do seu autor.

Acknowledgments

I would like to express my gratitude to my supervisor Dr. Edgar Gomes, for giving me the opportunity to perform my thesis in his new lab. I am very grateful for his support throughout my PhD and for his sharing of knowledge, experience and out of the box ideas. After this challenging but gratifying project, I know now that science can be “cool”, exciting and curiosity driven.

I would like to thank all former and present members of the Edgar Gomes group, for the productive and friendly working atmosphere and for all the group activities inside and outside the lab. In particular, I am grateful to Bruno Cadot and Valerie Vilmont, for receiving me in Paris, making me feel welcomed and helping me with all the initial technicalities and bureaucracies. I would like to thank Judite Costa for all the support and advice, and for always making me see the better side of things. I am thankful to Sara Ferreira for taking care of our lab and making our lives infinite times easier. Many thanks to the muscle team, for all the hours spent doing primary cells (or trying), for all the troubleshooting and shared frustrations. I am especially thankful to Graciano Leal, who became my mRNP mentor/ encyclopedia, and to Helena Pinheiro, who is my science soulmate and makes me enjoy every little detail in our joint scientific lives. I would like to thank my front neighbor, Francisco Calero, for all the molecular biology teachings no matter how hopeless they were. Most importantly, I am grateful to William Roman for changing my paradigms in science and beyond.

I would like to thank our neighbor lab, especially to Claudio Franco, for all the meaningful input in our meetings and to Pedro Barbacena for being always there for me. I would like to thank the Figueirencios, for being simply the best ex-lab ever and never stopping taking care of me. I acknowledge the IMM community for being so friendly and helpful all the way.

Finally, I would like to express my gratitude to my family and friends for their constant support and immense belief in me. You remind me every day why it is worth it.

Thank you!

Table of contents

List of figures

List of tables

List of abbreviations

A band	-	anisotropic band
AchR	-	Acetylcholine receptor
ADP	-	Adenosine diphosphate
ANOVA	-	analysis of variance
ATP	-	Adenosine triphosphate
bp	-	Base pairs
CDS	-	coding sequence
ChR2	-	Channelrhodopsin-2
CNM	-	centronuclear myopathy
DHPR	-	dihydropyridine receptor
E-C coupling	-	Excitation contraction coupling
ECCE	-	excitation-coupled Ca^{2+} entry
EDL	-	extensor digitorum longus
ER	-	endoplasmic reticulum
GO term	-	Gene Ontology Term
h	-	hours
hLamA/C	-	human Lamin A/C
I band	-	isotropic band
IF	-	intermediate filaments
kb	-	Kilobases
kD	-	kiloDalton
Kif	-	Kinesin family
LE	-	Localization element
LUT	-	Look up table
MAP	-	microtubule associated protein
MBP	-	myelin basic protein
MCI	-	mRNA clustering index
mDa	-	megaDalton
MHC	-	Myosin Heavy Chain
MIP	-	Maximum intensity projection
MRF	-	myogenic regulatory factors
mRNA	-	messenger ribonucleic acid
mRNP	-	messenger ribonucleic particle
ms	-	milliseconds
MT	-	microtubules
MTJ	-	Myotendinous junction
MTOC	-	Microtubule organizing center
MW	-	molecular weight
NMJ	-	neuromuscular junction
PAX	-	paired box gene
RBP	-	RNA binding protein
RNA	-	ribonucleic acid
RYR	-	Ryanodine receptor

SD	-	spinning disk
sec	-	second
SERCA	-	sarco/endoplasmic reticulum Ca^{2+}-ATPase
smFISH	-	single molecule fluorescence in situ hybridization
SOCE	-	store-operated Ca^{2+} entry
SR	-	sarcoplasmic reticulum
SUM	-	image SUM projection
TL	-	Transmitted light
um or µm	-	micrometers
UTR	-	untranslated regulatory region
wt	-	wild type

Summary

Skeletal muscle is formed by multinucleated myofibers, the biggest cells in the human body. The multiple nuclei in these cells are regularly positioned so that the distance between them is maximized. It was previously found that nuclear positioning is important for skeletal muscle function (Metzger et al., 2012). However, mechanistic insight was missing since no evident structural abnormalities were found as a consequence of nuclear mispositioning. We hypothesized that each nucleus influences the nearby cytoplasm by determining mRNA localization along myofibers. As a consequence, protein translation and regulation would be hampered in situations of nuclear mispositioning, such as in centronuclear myopathies.

Using highly matured mouse myofibers differentiated *in vitro*, we found that overall mRNA distribution depends on nuclear position. Using smFISH we observed that during myofiber maturation and myofibril organization, mRNAs are pushed towards the sarcolemma. We also validated the nuclear domain theory (Pavlath et al., 1989) by detecting total mRNA clustering around peripheral nuclei. This seems to be the default localization of mRNAs in myofibers since both muscle specific and housekeeping transcripts display the same pattern.

This perinuclear clustering is an active mechanism, dependent on the minus end directed microtubule motor dynein and its activator dynactin. We have also established that the levels of protein translation can depend on nuclear location. Ribosome content is higher in the nuclear region, independently of Dynactin2 expression. Using a heterokaryon system, we show that at least some proteins in the cell remain localized close to their nucleus of origin. Moreover, contractibility of the cells correlates with the position of the nucleus and thus with overall mRNA localization.

Interestingly, a peculiar subset of mRNAs localizes regardless of where the nucleus is placed. A common feature of these transcripts is their extremely big length. We confirmed that this differential distribution is also happening *in vivo*. We propose that an active mechanism is responsible for this “giant” mRNA localization

in order to ensure and facilitate the localization of the encoded proteins. Understanding the mechanisms of mRNA transport and anchoring that govern its subcellular destinations in myofibers may be the key to understand how nuclear positioning impacts muscle activity.

Keywords: skeletal muscle, mRNA localization, microtubules, translation, contraction

Resumo

O músculo esquelético é formado por longas células excitáveis e contrácteis denominadas fibras musculares. Estas são as maiores células no corpo, altamente complexas e especializadas (Marieb and Hoehn, 2007). As fibras musculares têm origem na fusão de dezenas a centenas de células percursoras – os mioblastos – durante a embriogénese. O seu citoplasma está maioritariamente preenchido pelas miofibrilas, compostas pelos filamentos de actina e miosina, efetores da contracção muscular. A fibra muscular é um dos raros sincícios existentes no corpo humano. Os múltiplos núcleos existentes em cada fibra organizam-se durante o desenvolvimento de modo a posicionarem-se à periferia da célula e a que se maximize a distância entre eles (Bruusgaard et al., 2003; Roman and Gomes, 2017). Este posicionamento é altamente conservado evolucionariamente, o que sugere relevância biológica (Liu et al., 2009). Adicionalmente, em certas patologias o posicionamento do núcleo encontra-se afectado, apresentando-se ao centro da célula e muitas vezes em agregados (Biancalana et al., 2012). As consequências desta alteração morfológica na função muscular dos pacientes não são totalmente entendidas (Romero, 2010).

Ainda não é clara a extensão da influência que cada núcleo pode exercer no citoplasma de uma fibra muscular. Foi reportado anteriormente que o posicionamento do núcleo afecta a função muscular, mas até então não se sabia exactamente através de que mecanismo (Metzger et al., 2012). Nós colocámos a hipótese de que cada núcleo é responsável por uma porção do citoplasma envolvente através do controlo da localização do RNA mensageiro (mRNA) que transcreve e exporta. De acordo com esta hipótese, um posicionamento incorrecto dos núcleos levaria a uma distribuição anormal de produtos de expressão génica potencialmente importantes para a contracção e homeostasia do músculo. A localização do mRNA já foi descrita como importante para diversos mecanismos biológicos, nomeadamente a formação e manutenção de sinapses no sistema nervoso (Sutton and Schuman, 2006). A deficiência dos mecanismos moleculares necessários para a correcta localização de certos transcritos também já foi associada a diversas patologias (Brinegar and Cooper, 2016; Wurth and Gebauer, 2015). Embora todos os mecanismos descritos até à data sejam específicos para

cada espécie de mRNA, geralmente é comum a todos a ocorrência de transporte activo através de uma proteína motora do citoesqueleto e proteínas adaptadoras ligadas ao transcrito, muitas vezes através do 3'UTR (Buxbaum et al., 2015).

No músculo esquelético a localização do mRNA tem sido alvo de interesse, mas a sua estrutura e complexidade dificultaram estudos mais aprofundados e com maior especificidade. Adicionalmente, dada a delicadeza fisiológica destas células, são escassos os estudos dinâmicos com relevância similar ao que acontece em músculo completamente formado e funcional. Utilizando um sistema *in vitro* para o desenvolvimento de fibras musculares altamente diferenciadas nós confirmámos que a distribuição do mRNA depende do posicionamento nuclear. Este sistema permite desenvolver fibras musculares de ratinho de modo a apresentarem as características de fibras musculares *in vivo* (Pimentel et al., 2017). Permite também a manipulação e observação microscópica com alta resolução de todo o processo de diferenciação. O desenvolvimento inicia-se com mioblastos recolhidos de recém-nascidos que durante 10 dias formam fibras musculares com forma tubular, miofibrilas alinhadas, contracção espontânea, núcleos à periferia e tríades em dupletos a flanquear o disco Z dos sarcómeros (Falcone et al., 2014).

Através de smFISH (hibridação de sondas fluorescentes in situ para marcação de moléculas individuais) observámos que durante a maturação da fibra muscular e dos seus filamentos (mofibrilas) os mRNAs são excluídos para a periferia das células levando à sua acumulação perto da membrana citoplasmática. Confirmámos adicionalmente a teoria dos domínios nucleares de Pavlath que durava há décadas no campo da investigação muscular (Pavlath et al., 1989) ao detectar um enriquecimento significativo de mRNA na zona envolvente dos núcleos à periferia da célula. Esta restrição da distribuição de transcritos já tinha sido observada na junção neuromuscular mas não em núcleos não sinápticos, dada a maior dificuldade em entender a origem dos transcritos no sincício (Merlie and Sanes, 1985). Esta parece ser a localização preferencial dos transcritos em geral dado que tanto transcritos específicos de musculo como transcritos *housekeeping* partilham desta localização. A disrupção do posicionamento nuclear através da depleção de *kif5b* leva a regiões cuja densidade de transcritos é diminuída.

A localização perinuclear do mRNA é um mecanismo activo dado que é dependente do motor Dineína, um complexo proteico que transporta cargas para a extremidade positiva dos microtúbulos. O complexo auxiliar Dinactina também é importante para a manutenção de mRNAs em volta do núcleo. Não observámos o envolvimento de nenhuma das Cinesina testadas na localização de mRNA em fibras musculares. No entanto, algumas delas afectaram consideravelmente o desenvolvimento celular sendo possível que estejam implicadas no transporte de mRNA. Adicionalmente, também observámos que os ribossomas estão enriquecidos na zona perinuclear através da marcação do RNA ribossomal 18S e das proteínas P. Utilizando o ensaio de puromicilação, confirmámos que os níveis de tradução são proporcionalmente mais elevados perto do núcleo do que no em zonas longe dos mesmos. Para determinar com precisão a localização de proteínas específicas relativamente ao seu núcleo de origem, optimizamos a formação de heterocários em que um núcleo humano é incorporado numa célula contendo múltiplos núcleos de ratinho. Utilizando anticorpos específicos para proteínas humanas detectamos um enriquecimento das mesmas perto do único núcleo humano na célula. Em células contendo apenas núcleos de ratinho não foi observado um enriquecimento proteico na região perinuclear. Isto deve-se possivelmente ao facto de que o espaçamento nuclear permite que as proteínas se encontrem devidamente distribuídas em fibras musculares saudáveis.

Para tentar compreender a possível implicação desta assimetria na distribuição do mRNA e respectiva tradução, medimos a função muscular através da contracção. Utilizando uma ferramenta optogenética que consiste num canal de catiões activado pela luz (Channelrodopsin2) pudemos concluir que a região nuclear da fibra muscular é mais facilmente induzida a contrair do que regiões afastadas do núcleo. Estes resultados apontam para a importância da distribuição equidistante dos múltiplos núcleos nas células de músculo.

Paralelamente, encontrámos um conjunto de mRNAs que não se acumula na periferia do núcleo. A única característica comum que conseguimos apurar entre eles foi o seu tamanho acima do normal. Um deles é o mRNA para a Titina, a maior proteína codificada no genoma, específica e essencial para o músculo. De facto, várias das maiores proteínas musculares são anormalmente grandes em parte devido à sua função estrutural. Os mRNAs que codificam para estas

proteínas encontram-se amplamente distribuídos nestas células. Apesar de não termos encontrado nenhuma proteína motora que afecte o transporte dos mesmos (em parte devido à possível toxicidade do seu fenótipo de depleção), observámos que estes transcritos se encontram altamente concentrados nas extremidades celulares. Essa localização sugere uma dependência da orientação positiva dos microtúbulos, embora não tenhamos estabelecido uma conexão com nenhuma das Cinesinas testadas. O transporte diferencial de mRNAs “gigantes” traria benefícios que poderiam ser passiveis de selecção evolucionária. Ao localizar estes mRNAs ao longo de toda a célula, as várias proteínas traduzidas a partir dos mesmos não teriam de percorrer distâncias tão elevadas e exigentes energeticamente. A topologia destas proteínas também pode requerer que estas sejam traduzidas localmente, tendo especialmente em conta a elevada densidade do citoplasma muscular (sarcoplasma).

Em conjunto estes resultados demonstram a relevância do posicionamento nuclear em fibras musculares ao nível da distribuição dos mRNAs em geral. Também implicam que um incorrecto positionamento pode potencialmente original zonas da célula em que a contracção não é tão eficiente. Este estudo revela a localização especial de um conjunto de transcritos, os mRNAs “gigantes” que nunca tinha sido descrita anteriormente. A distribuição particular destes mRNAs constitui um novo exemplo que fundamenta a importância da localização de certos transcritos para a optimização de funções biológicas específicas.

Palavras-chave: músculo esquelético, localização de mRNA, microtúbulos, tradução, contracção

1 Introduction

1.1 Skeletal muscle biology

Skeletal muscle tissue is by far the most abundant in a mammalian organism, composing up to 40% of the human body (Janssen et al., 2000). It can be divided in two groups – **striated and smooth muscle** – based on the internal arrangement of contractile filaments. Striated muscle exhibits clear arranged striations under a brightfield microscope in comparison to the smooth counterpart. It can be further subdivided into **skeletal and cardiac** tissues. Although with a very similar contractile machinery, they are quite distinct not only in function but also in cellular organization. Skeletal muscles attach to bones through tendons and are responsible for all voluntary movements of the body, posture and heat generation. Each muscle is composed of long multinucleated cells that span the entire organ length. On the other hand, cardiac muscle generates involuntary heart beat and is generally composed of mononucleated cells connected by specialized junctions called intercalated disks. Despite their different biogenesis, many proteins and pathways are shared between the two types of striated muscle and so the two fields of research are often connected.

1.1.1 Skeletal muscle structure

Skeletal muscle is a highly complex and organized organ composed of several types of tissue (Figure 1,Figure 1 – Structural organization of skeletal muscle. Aminoff, 2005). The predominant cell type – skeletal muscle fibers or **myofibers** – are long multinucleated cells encapsulated by a basement membrane. Several myofibers surrounded by connective tissue (endomysium) bundle into a fascicle. Multiple fascicles are bound by an epimysium and ultimately compose the muscle organ, connected to bone usually through tendons. In addition to the supportive layers of connective tissue, each muscle has an intricate network of small capillaries. These are derived from a central artery and branch along each myofiber in order to serve its high metabolic needs. Furthermore, each muscle is innervated by at least one motor neuron being each myofiber controlled by only one axon branch, at the neuromuscular junction.

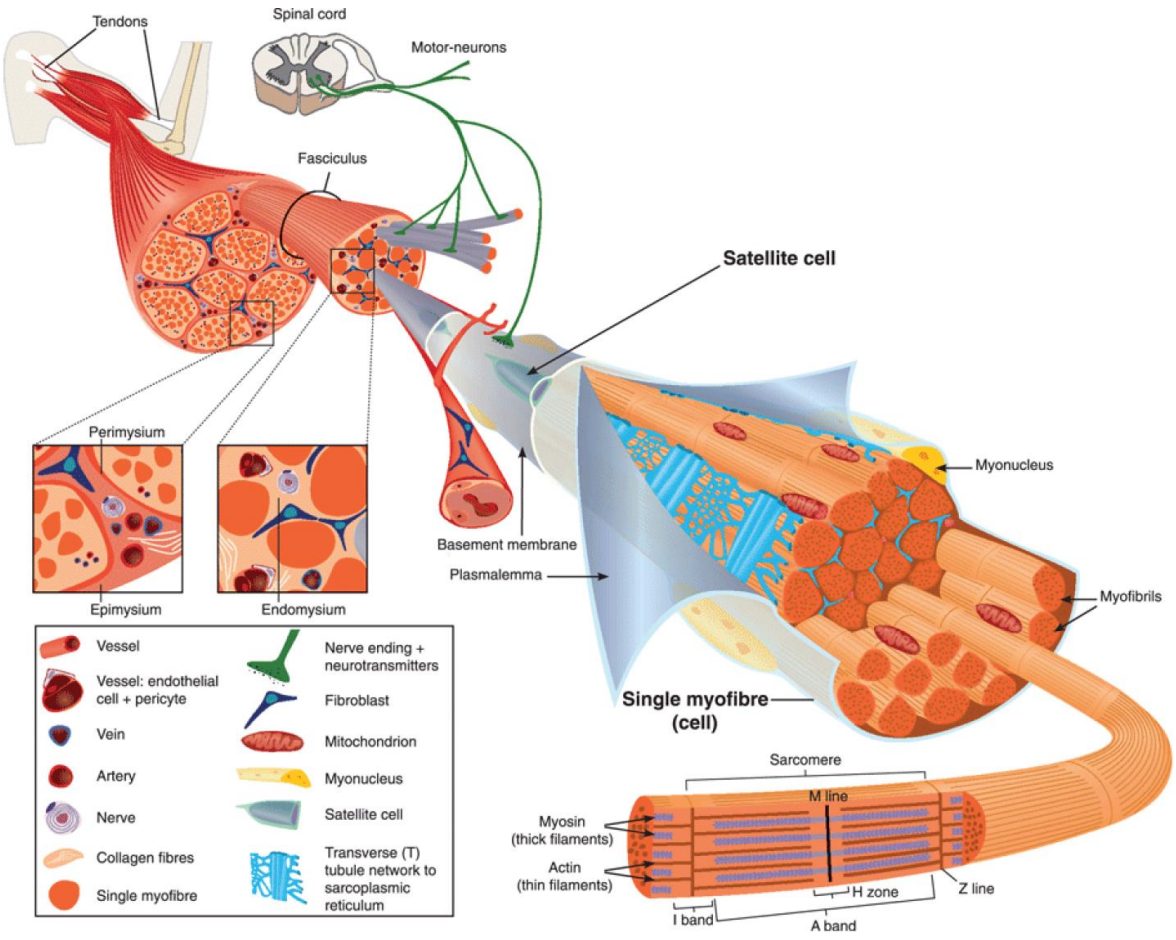

Figure 1 – Structural organization of skeletal muscle.

Skeletal muscle is highly vascularized and is innervated by axon branches of motor neurons. It is mainly composed of several fascicles which aggregate multiple myofibers (muscle cells), spanning the organ length. Each cylindrical myofiber has numerous myofibrils containing arrays of contractile units, the sarcomeres. The multiple nuclei are positioned at the cell periphery, under the sarcolemma. The organization and function of muscle is also dependent on its several layers of connective tissue. Adapted from Tajbakhsh, 2009.

At the myofiber level, intracellular organization is also highly complex (Marieb and Hoehn, 2007). Each tubular cell has multiple nuclei positioned at the periphery, under the membrane, known as **sarcolemma**. Inside, the **sarcoplasm** (muscle cytoplasm) surrounds a dense arrangement of filament bundles termed **myofibrils**. These cylindrical myofibrils are sequential repetitions of the contraction units, the **sarcomeres**, in which filaments of myosin slide over actin filaments to generate force (Figure 2)Figure 2 – Sarcomere basic components and organization.. Each sarcomere extends from one **Z line** (or Z disk) to another, a very dense structure containing **α-actinin** for actin filaments anchorage (Clark et

al., 2002). The center of the sarcomere is termed **M line**, given that myosin tails are fixed in this region. By opposition, the region around the Z lines contains only actin and it is known as the **I band**. The I band has **I**sotropic light properties in comparison to the **A**nisotropic nature of the complementary **A band** (where myosin polarizes light). The gigantic protein **Titin** spans all the way from the Z line to the M line (Tskhovrebova and Trinick, 2003). Being the biggest protein encoded in the genome, it is 1 µm in length and 4 MDa in weight. Importantly, the elastic properties of the Titin filament provide resistance to excessive stretching while keeping the Myosin filament in place.

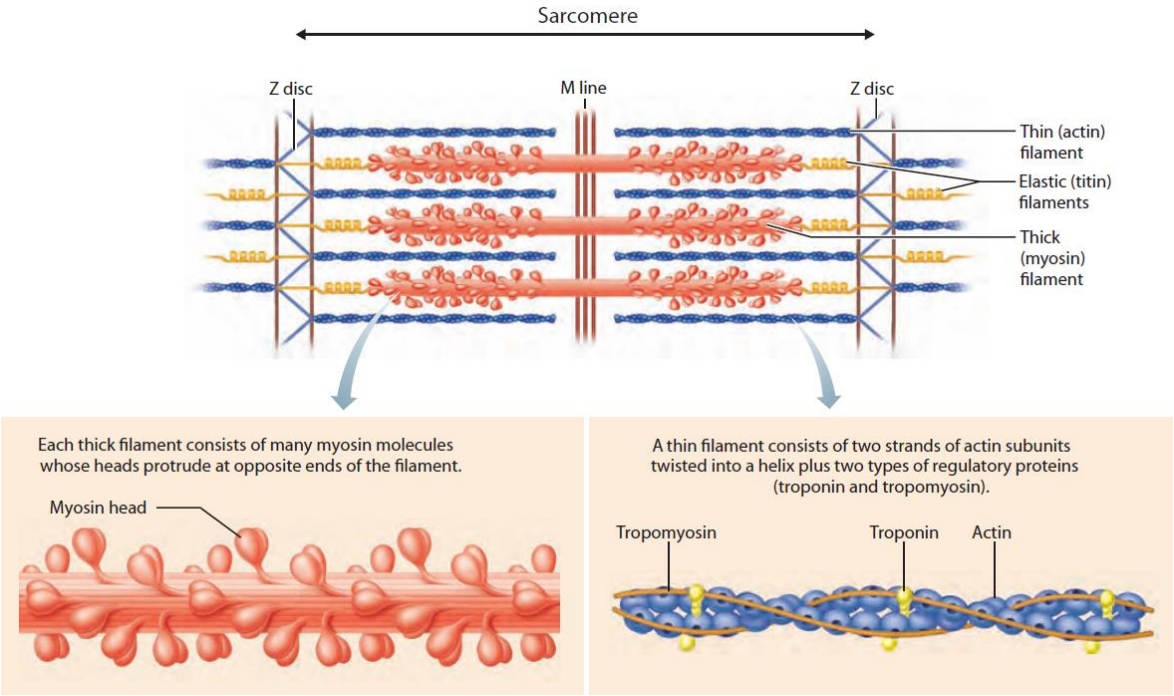

Figure 2 – Sarcomere basic components and organization.

Each sarcomere is bordered by the Z lines (or Z disks) where the actin filaments get anchored to α-actinin. The myosin filaments stem from the center of the structure with their heads towards the actin filaments. During contraction, troponin binds to Ca^{2+} and changes tropomyosin conformation, making actin accessible to myosin. The myosin binds and slides to the next actin site at the expense of one ATP. Titin is a gigantic protein that spans half of the sarcomere. It keeps the myosin filament in place and its elasticity offers resistance to stretch. Adapted from Marieb and Hoehn, 2007.

Each sarcomere is laterally aligned with the adjacent sarcomeres in neighboring myofibrils. This ultrastructural myofibril alignment and the different filament density are the reasons behind the striated pattern appearance, typical of striated muscle (Figure 3). This precise patterning enables the crosslinking of all myofibrils through their Z lines, by the intermediate filament **Desmin** (Capetanaki et al., 2007). It also paves the way for the organization of **Triads**, membrane structures crucial for muscle contraction (described in section 1.1.3). These also span transversely the whole cell section, residing immediately next to each A band.

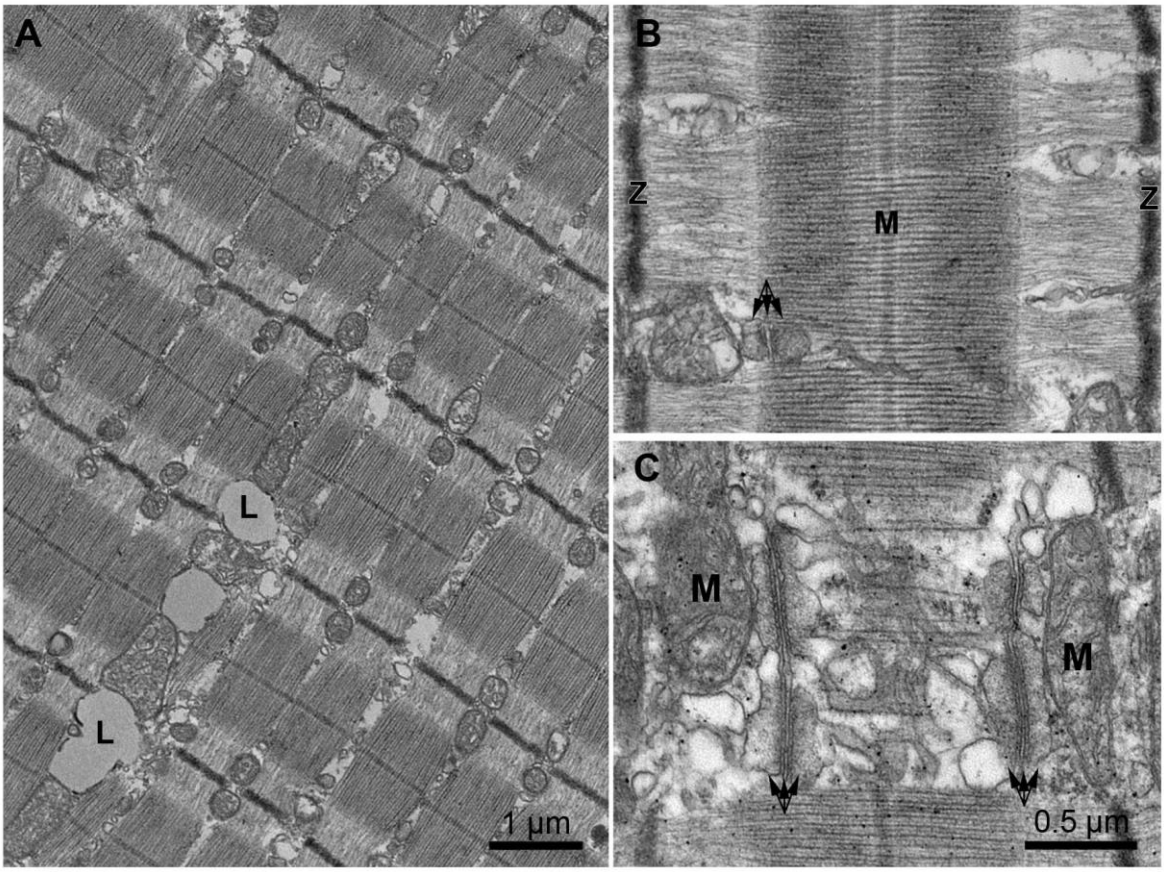

Figure 3 – Ultrastructure of a skeletal muscle cell.

A) Low magnification electron micrograph of human vastus lateralis biopsy displaying the typical striated pattern of aligned myofibrils. B) Sarcomere detail with aligned Z line (Z) and M band (M). C) Membrane components positioned at the edge of the A band (triple arrows indicate a triad), next to mitochondria. (Pietrangelo et al., 2013)

Importantly, sarcomere and thus myofibril alignment results in efficient muscle force generation. Yet, this contractile machinery has to be anchored to the cell membrane for force transmission to the muscle tissue. Given the magnitude of the contraction force, the subsarcolemmal area has a specialized structure termed **costamere** for connection to the extracellular matrix at the Z line (Ervasti, 2003; Jaka et al., 2015). The dystrophin–glycoprotein complex is a main costamere component, linking the intermediate filaments network of desmin to the extracellular matrix. The costamere is subjected to immense straining, being the origin of a multitude of muscular dystrophies (Cardamone et al., 2008).

1.1.2 Skeletal myogenesis

Myofibers are the biggest human cells, originated from the fusion of numerous muscle precursors – the **myocytes** (Bentzinger et al., 2012). This happens intensively throughout embryogenesis, as well as sparsely during adulthood in order to maintain tissue homeostasis.

The main intrinsic signaling pathways underlying embryonic progenitor and adult satellite cell fusion are broadly similar and well established. Essentially, a cascade of hierarchical transcription factors is induced to orchestrate the transition of **progenitors** through specification and commitment into the **myoblast** stage. The most often referred players are paired-homeobox transcription factors (e.g. Pax3 and Pax7) which regulate early specification, and myogenic regulatory factors (MRFs) which are common markers for committed myoblasts (e.g. Myf5 and MyoD) (Buckingham and Relaix, 2015).

Following proliferation, myoblasts give place to myocytes ready to fuse expressing MyoG and MRF4. The nuclei from these fusing myocytes are placed in the cell center giving rise to a multinucleated **myotube** (Cadot et al., 2015). The myotube differentiates into a **myofiber** once the excitation and contraction components are properly expressed and assembled. The process of **myofibrillogenesis** starts with arrays of sarcomeres being assembled close to the cell membrane (Sparrow and Schöck, 2009). It is believed that integrins anchor premyofibrils, which resemble actin stress fibers containing α-actinin and non-muscle myosin II. While premyofibrils develop, they incorporate titin and muscle myosin II. The correct

length of the actin and myosin is regulated by several components (e.g. Titin and Nebulin) as Z disks are formed. The newly formed myofibrils become aligned in a contraction dependent manner. Concomitantly, the nuclei move to the cell **periphery** and spread so that the distance between them is maximized (Bruusgaard et al., 2003; Roman et al., 2017).

Finally, the mature myofiber can undergo **hypertrophy** (increase in size) in response to exercise. Interestingly, new myoblasts can fuse during hypertrophy suggesting that the number of nuclei is proportional to the cell volume in certain muscles (Bruusgaard et al., 2010; Gundersen, 2016).

Some muscle progenitor cells do not fully engage in the myogenic process and become quiescent after specification (Bentzinger et al., 2012). These will give rise to the adult **satellite stem cell** pool that upon activation replenishes muscle with myoblasts for hypertrophy or muscle damage repair.

1.1.3 Muscle function

The main function of muscle tissue is the voluntary generation of force. This is why the main switch to induce contraction is an **action potential** from a somatic motor neuron. In the same muscle, one motor neuron can have multiple axon branches connecting to multiple myofibers. This is known as a **motor unit**. The smaller the average motor unit size, the more precise and controlled is a muscle.

Once the action potential has reached the axon terminal it has to be passed on to the myofiber. This occurs at the **neuromuscular junction**, a unique site where both the neuron and myofiber specialized in order to communicate. In there, Acetylcholine (ACh) is released and binds to its receptors at the muscle postsynaptic membrane. As a consequence, the activated receptors open and lead to local membrane depolarization (K^+ efflux). Since only one neuromuscular junction exists per myofiber, the excitation signal has to be propagated throughout the entire cell length for contraction to occur. Essentially, this is made possible by the voltage gated Na^+ channels spread along the sarcolemma that open sequentially upon the initial depolarization (Na^+ influx).

After the myofiber has been thoroughly stimulated, the contractile machinery has to be activated. This link between the two events is termed **Excitation-Contraction (E-C) coupling** and relies on the specialization and organization of two different membrane structures (Figure 3C and 4). The first has origin in the sarcolemma, which invaginates and forms transversal tubules that go into the cell center while surrounding the myofibrils. These so called **T Tubules** transmit the action potential from the cell surface to every sarcomere, and flank each Z line at the junction between the A and I bands. The second originates from the **sarcoplasmic reticulum (SR)**, the endoplasmic reticulum of muscle that governs calcium levels (Rossi and Dirksen, 2006). The SR has two domains: the longitudinal SR, which is tubular and surrounds myofibrils; and the junctional SR, composed of **terminal cisternae** which are also at the A-I band junction. Invariably, each T tubule is bordered by two terminal cisternae and this structure is a **triad**. The triad is where E-C coupling occurs. Briefly, a structural change in the voltage dependent calcium channel **DHPR** (at the T tubule) leads to Ryanodine receptor (**RyR**) opening which massively releases Ca^{2+} from the SR.

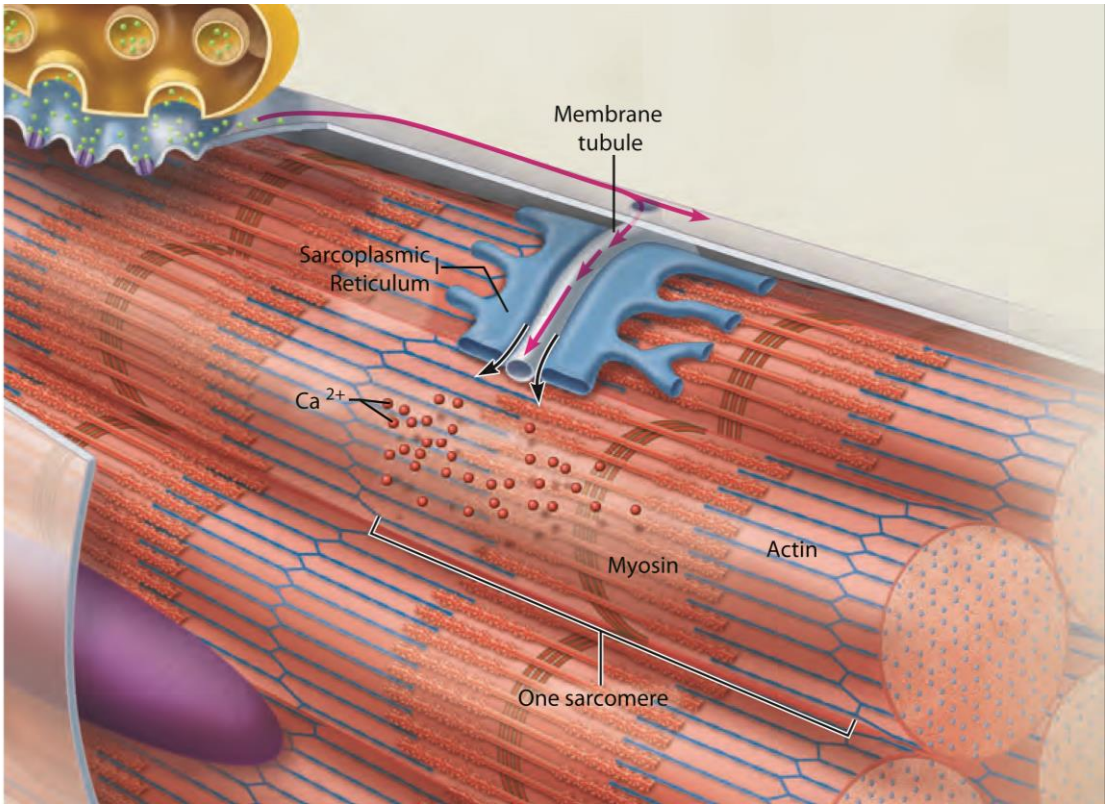

Figure 4 – Excitation-contraction coupling.

After local depolarization at the neuromuscular junction, an action potential is generated and travels along the sarcolemma into the T tubules all the way to the cell center. The t tubules are flanked by two terminal cisternae of the SR, making one triad. It is due to the close proximity triad proteins that the membrane depolarization signal is transmitted to the contractile apparatus. DHPR senses the T tubule voltage inducing RyR opening and massive calcium release in the SR. Adapted from Marieb and Hoehn, 2007.

Muscle contraction structurally consists of linking myosin globular heads to accessible actin attachment sites (Figure 2). These cross bridges are formed upon Ca^{2+} release and binding to troponin, which in turn changes tropomyosin configuration leaving actin exposed. Consecutively, myosin binds actin, releases previously hydrolyzed ATP (ADP + P_i) and moves to the following actin site. A new ATP readily binds to myosin and as a consequence myosin detaches from actin. The unbound but energized myosin head undergoes ATP hydrolysis and is ready for a new cycle of attachment, as long as Ca^{2+} and ATP are available. This sequential sliding of multiple myosins over actin, will lead to muscle shortening if the combined force produced by all sarcomeres in several myofibers surpasses the resistance offered to the muscle organ. Of note, whereas an action potential lasts 1-2 ms, the consequent contraction lasts at least 10ms and up to hundreds of milliseconds.

Contraction needs to be tightly controlled at all levels for muscle homeostasis: At the neuromuscular junction, Ach is rapidly degraded by acetylcholinesterase after binding to its receptors for neuronal control precision; As a consequence of membrane depolarization by Na^+ channels, voltage gated K^+ channels are quickly activated (K^+ efflux). During this brief period of membrane repolarization (1-2 ms) an action potential cannot be triggered; To compensate this Na^+-K^+ ionic unbalance, the ATP-dependent Na^+-K^+ pump works at a relatively slow rate over the course of several contractions until fatigue (contraction inability) eventually occurs (Allen et al., 2008); Calcium stocks are also limited in the SR and so after each contraction they are at least partially restored by the sarco/endoplasmic reticulum Ca^{2+}-ATPase (SERCA).

There are many other levels at which muscle function can be regulated, on the short and long term. The functional interaction of the numerous proteins involved is usually modulated by a third party. For example, Ca^{2+} is buffered in the SR by

Calsequestrin, which regulates Ryr opening through Triadin and Junctin (Beard et al., 2009). Total calcium levels can also be controlled by store-operated Ca^{2+} entry (SOCE) (Kurebayashi and Ogawa, 2001) or excitation-coupled Ca^{2+} entry (ECCE) (Cherednichenko et al., 2004). Different myofibers can also have different contraction kinetics, due to the expression of different protein variants and usage of energy sources. Myofibers can be classified in three types: slow oxidative (type 1), fast oxidative (type 2A and 2X) and fast glycolytic (type 2B) (Schiaffino and Reggiani, 2011). In particular, they express different myosin isoforms and use either the aerobic oxidative pathway or the glycolysis for ATP production. Different muscles will have different proportions of these fiber types depending on the kind of contraction they are used for. Altogether, the intrinsic ability for a muscle to contract sustainably depends on the correct expression, at the right place, of numerous proteins with countless possible interactions.

1.1.4 Muscle disorders

Most muscle inherited disorders can be classified as either a Dystrophy or a Myopathy (Cardamone et al., 2008). The pathogenesis of dystrophies is very heterogeneous but often related to structural muscle proteins, mostly at the costamere or its interacting proteins (Mercuri and Muntoni, 2013). Dystrophy symptoms have on average a later onset than Myopathies and there is progressive degeneration over time. Histologically, the dystrophic muscle shows severe necrosis, fibrosis and regeneration signs. The most common and best studied dystrophy is the Duchenne Muscular Dystrophy (DMD). In DMD the Dystrophin gene is mutated so that the protein is absent, affecting the structural integrity of myofibers and possibly mechanotransduction (Cohn and Campbell, 2000). Muscle weakness is one of the first symptoms although patients eventually die of heart or respiratory failure.

Myopathies are rarer than dystrophies, and usually the cause is a mutation affecting the efficiency of contraction. Myopathy biopsies show no signs of necrosis or regeneration. Instead, myofibers have distinct morphological changes such as the centrally located rows of nuclei in **Centronuclear myopathies** (CNM) (Figure 5, Biancalana et al., 2012). Several genes have been linked with CNM (e.g. DNM2, BIN1, MTM1, RYR1, TTN) although 20% of patients do not have a

genetic origin identified so far (Romero, 2010). The etiology of some structural abnormalities has been elucidated over the recent years, being mostly due to mutations in the E-C coupling machinery or in upstream components of membrane trafficking and metabolism (Jungbluth and Gautel, 2014). Myopathies have a much smaller incidence than dystrophies but are mostly congenital and usually present severer symptoms and mortality rates (Cardamone et al., 2008). Unfortunately, there is no cure for any of the disorders but disease specific interventions can sometimes improve the quality of life and longevity of the patients (Manring et al., 2014).

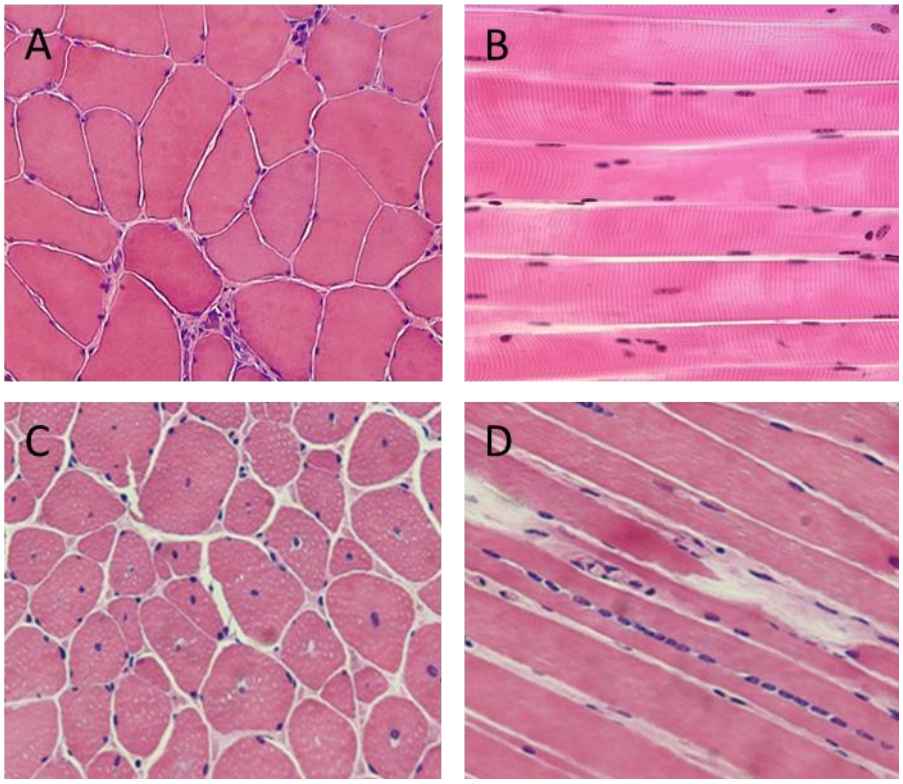

Figure 5 – Hematoxylin and eosin staining of healthy and CNM muscle sections

Healthy muscle biopsies display spaced peripheral nuclei (A,B) whereas CNM patients often have chains of centrally located nuclei (C,D), without showing signs of necrosis or regeneration. A,C transversal cuts; B,D longitudinal cuts. Adapted from Julio, 2013; Park et al., 2014b; Song et al., 2012.

1.2 Nuclear positioning and nuclear domains

1.2.1 Nuclear positioning in skeletal muscle

The multiple nuclei in a mature myofiber are positioned at its periphery, under the sarcolemma. In order to reach this location, several intermediary movements occur sequentially during myogenesis: centration, alignment, spreading, peripheralization and anchoring (Figure 6)Figure 6 – Events of nuclear movement during myogenesis. The steps leading to movement to the periphery have been well characterized, being dependent initially on microtubules and later on desmin filaments (Cadot et al., 2012; Falcone et al., 2014; Gimpel et al., 2017; Metzger et al., 2012; Roman and Gomes, 2017; Roman et al., 2017).

Once at the periphery, nuclei eventually get anchored and stop their longitudinal microtubule dependent movements (Bruusgaard et al., 2003; Englander and Rubin, 1987). Importantly, the nuclei are positioned so that the distance between them is maximized, in a non-random manner (Figure 7, Bruusgaard et al., 2003, 2006). The exact trigger for this nuclear caging by microtubules and desmin remains to be elucidated (Roman and Gomes, 2017). The LINC complex components (Nesprin1α2 and Sun1/2) and desmin have been shown to be impact anchorage (Chapman et al., 2014; Lei et al., 2009; Milner et al., 1996; Stroud et al., 2017; Zhang et al., 2007b). It is still unclear whether nuclear spacing and anchorage are interdependent at the periphery, as most phenotypes reported are static observations of nuclear clustering. This is in part due to a lack of appropriate system to dynamically address the question, independently of the preceding nuclear movements.

In a fully matured myofiber, three different areas can be distinguished: the neuromuscular junction (NMJ), at the center of the cell where around 5 subsynaptic nuclei are clustered under the axon terminal (Englander and Rubin, 1987); the myotendinous junction (MTJ), at the tips of the myofiber for attachment to tendons; and the extra-junctional area, where the remaining and majority of nuclei reside. The subsynaptic nuclei in the NMJ express specific genes important for the respective local functions (Fontaine and Changeux, 1989; Nazarian et al., 2005). The tyrosine kinase receptor Musk, when activated by the neuro-secreted

agrin, induces the transcription of specific NMJ genes with N-box elements (Hippenmeyer et al., 2007; Shi et al., 2012). Subsynaptic nuclear clustering and maintenance was also shown to be Desmin-Plectin and Nesprin1-Sun1 dependent (Grady et al., 2005; Lei et al., 2009; Mihailovska et al., 2014). Proteins important for membrane integrity, signaling and adhesion also accumulate specifically at the MTJ (Can et al., 2014; Dix and Eisenberg, 1990; Wang et al., 2013). However, nuclear clustering is only occasionally observed at the MTJ, probably as a consequence of regeneration or myocyte fusion (Bruusgaard et al., 2003). Thus, a specific pool of nuclei at the MTJ with a particular expression signature has not been described so far.

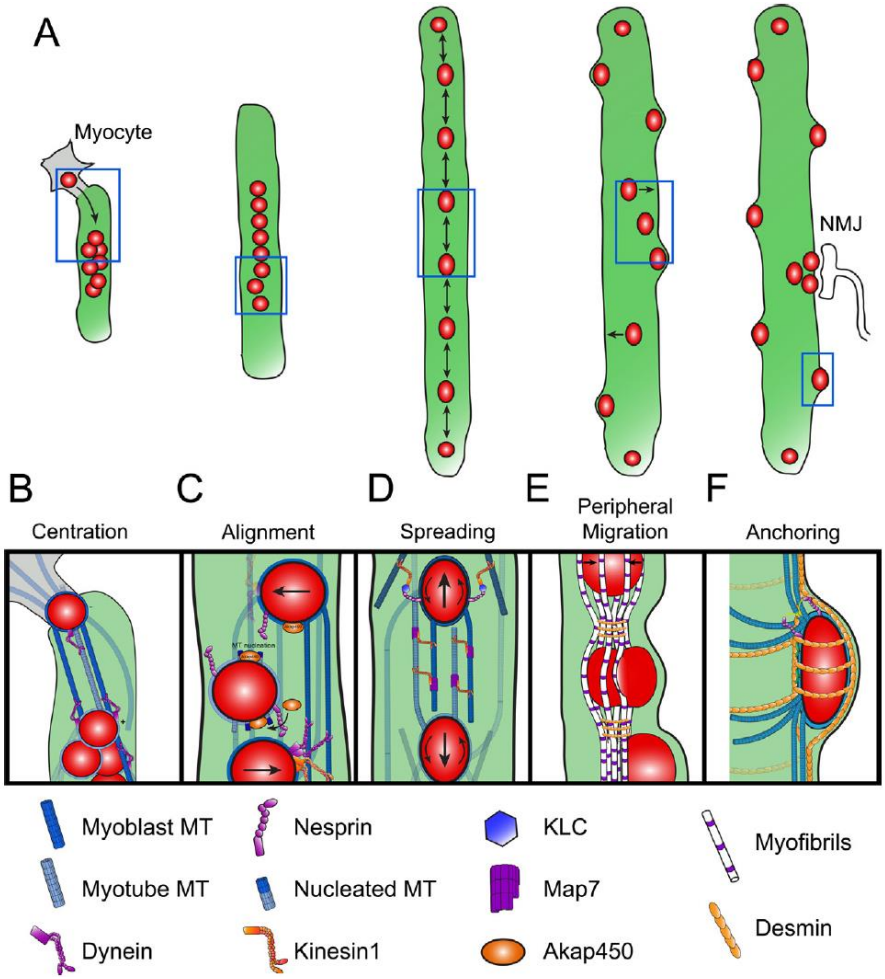

Figure 6 – Events of nuclear movement during myogenesis.

After myocyte fusion, dynein clusters nuclei at the center of the cell (B) and are afterwards aligned with the microtubule array in a Nesprin and dependent manner (C). Anti-parallel microtubules later allow the spreading of nuclei via Map7 and Kif5b (D). With myofiber differentiation, nuclei move to the periphery of the cell due to the tension generated by contraction and Desmin crosslinking (E).

Throughout differentiation nuclei move longitudinally inside the myofiber, except at highly mature stages where they get anchored by ITs and MTs (F). From Roman and Gomes, 2017.

1.2.2 Nuclear domain theory

The role for nuclear positioning is intuitive in certain circumstances, such as diving cells (Gundersen and Worman, 2013). However, the nucleus can also be asymmetrically positioned in terminally differentiated cells. The developed myofiber represents such cases in which the role for nuclear positioning might not be as evident (Folker and Baylies, 2013).

Bruusgaard and Gundersen contributed immensely to the current knowledge on nuclei number and distribution depending on muscle type and volume. By analyzing specifically myonuclei, they have undoubtedly established that: 1) nuclear distribution is fairly equidistant and not random; 2) the number of nuclei is proportional to cell volume in the slow/oxidative soleus muscle and 3) the number of nuclei is related to the cell surface area in the fast/glycolytic EDL muscle (Bruusgaard et al., 2003). Contradicting studies have sparked controversy, although most did not take into account the cellular heterogeneity of muscle tissue thus giving rise to skewed conclusions (Discussed in Gundersen, 2016; Gundersen and Bruusgaard, 2008). The authors have further confirmed by *in vivo* imaging that myonuclei number increases as a consequence of hypertrophy through satellite cell fusion (Bruusgaard et al., 2010). Moreover, they have unarguably shown that myonuclei number does not reduce during atrophy, contrarily to muscle size (Bruusgaard and Gundersen, 2008; Bruusgaard et al., 2010). These and other results have suggested the hypothesis of “muscle memory” in which the number of nuclei in a myofiber reflects its maximum size in the past. Accordingly, myofibers with increased myonuclear number but normal size due to testosterone induced hypertrophy and a period of withdrawal, have a much faster regrowth than the control and do not incorporate new myonuclei (Egner et al., 2013). These findings emphasize the importance of myonuclei position and number as they seem to be tightly controlled.

The reason for the particular position of myonuclei and its number regulation is still uncertain although Pavlath et al. provided a possible explanation by stating the

nuclear domain theory (Pavlath et al., 1989). Accordingly, each nucleus in a myotube is surrounded by a region of limited distance where its genetic products can exert their effects (Figure 7E, top). The formation of these nuclear domains by some mRNAs and proteins was shown in a myotube context, by fusing cells of different genetic backgrounds (Ralston and Hall, 1992; Ralston et al., 1997). In fact, this exactly the case for the subsynaptic nuclei clustered at the NMJ. In this functionally specialized region of the muscle cell, the respective mRNAs and proteins accumulate and do not spread (Merlie and Sanes, 1985). It remains to be demonstrated that the majority of myofiber nuclei also have domains of influence where E-C coupling takes place. If Pavlath's theory applies, mispositioning of nuclei might impede crucial mRNAs and respective proteins to completely reach their cellular targets and exert their functions (Figure 7E).

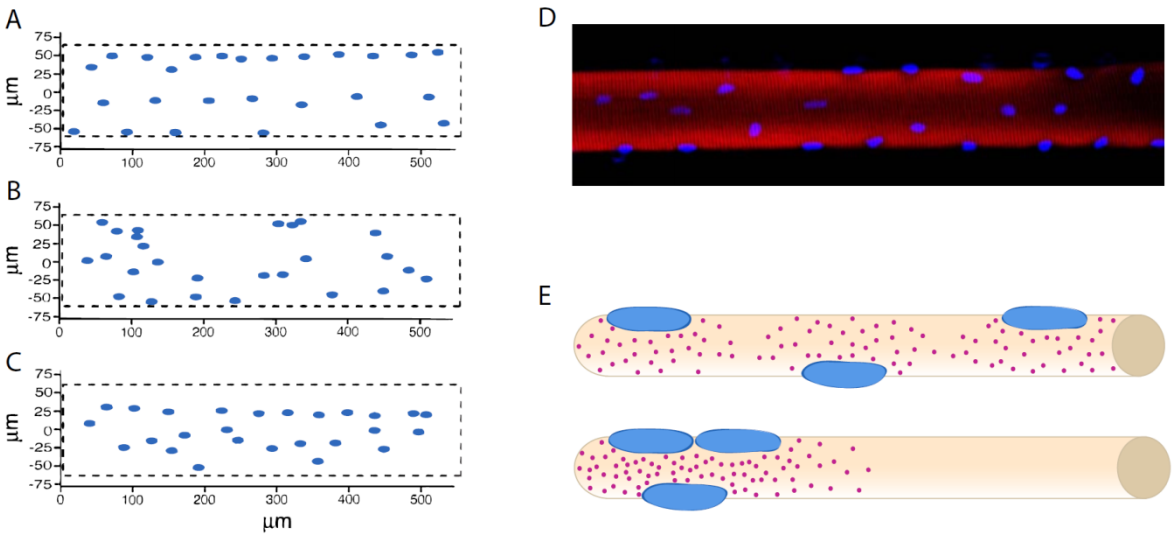

Figure 7 – Myofiber nuclear position and nuclear domains.

(A-C) Bruusgaard et al. compared *in vivo* nuclear positioning (B) with computational predictions of random distribution (B) and optimal distance between nuclei in 3D (C). All representations are of a myofiber flattened surface. Adapted from Bruusgaard et al., 2003 (D) Example of nuclear distribution in an isolated human myofiber, adapted from Qaisar and Larsson, 2014 (E) Simplified representation of nuclear domains in wild-type (top) and in nuclear mispositioning (bottom) conditions. Nuclei in all panels are depicted in blue.

In accordance to the nuclear domain theory, proper nuclear positioning seems to be important for drosophila skeletal muscle function (Metzger et al., 2012).

Moreover, mispositioned nuclei are a not yet understood hallmark of Centronuclear Myopathies (Al-Qusairi and Laporte, 2011), without being a consequence of regeneration. Interestingly, myoblast transplantation into DMD patients led to expression of dystrophin restricted to the new nuclei surroundings (Gussoni et al., 1997). Muscle fiber identity was also shown to decline in elder individuals in distinct nuclear associated domains (Andersen, 2003).

1.2.3 Skeletal muscle research models

There are multiple skeletal muscle models, depending on the biological question. The two most used systems are extremes opposite to one another: the murine *in vivo* experiments and the *in vitro* C2C12 culture. *In vivo* approaches provide by far the most physiologically complete results, with the drawbacks of being mostly static and excessively complex (Meng et al., 2014). They integrate the neurological and systemic response of matured myofibers modulated by the surrounding cells, to the experimental manipulation (e.g. induced damage, gene knock-out or contraction stimulation/inhibition). The second one, although more malleable, is highly limited by the differentiation level that can be reached and by the absence of a neuronal component. C212 cells were isolated from an adult CH3 mouse tight after injury (Yaffe and Saxel, 1977) and immortalized by serial passaging and subcloning (Blau et al., 1983). They constitute an excellent early developmental model, being accountable for most of the knowledge we have on myotube formation and development.

Another frequently used model is the isolation of adult mouse myofibers, either mechanically or enzymatically (Cheng and Westerblad, 2017; Pasut et al., 2013). This delicate ex vivo approach is particularly useful for studying satellite cell activation and fusion, as well as myofiber structure and contraction. It provides a slightly more dynamic insight into adult muscle biology, although limited technically and in time by the biophysical and physiological properties of these cells.

An approach that is being increasingly adopted is the use of *in vitro* systems with a degree of differentiation significantly higher than classic immortalized cultures. Early work with neonatal rat myoblasts unraveled not only the possibility for *in vitro* culture improvement but also underlined the different species inherent

differentiation potential (Flucher, 1992; Flucher et al., 1991). In fact, human myofiber *in vitro* differentiation is still limited despite all the investment driven by therapeutic interest (Guo et al., 2013).

With the recent progress of biotechnology, 3D systems were able to greatly enhance greatly *in vitro* myofiber development (Hinds et al., 2011; Madden et al., 2015). All 3D setups point out the importance of the extracellular matrix structure and composition for proper differentiation. In particular, the technique by Falcone and Roman differentiates primary neonatal mouse myoblasts into highly mature myofibers with peripheral nuclei, transversal triads and twitching capability (Figure 8Figure 7, Falcone et al., 2014; Pimentel et al., 2017). This method does not require specific hardware or highly-skilled manipulation and it is amenable to genetic manipulation and continuous imaging. Because of the simplicity of the setup, it can be adapted for combination with other techniques (e.g. neuron co-culture (Vilmont et al., 2016a)).

Given that *in vitro* developed myofibers have a smaller diameter, the utilization of high 3D resolution techniques is facilitated (due to increased sample permeation, higher specimen proximity and reduced auto-fluorescence). Additionally, the live imaging and developmental aspects provide a more integrated understanding of muscle biology compared to mammalian *in vivo* studies. For instance, nuclear dynamics can provide valuable insight into how muscle is compartmentalized and how other organelles are relatively positioned. As such, this *in vitro* system constitutes a unique skeletal muscle model of great potential in the field.

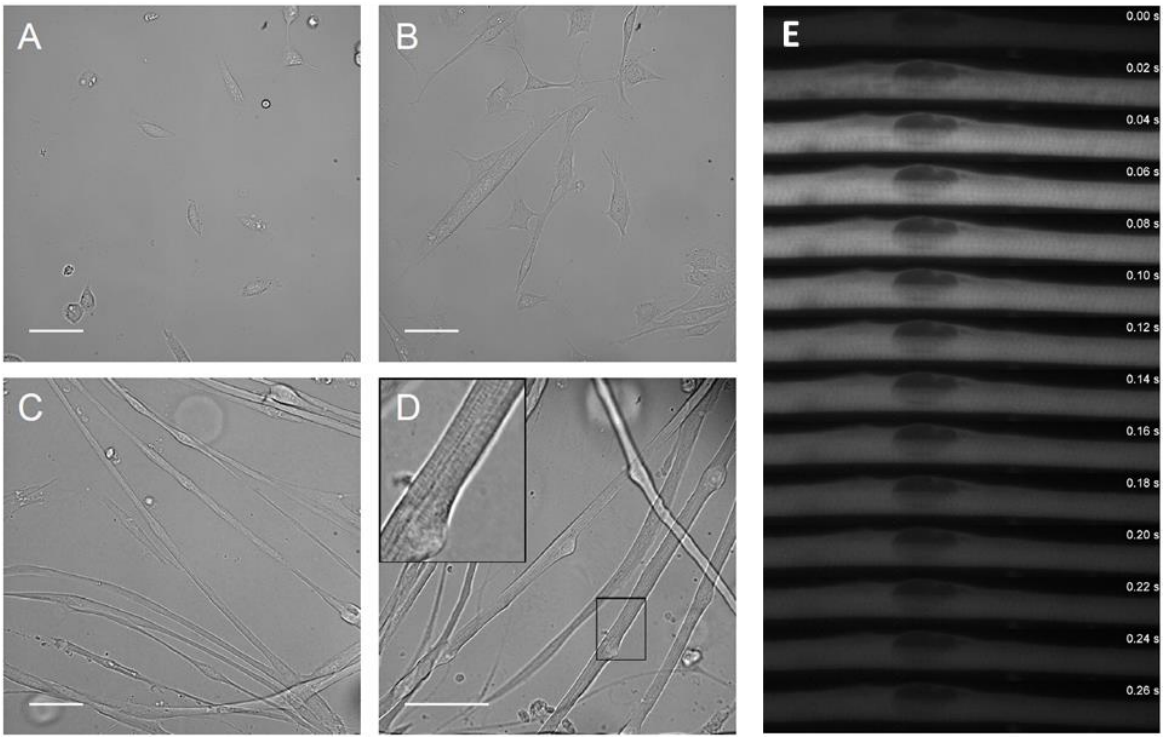

Figure 8 – Differentiation of mouse primary myofibers *in vitro*

(A-C) Transmitted light images showing the differentiation of myoblasts into myofibers with at day 2, 3, 6 and 11 respectively. Inset in D shows peripheral nuclei and striations of a highly matured myofiber. Scale bar 50µm. (E) Contraction event visualized through the expression of a cytoplasmic calcium sensor (20 ms/frame). Adapted from Pimentel et al., 2017.

1.3 Subcellular mRNA localization

The first in situ observation of polarized mRNA distribution dates to 1983 (Jeffery et al., 1983). The egg of the ascidian *Styela* has three visually distinct cytoplasmic domains, each giving rise to different cell lineages. William Jeffery observed that contrarily to total mRNA, the non-muscle actin mRNA was enriched at the myoplasm in the egg periphery. The potential functions for mRNA localization and localized protein expression were hypothesized, with translation control for cytoplasmic fate determination being proposed. Remarkably, the authors interrogated the mechanism for this cytoplasmic segregation and speculated on a contribution from the cytoskeleton, membranes and organelles. The discussed theories were proven right later on, being still applicable to countless transcripts and spanning many types of organisms.

1.3.1 Relevance of mRNA localization

The field of mRNA localization flourished with further developmental biology studies showing critical roles for specific mRNAs in oocyte, egg and embryo patterning. A classical functional example is the *Xenopus* Vg1 mRNA. This maternal transcript localizes to the oocyte vegetal pole being necessary and sufficient for mesoderm induction (Birsoy et al., 2006; Dale et al., 1993; Melton, 1987; Thomsen and Melton, 1993).

Eventually, the most widely used model to study mRNA localization became the *Drosophila* oocyte. In particular, the localization of the maternal mRNAs *gurken*, *bicoid*, *oskar* and *nanos* is a textbook example of anteroposterior (AP) and dorsoventral (DV) patterning. The localized translation of Gurken in the posterior pole initiates a signaling cascade that leads to cytoskeleton reorganization, nuclear repositioning and DV axis determination (González-Reyes et al., 1995; Guichet et al., 2001; Neuman-Silberberg and Schüpbach, 1993; Roth et al., 1995). As a consequence, *bicoid* and *oskar* can diverge to the anterior and posterior poles respectively, specifying the AP axis (Berleth et al., 1988; Ephrussi and Lehmann, 1992; St Johnston et al., 1991). The posterior translation of Oskar enables the localization of *nanos* at the posterior pole, which is crucial for abdominal and germline development in the embryo (Figure 9 A and A', Ephrussi

and Lehmann, 1992; Gavis and Lehmann, 1992; Gavis et al., 2008; Wang and Lehmann, 1991).

Several purposes for mRNA localization are recognized nowadays beyond embryonic determination, from bacteria to mammals (Buxbaum et al., 2015; Holt and Bullock, 2009). In 1986, Lawrence and Singer described the polarized localization of cytoskeletal mRNAs in migrating myoblasts (Lawrence and Singer, 1986). In particular, the localization of β-actin mRNA at the lamellipodia of migrating fibroblasts became one of the most studied examples (Figure 9). Abolishment of β-actin mRNA transport leads to altered cell morphology and decrease in the directionality and persistency of cell movement (Kislauskis et al., 1994, 1997; Shestakova et al., 2001). More precisely, these phenotypes were shown to be due to impairment of **local translation** of β-actin and consequent reduction of focal adhesion stability (Katz et al., 2012; Rodriguez et al., 2006).

In epithelial cells mRNA localization is also polarized, and this seems to be important for adherens junction assembly and signaling (Gutierrez et al., 2014; Kourtidis et al., 2017; Nagaoka et al., 2012). Recent work on the mouse intestinal epithelium has shown that apical mRNA polarization upon feeding increases translation efficiency, required for nutrient absorption (Moor et al., 2017).

Independent genome wide studies emphasize how common mRNA localization seems to be. In one particularly striking study, over 70% of the observed mRNAs localize to specific subcellular compartments in the drosophila embryo, usually at the same location as the encoded proteins (Lécuyer et al., 2007). In line with this, a significant number of mRNAs was found to be enriched in specific cytoplasmic regions of mammalian cells (Cajigas et al., 2012; Mardakheh et al., 2015; Mili et al., 2008; Poon et al., 2006; Weatheritt et al., 2014). Many of these global studies were performed in neurons, with the localization of several individual mRNA species nowadays confirmed and well described (Doyle and Kiebler, 2011; Jung et al., 2012; Spaulding and Burgess, 2017).

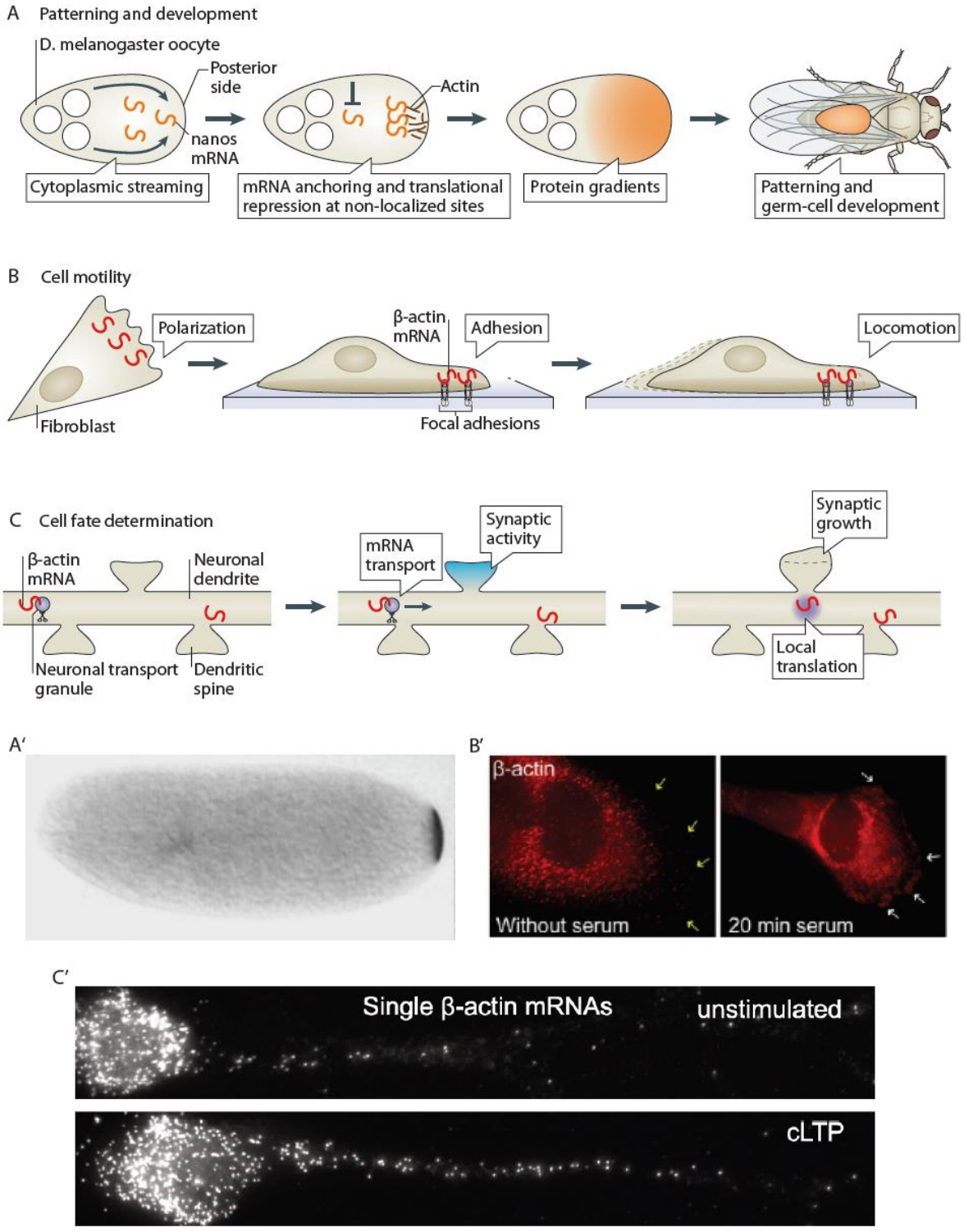

Figure 9 – Overview of roles and mechanisms for mRNA localization

A and A') mRNA localization in oocytes determines developmental fates (e.g. *nanos* mRNA at the posterior pole determines abdomen and germ cell lineage) (Wang and Lehmann, 1991). B and B') Localization of cytoskeletal mRNAs (e.g. β-actin) at the cell edge determines the efficiency of cell migration (Ben-Ari et al., 2010). C and C') mRNA localization and local translation in synapses is crucial for their development and plasticity (Buxbaum et al., 2014). Schemes adapted from Buxbaum et al., 2015.

Neurons constitute an excellent model for mRNA localization studies, since they are highly polarized and their functionality can be easily evaluated. Given that axon length can reach the meter range, it seems intuitive that transport of mRNA in a repressed form would be a very effective way to rapidly localize proteins upon local stimulation (Figure 9C and C'). In fact, β-actin mRNA localization and local translation is also important in neurons for dendritic morphology, neuronal outgrowth and long-term potentiation (Eom et al., 2003; Hüttelmaier et al., 2005; Ramachandran and Frey, 2009).

Defects in the RNA localization machinery have been associated with neuronal and oncogenic disorders (Brinegar and Cooper, 2016; Wurth and Gebauer, 2015). However, out of a *in vivo* context the functional consequences of abolishing mRNA targeting may appear only mild (e.g. β-actin in migrating fibroblasts; Katz et al., 2012). This indicates that the proteins from remaining sources can still partially execute their functions under certain experimental conditions. Nevertheless, there are undoubtedly many advantages at the molecular level that can explain the evolutionary conservation of this mechanism: increased cost effectiveness by transporting few mRNAs that can generate many protein copies at the destination; facilitation of protein complex assembly by approximation of functionally related mRNAs; synthesis of proteins with distinct properties such as posttranslational modifications depending on the subcellular environment; possibility for local control of translation by repression alleviation in response to cues and thus finer control of protein localization and activity (Eliscovich et al., 2008; Hüttelmaier et al., 2005; Mingle et al., 2005; Weatheritt et al., 2014).

The ability to locally translate is important regardless of mRNA localization. By keeping mRNAs repressed but poised for translation, the relative efficiency of local protein enrichment is improved and ectopic action of potentially detrimental proteins is prevented. A good example is the myelin basic protein (MBP) mRNA localized and translated solely at the distal oligodendritic processes, avoiding aberrant myelination patterns (Lyons et al., 2009). In fact, it is generally believed that mRNAs need to be kept in a repressed state for processive transport, although simultaneous translation and transport have been reported (Katz et al., 2016; Wu et al., 2016). Through local translation, a decentralized and faster control of protein expression occurs at the cytoplasmic regions that directly

perceive extracellular cues. This mechanism is the basis of synaptic plasticity and memory formation, since strengthening and weakening of synapses (long-term potentiation and depression) have to be restricted in space while continuous in time (Sutton and Schuman, 2006). Thus, mRNA localization and local translation are mechanisms that often hold hands and allow for fine-tune post-transcriptional gene expression control.

1.3.2 Sequence determination and RBPs

What determines the destination of an mRNA in the cell? There is no consensus answer, as different mRNA species can exhibit very different localization mechanisms. Nevertheless, the involvement of specific regulatory proteins and the cytoskeleton in the process seems to be ubiquitous. mRNAs are constantly associated with RNA-binding proteins (**RBPs**) in the form of mRNA–protein complexes (**mRNPs**). When these complexes reach large sizes they can be loosely termed RNA granules, particularly in neurons. Several different RBPs will bind to a transcript depending on the cis-acting elements in its nucleotide sequence, known as **localization elements (LEs)** or zipcodes.

LEs are found typically in the 3'UTR but can also be located in 5'UTRs, coding sequence, retained introns, exon-junctions and even promoter regions (Buckley et al., 2011; Ghosh et al., 2012; Macdonald and Struhl, 1988; Saunders and Cohen, 1999; Zid and O'Shea, 2014). The higher frequency of LEs in UTRs may reflect their ability to evolve without constrains of retaining coding information. Importantly, RBPs often recognize secondary structures instead of the nucleotide sequence itself (Ferrandon et al., 1994, 1997). Thus, it is not surprising that LE sequences are not conserved across mRNAs known to be bound to the same RBP. Additionally, each transcript can have multiple LEs, either different or repeated. Redundant LEs can act cooperatively towards increased efficiency whereas diverse LEs can also function as modules dedicated to intermediate steps or different contexts for localization (Chartrand et al., 2002; Macdonald and Kerr, 1997; Macdonald et al., 1993). To add even more complexity, in some cases the transcripts must oligomerize for efficient mRNP assembly and localization (Ferrandon et al., 1997).

Translation may also be required to localize some proteins, as it is the case of some secreted and transmembrane proteins that get their nascent signal recognition particle anchored to ER resident proteins (Cui and Palazzo, 2014). Given that multiple RBPs can bind one transcript, it is the combinatorial composition of each mRNP that will dictate its localization in a particular cellular context (Figure 10).

A particularly complex mechanism localizes *bicoid* in the anterior of the *Drosophila* oocyte (Figure 10B). The different LEs in the 3'UTR of the transcript form stem loops necessary for its stepwise transport, from nurse cells to the anterior of the oocyte where it is anchored (Ferrandon et al., 1997; Macdonald and Kerr, 1997; Macdonald and Struhl, 1988; Macdonald et al., 1993). Moreover, dimerization of the mRNA is necessary for binding to the RBP Staufen, necessary for *bicoid* localization in the later steps of oogenesis (Ferrandon et al., 1997; St Johnston et al., 1991; Weil et al., 2006).

The detection of LEs facilitates the discovery of its respective RBPs, especially when different RBPs have redundant effects among their multiple mRNP targets. Once the sequence is known, it can be manipulated and used in reporters for better understanding of the function of its binding partners. This was the case for the β-actin zipcode that led to the identification of zip-code binding (ZBP) proteins (Figure 10A, Kislauskis et al., 1994; Ross et al., 1997). The recognition of the 54-nucleotide motif in the 3'UTR of the transcript by ZBP1 is sufficient and necessary for localization at the leading edge (Oleynikov and Singer, 2003). The hexanucleotide sequence ACACCC in the motif is evolutionarily conserved in the β-actin transcript of other species and the chicken ZBP1 also has orthologues like the mammalian IMP1 and the Xenopus Vg1RBP/Vera. More RBPs are now known to bind the β-actin mRNA, such as ZBP2 that binds co-transcriptionally and mediates the rapid engagement of ZBP1 upon its release (Gu et al., 2002; Pan et al., 2007). ZPB2 illustrates how the journey of each transcript starts being determined early in the nucleus, despite its absence in the cytoplasmic mRNPs.

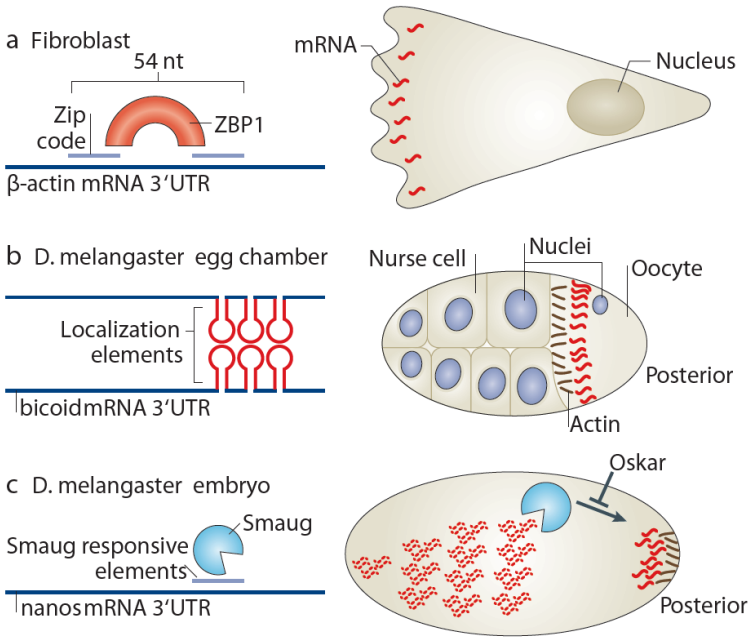

Figure 10 – RBP binding to localization elements determines mRNA localization

A) The zip code sequence of the β-actin 3'UTR recruits zipcode-binding protein1 (ZBP1) that will determine its transport to the leading edge and to synapses. B) Several 50nt stemloops in the *bicoid* 3'UTR allow its dimerization and binding to Staufen for anchoring at the anterior pole of the Drosophila oocyte. C) Smaug binds to its responsive elements in the 3'UTR of *nanos* in the absence of Oskar, leading to its degradation in the embryo anterior. Adapted from Buxbaum et al., 2015.

Biochemical approaches have determined that the same RBP can be linked to different mRNAs and vice versa (Fritzsche et al., 2013). Yet, these approaches do not elucidate the functions of these interactions nor specify how diverse each type of granule can be. In fact, the mode of action of most identified RBPs remains undemonstrated in the context of mRNA localization. **Three main roles have been assigned for RBPs: active transport, anchoring and local stabilization/degradation.** The most commonly observed is the facilitation of active-transport by interaction with motor proteins. Although evidence for direct binding is scarce, RBPs have been shown to increase the binding affinity of mRNPs to motors, their processivity and run length (Alami et al., 2014; Amrute-Nayak and Bullock, 2012; Fusco et al., 2003; Sladewski et al., 2013).

The two remaining functions for RBPs in mRNA localization are well represented by the localization of *nanos* in the Drosophila embryo (Figure 10C). During late

oogenesis, a cytoplasmic streaming moves *nanos* from the nurse cells to the posterior pole of the oocyte (Forrest and Gavis, 2003). There the mRNA gets anchored to actin through multiple RBPs (Becalska et al., 2011; Jain and Gavis, 2008). At the embryo stage, binding of the RBP Oskar stabilizes *nanos* at the posterior pole whereas it gets degraded by Smaug at other locations (Zaessinger et al., 2006). The combination of these mechanisms enables the concentration of only 4% the mRNAs at the posterior pole where Nanos is locally translated (Bergsten and Gavis, 1999). Remarkably, this is sufficient for a local protein enrichment of more than one hundred times.

1.3.3 mRNP transport by cytoskeleton motors

mRNPs have been described to localize mainly by active transport via direct or indirect binding to motor proteins. Most studies showing association to motor proteins are rather static, either by biochemical or loss-of-function approaches. As a consequence, an integrated understanding of the exact biophysical mechanism by which mRNAs are transported is generally missing.

Reporter mRNA tracking experiments in COS-7 cells demonstrated that it exhibits four types of movement: stationary, corralled, diffusive and directed (Fusco et al., 2003). The authors concluded that in the absence of LEs, passive mRNA movement accounts for 61% of its behavior whereas active transport only represents about 3%. Addition of the β-actin zipcode to the reporter decreased its static behavior and increased the percentage of particles displaying directed movement to 22%. While transported, targeted mRNAs had the same average speed as non-targeted (1-1.5 μm/sec) but these events lasted longer periods. Live imaging of the β-actin mRNA in fibroblasts revealed different dynamics depending on the cytoplasmic location (Yamagishi et al., 2009). These mRNAs exhibited restricted Brownian motion in the perinuclear region in opposition to the leading edge, where their diffusive behavior was about 10 times faster.

The fact that transcripts without any known LE still display residual active transport raises the hypothesis of an intrinsic bias for motor mRNA interaction (Buxbaum et al., 2015; Soundararajan and Bullock, 2014). This less processive displacement in combination with a predominant diffusive behavior could be accountable for a

homogenous mRNA distribution. Binding of context-modulated RBPs could then influence the processivity of the motors in the mRNP complex. Although motors and RBPs are clearly implicated in mRNA localization, very little is known about their interaction except for a few isolated cases.

In the budding yeast, the actin cytoskeleton seems to be preferred for mRNA transport. The best described example is the transport of ASH1 mRNA to the bud tip, where it determines the daughter cell fate (Bobola et al., 1996; Sil and Herskowitz, 1996). ASH1 is transported by the Myo4p-She3p complex, a myosin V that dimerizes and becomes highly processive when bound to the RBP She2p, in a mRNA dependent manner (Hodges et al., 2008; Sladewski et al., 2013).

In other cell types, mRNA transport is mostly associated to a polarized microtubule network. It is challenging to unravel how mRNA moves along the complex microtubule cytoskeleton due to its many components, tunable dynamics and multilayered polarity (Figure 11). Microtubule motors can be of two types – dyneins and kinesins – being both ATP dependent (Gibbons and Rowe, 1965; Vale et al., 1985). The cytoplasmic dynein complex is directed to the minus end of microtubules and its core is composed of dimers of heavy chains (DHC), intermediate (DIC), light intermediate (DLIC) and three different light chains (DLC), with a total size of approximately 1.4 MDa (King et al., 2002; Roberts et al., 2013; Trokter et al., 2012). Additional regulators and adapters can interact with the complex, such as the 1.2 mDa dynactin complex which is necessary to generate a processive invitro complex (Cianfrocco et al., 2015; Gill et al., 1991; Schlager et al., 2014). Conversely, kinesins are smaller and simpler complexes usually directed to the plus end of microtubules (N-kinesins) but with a diversity encoded in 45 genes, grouped in 15 different kinesin families (KIF) (Hirokawa et al., 2009; Miki et al., 2001). Thus, it is understandable that the localization mechanism of the majority of mRNAs remains unknown, even if assuming that transport can be dictated by one single type of motor.

The fragile X mental retardation protein (FMRP) is a RBP that has been linked to Kinesin-1 and Kinesin-2 in independent studies (Davidovic et al., 2007; Dictenberg et al., 2008). Thus it could be possible that different kinesins have redundant roles (Messitt et al., 2008). Additionally, several mRNPs are seen travelling in a

bidirectional manner, suggesting simultaneous binding to motors of opposing directions (Bullock et al., 2006; Knowles et al., 1996). In fact, biochemical interaction between a mRNP and both dynein and a kinesin has been observed and other cellular cargos have also been simultaneously associated to different motors (Dictenberg et al., 2008; Holzbaur and Goldman, 2010; Ma and Chisholm, 2002; Rogers and Gelfand, 1998; Rogers et al., 1997). Moreover, the interaction of dynein and kinesin has been detected either directly or through linkers such as the dynactin complex or Bicaudal (Berezuk and Schroer, 2007; Deacon et al., 2003; Grigoriev et al., 2007; Ligon et al., 2004).

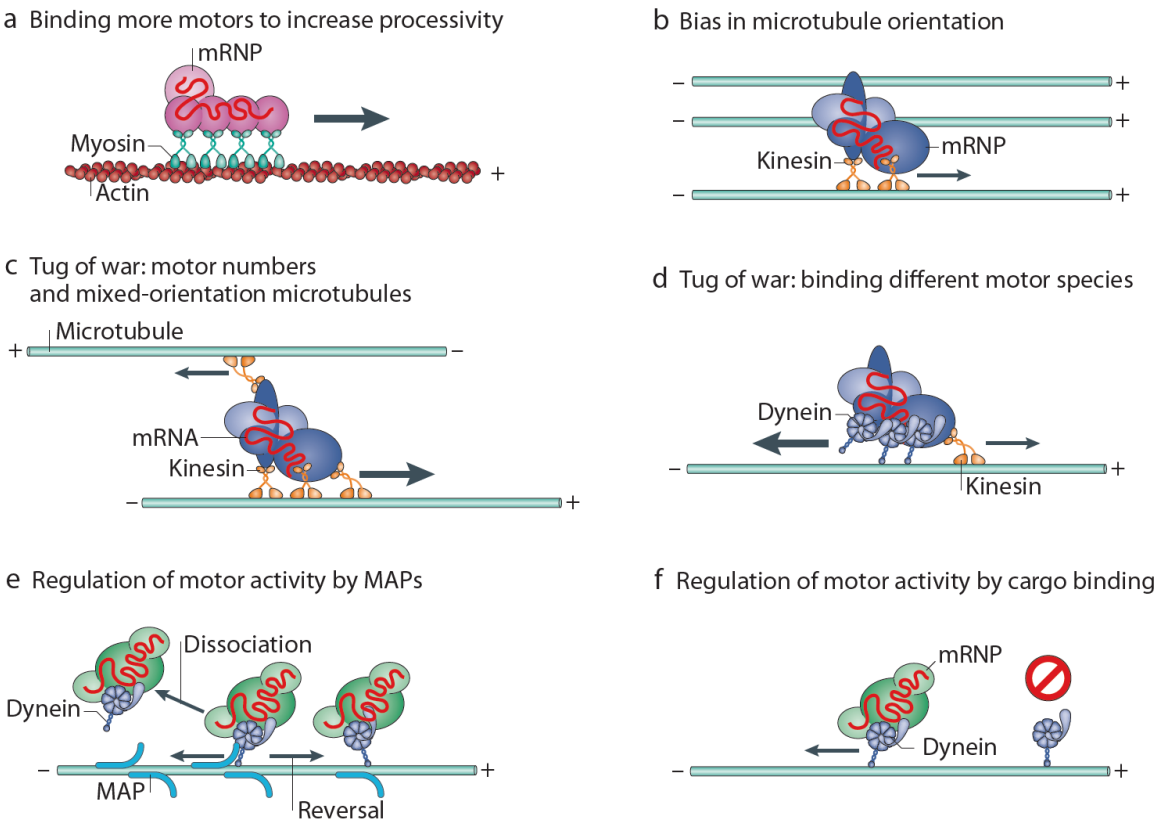

Figure 11 – Regulation of motored mRNA transport.

A) Processivity of transport might be increase by the binding of multiple motors (e.g. The 4 LEs of ASH1 bind four myosins (Sladewski et al., 2013)). B) Local bias in microtubule orientation might determine direction of mRNA transport. C,D) When microtubule and motor orientation is mixed the resulting direction will be determined by the overall force balance. E) MAPs can alter the binding and processivity of specific motors (Soundararajan and Bullock, 2014). F) The cargo itself might affect the function of the motor. Adapted from Buxbaum et al., 2015.

The direction of mRNPs on such scenario would be determined either by motor regulators or by the balance of antagonist strengths (Gagnon and Mowry, 2011). The outcome of this “tug of war” depends on the number of each motor type and respective mechanical strengths. In contradiction to this model, some experiments of loss-of-function suggested motor co-dependence given that motility was impaired in both directions (Hancock, 2014).

Further *in vivo* tracking studies are required to understand the dynamics of cellular transport and its specificities depending on the cargo. Also, whether different motors interact simultaneously with mRNPs or not remains elusive. The spatial heterogeneity of microtubule posttranslational modifications and orientations could account in many cases for irregular motor movements (Tas et al., 2017; Wang et al., 2017). Additionally, the intrinsic irregular motion displayed by dynein (Mallik et al., 2004; Roberts et al., 2014) and the transport of the motor proteins themselves is often overlooked (Duncan and Warrior, 2002; Palacios and Johnston, 2002; Ross et al., 2006). Regardless, bidirectional transport is particularly important in neurons as it is a premise for the “sushi belt model” (Doyle and Kiebler, 2011). This model states that mRNPs patrol neurites back and forth until they get summoned by synaptic activity, contributing for its plastic properties.

The best understood case of mRNA transport on microtubules is the one of pair-rule transcripts by the dynein complex in Drosophila. The minus-end-directed motor associates to these mRNAs through the adaptor BicaudalD and the RBP Egalitarian transporting them towards the apical cytoplasm of the embryo (Bullock and Ish-Horowicz, 2001; Dienstbier et al., 2009). BicaudalD was further shown to increase dynein-dynactin stability and therefore the processivity of the motor (Hoogenraad and Akhmanova, 2016; Jha et al., 2017; Splinter et al., 2012).

The dynein–BicaudalD–Egalitarian pathway is also likely to transport *gurken*, *bicoid*, *oskar* and *K10* the mRNAs from nurse cells to the oocyte (Bullock and Ish-Horowicz, 2001; Clark et al., 2007; Mische et al., 2007). Subsequently, these mRNAs follow different paths in the cell, each with specific mechanisms. For instance, *oskar* shifts to a kinesin-1 and Staufen dependent posterior transport and gets anchored by the Oskar protein (Brendza et al., 2000; Vanzo and Ephrussi, 2002). The orientation of the microtubules in the oocyte is fundamental for *oskar*

delivery and dynactin was shown to be necessary at the microtubule plus end to increase growth persistence (Nieuwburg et al., 2017; Trong et al., 2015; Zimyanin et al., 2008). The complex localization of *oskar* mRNA is a classic but controversial example, and only recently the molecular link to kinesin-1 was found to be an atypical tropomyosin (Erdélyi et al., 1995; Gáspár et al., 2017; Veeranan-Karmegam et al., 2016).

Other examples of plus-end directed mRNA transport have been unraveled, such as β-actin by ZBP1 bound directly to Kif11 in migrating fibroblasts (Song et al., 2015). In addition, a myosin IIB and myosin Va dependent localization has also been reported, suggesting that multiple motors act towards the localization of β-actin mRNA (Latham et al., 2001; Salerno et al., 2008). Interestingly, it seems that in neurons a different mechanism is employed as dynein, Kif5a, huntingtin and HAP1 are present in β-actin granules (Ma et al., 2011). The development of the b-actin mRNA fluorescent mouse highlighted the discrepancies between the kinetics of endogenous and exogenous transcripts, albeit their localization pattern is conserved (Park et al., 2014a). This is not totally surprising, given the described involvement of splicing and of the mRNA-RBP stoichiometry in mRNA localization (Bullock et al., 2006; Donnelly et al., 2011; Ghosh et al., 2012).

1.3.4 mRNP anchoring and hitchhiking

Although microtubules seem to be preferred for mRNA localization in multicellular organisms, the actin cytoskeleton is often important for mRNP anchorage. The difference between a role on anchoring and long-range transport might be difficult to determine, particularly in small cells with less spatial resolution. Moreover, some molecular players might be the same for both events thus masking possible different consecutive roles.

The β-actin mRNA is anchored to F-actin in protrusions through ZBP1 and the elongation factor 1α (Farina et al., 2003; Liu et al., 2002). It has also been suggested that actin polymerization is required for mRNA capturing by activated dendritic spines (Huang et al., 2007). The mRNA *nanos* is also anchored by actin to the posterior pole (Forrest and Gavis, 2003). For this late step of localization LEs are also necessary, although their role is often overlooked due to other

redundant LEs (Becalska et al., 2011; Jain and Gavis, 2008). Other mRNAs are anchored by short-range transport by myosin, such as *oskar* in the Drosophila oocyte. When depleted for the anchoring myosin V, *oskar* still to reaches the posterior pole but localization is not as efficient (Krauss et al., 2009). Interestingly, the Oskar protein itself anchors its upstream transcripts (Rongo et al., 1995).

Alternatively, mRNAs can also be anchored by dynein to areas of microtubule nucleation. An example is the *gurken* mRNA which is transported by dynein to the dorso-anterior corner of the oocyte. There, the mRNP loses Egalitarian and Bicaudal but not Squid, in order to get anchored (Delanoue et al., 2007). In contrast, *bicoid* is anchored to the oocyte by dynein, but independently of microtubule orientation (Trovisco et al., 2016; Weil et al., 2006). Whereas the *bicoid* RBP Exuperantia is required for localization in all oogenesis stages, Staufen is only required for the later ones (Cha et al., 2001; Ferrandon et al., 1994). Thus the localization and transport of mRNAs will change over space and time based on the RBPs bound.

More recently a novel pathway for mRNA transport – endosome hitchhiking – was described in the fungus *Ustilago maydis*. Originally, the microtubule dependent transport of mRNAs by the RBP Rrm4 was found to be necessary for hyphal growth (Becht et al., 2006; König et al., 2009). Later on, the characterization of the transport mechanism unveiled an overlapping with endosome trafficking and the respective motors Kin3 and Dyn1/2 (Baumann et al., 2012). Moreover, the endosome-mRNA adaptor was found to be a FYVE zinc finger domain protein – Upa1 (Pohlmann et al., 2015). Although a clear connection between mRNA transport and endosomes in higher eukaryotes is lacking, the process of endocytosis has been indirectly coupled to *oskar* anchoring by actin (Tanaka et al., 2011). Interestingly, ESCRT-II is required for *bicoid* localization although it seems to be independent of endosomal sorting (Irion and St Johnston, 2007)

1.3.5 mRNA localization in muscle

Given the multinucleated nature and size of skeletal muscle, the localization of its mRNAs has been a matter of study for decades. The first key observation was the clustering of AchR mRNA at the NMJ (Merlie and Sanes, 1985). After much

interrogation we now know that the main cause for this localization is the expression of postsynaptic genes only by those nuclei (Schaeffer et al., 2001).

Regarding nonsynaptic nuclei, the first description of mRNA distribution was of myosin heavy chain (MHC) in different muscle sections (Dix and Eisenberg, 1988). The authors described a non-uniform distribution, with enrichment at the sarcolemma, between myofibrils and close to myonuclei. They further suggested the existence of a distribution mechanism. Stretching of myofibers led to an increase in MHC mRNA at the MTJ, suggesting induced localization for myofibrillogenesis (Dix and Eisenberg, 1990). Meanwhile several lines of observation in different heterokaryon systems pointed to the fact that the gene products of heterologous nuclei do not completely diffuse in the cell (Figure 12A, Hall and Ralston, 1989; Karpati et al., 1989; Pavlath et al., 1989; Ralston and Hall, 1989a, 1989b, 1992). Interestingly, the perinuclear localization of the Transferrin Receptor mRNA in myoblasts was reported to be independent of its half-life and dependent on translation (Ralston et al., 1997).

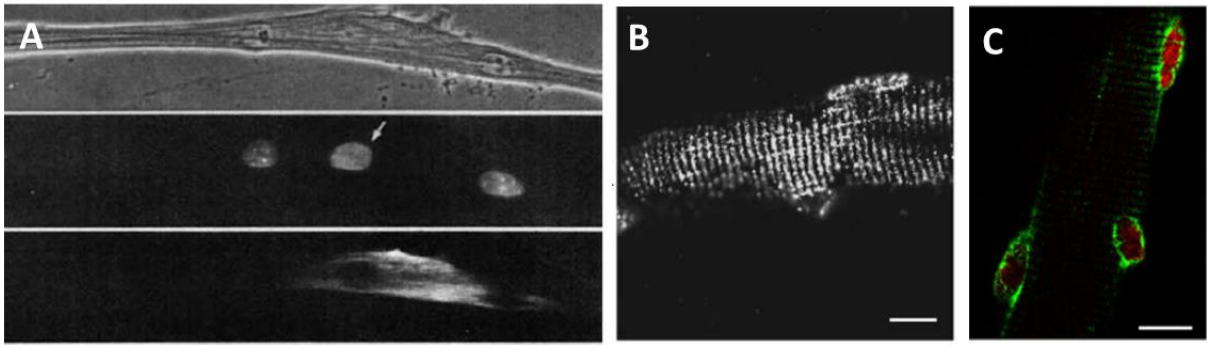

Figure 12 – Localization of mRNA in skeletal muscle cells

A) Human mRNA (slow myosin heavy chain, bottom panel) localizes close to the human nucleus in the myotube (arrow, middle panel). Adapted from Pavlath et al., 1989. B) Dihydropyridine receptor (DHPR) mRNA localization is isolated fibers are enriched at the sarcolemma. Adapted from Nissinen et al., 2005 C) Poly-A mRNA (green) is enriched at the sarcolemma in perinuclear regions (nuclei in red). Adapted from Nevalainen et al., 2013. Scale bars 10µm.

The mRNAs encoding for sarcomeric and costameric proteins (Titin, Nebulin, Vimentin, Desmin and Vinculin) were described to localize respectively at these sites (Fulton and Alftine, 1997; Morris and Fulton, 1994). Remarkably, the authors observed a temporal delay between Titin protein and mRNA localization. The latter is speculated to organize co-translationally as a consequence Titin protein arrangement. The authors underline the transport limitations of this protein, given its size (4 mDa) and low solubility, suggesting that mRNA localization might compensate for this. Calsequestrin and DHPR mRNAs were observed perinuclearly and at the sarcolemma, in a striated pattern (Figure 12B, Nissinen et al., 2005). These striations flanked the Z lines in accordance to their protein localization at the SR and T tubules respectively.

More recently, a similar distribution was observed for total mRNA in isolated fibers (Figure 12C, Nevalainen et al., 2013). In this study, ribosomes were also enriched in perinuclear regions and throughout the cell in a striated pattern corresponding to the A-I junction. At a higher molecular resolution, a striated mRNA and ribosome localization was also observed in adult cardiomyocytes (Lewis et al., 2018). Overall, different studies point to a perinuclear mRNA accumulation and to preference for subsarcolemmal regions compared to myofibril areas. The unique structure and dimension of myofibers has hindered a more detailed and mechanistic analysis of the localization of its mRNAs.

Importantly, the Microtubule Organizing Center (MTOC) shifts from the centrosome to the nuclear envelope early in skeletal myogenesis (Bugnard et al., 2005; Tassin et al., 1985). The Golgi is also relocalized to the nuclear envelope boundary and to dispersed cytoplasmic outposts, having microtubule nucleation capability (Oddoux et al., 2013; Ralston et al., 1999). As a consequence, microtubules are arranged in mostly longitudinal arrays throughout the multinucleated myofiber (Warren, 1974). In adult myofibers, the microtubules at the surface are dynamic and form a grid of both parallel and antiparallel bundles (Figure 13, Oddoux et al., 2013).

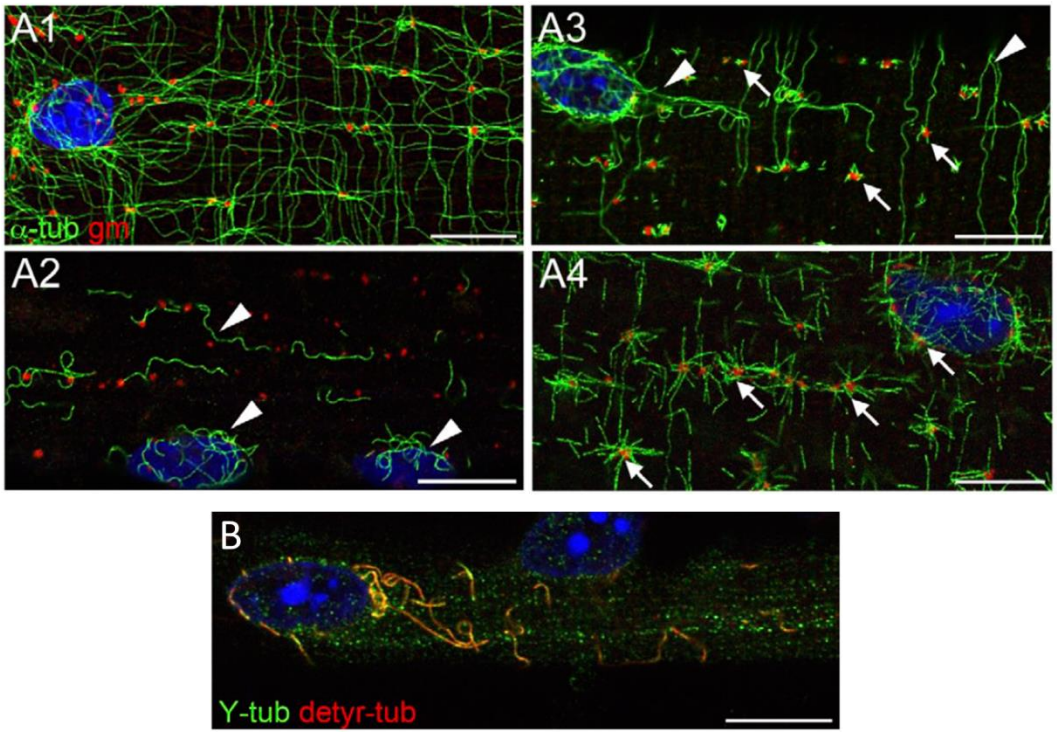

Figure 13 – Microtubule regrowth in isolated adult myofibers

A) Treatment of 4 h at 37°C in 4 µg/ml of nocodazole (NZ) and release shows microtubule regrowth from nuclear envelope and Golgi. A1: untreated control; A2: 4h NZ; A3: 2 min release; A4: few minutes after release. (Green, α-tubulin; Red, golgi; Blue, nucleus). B) Microtubules that remain after 4h of NZ are tyrosinated (green) and detyrosinated (red). Scale bars 10µm. Adapted from Oddoux et al., 2013.

Most microtubule studies in muscle have focused on the MTOC transition and on the functions of this network during myogenesis. Tubulin detyrosination, EB1, MURF and oMAP4 were also shown to be important for proper muscle differentiation (Chang et al., 2002; Mogessie et al., 2015; Spencer et al., 2000; Zhang et al., 2009). Tubulin tyrosine ligase expression peaks in neonatal muscles, and rapidly decreases with development (Arregui et al., 1997).

Surprisingly, not much is known regarding microtubules in mature myofibers except that detyrosination levels are increased in dystrophin-deficient *mdx* mice (Belanto et al., 2014; Khairallah et al., 2012). Furthermore, detryrosination seems to have a role in mechanotransduction since parthenolid inhibition altered the mechanical properties of contraction and alleviated *mdx* muscle injury (Kerr et al.,

2015). Microtubules have long been known to be essential for muscle development, but their precise roles and mechanisms in adult skeletal muscle biology remain largely unaddressed (Saitoh et al., 1988). Considering that microtubule-dependent nuclear positioning is important for skeletal muscle function and that nuclei are the main microtubule organizers, a careful analysis is needed to understand to what extent each nucleus is determinant for its surrounding cytoplasm.

2 Objectives

In this study we aimed to clarify how mRNA localization in muscle correlates with nuclear position and consequently with muscle function. Hence we asked:

1) What is the localization of mRNAs important for muscle function relatively to the multiple nuclei in the cell?

2) What are the mechanisms that localize mRNA in myofibers?

3) Is the physiological function of skeletal muscle dependent on nuclear position because of a polarized mRNA distribution?

3 Materials and Methods

3.1 Myoblast isolation and *in vitro* myofiber differentiation

Primary mouse myoblasts were isolated and differentiated as previously described (Pimentel et al., 2017).. The tibialis anterior, extensor digitorum longus, gastrocnemius and quadriceps of P5-P8 C57BL/6 pups were dissected into DPBS at 4 °C. The muscle was minced and transferred to digestion solution, in which was incubated for 90 min at 37 °C with agitation. Digestion was stopped with 1 volume of Dissection medium and the suspension was centrifuged at 75 x g for 5 min for debris removal. The supernatant was centrifuged at 350 x g for 5 min and resuspended in Dissection medium. The cell suspension was filtered through a 40 µm cell strainer and plated for 4 h in a cell culture incubator (37 °C and 5% CO2) to allow for fibroblast adhesion. While pre-plating, cell culture dishes were coated with basement membrane matrix (Matrigel) diluted 1:100 in cold IMDM for 1 h at RT. After 4 h of pre-plating the non-adhered cells were collected, centrifuged for 350 x g for 5 min and resuspended in Growth medium. Cells were counted and the density was adjusted to 160,000 to 220,000 cells per mL, depending on the differentiation efficiency of recent cultures. Of the adjusted cell suspension, 1 mL was added to Fluorodishes (WPI #FD35-100) used for imaging, 2 mL to 35cm culture dishes for RNA extraction and 0.75 mL to Membrane Ring (Zeiss #415190-9131) for LCM. Typically one animal yields sufficient myoblasts for approximately 2 Fluorodishes. After 3 days of proliferation, cells were changed to Differentiation medium. The following day, after removing the medium cells were coated with Matrigel diluted 1:2 in cold Differentiation medium for 30 min in a cell culture incubator (37 °C and 5% CO2). Following matrix jellification, fresh Differentiation medium supplemented with 100 ng/mL of Agrin was carefully added. Half of the Differentiation medium was changed every 2 days and Agrin supplemented. The lifespan of the cultures was typically of 7 days p.d. (post-differentiation). All necessary reagents and compositions are listed in Table 1.

Table 1 – Reagents for primary myofiber *in vitro* differentiation

Reagent	Final formulation	Source
Digestion Solution	5 mg/ml Collagenase type V	Gibco #17105041
	3.5 mg/ml Dispase II	Sigma-Aldrich #C9263
	in DPBS	Gibco #14190094
Dissection Medium	10% FBS	Eurobio # CVFSVF0001
	1% Penicillin-Streptomycin	Thermo Fisher #15140122
	in IMDM Glutamax	Gibco #31980022
Matrigel	Matrigel Growth reduced factor 1% or 50% in medium	Corning #354230
Growth Medium	20% FBS	Eurobio # CVFSVF0001
	1% Chicken Embryo Extract	Made in-house (Danoviz and Yablonka-Reuveni, 2012)
	1% Penicillin-Streptomycin	Thermo Fisher #15140122
	in IMDM Glutamax	Gibco #31980022
Differentiation Medium	2% Horse Serum	Invitrogen #13778-150
	1% Penicillin-Streptomycin	Thermo Fisher #15140122
Recombinant rat agrin	100 ng/mL	R&D systems #550-AG-100

3.2 Immortalized human myoblast culture and co-culture

The human myoblast cell line C8220 was a kind gift from Vicent Mouly (Institute of Myology). Cells were grown in Human Growth Medium (Skeletal Muscle Cell Growth Medium Promocell #C-23160) in cell culture dishes. Confluence was kept between 20-60% in order to avoid committing the cells to differentiation. For passaging, cells were washed with DPBS and trypsinized with TrypLE™ Express (Gibco #12605028) until detachment, followed by resuspension in fresh Skeletal Muscle Growth Medium at plating at appropriate dilution. For cell freezing, cell suspension was centrifuged at 350 x g for 5 min and resuspended in Freezing Medium (10% DMSO Sigma-Aldrich #D2650, 20% FBS, 70% Human Growth Medium).

For co-cultures, several conditions were tested in order to have enough human cells fusing (ideally one per myofiber) without impairing myofiber development due to the low fusogenic properties of immortalized cell lines. The best condition found

required growing the human cells until confluency to induce differentiation. When 100% confluence was reached, cells were kept in mouse Growth Medium for at least 6h. Cells were then trypsinized, centrifuged and resuspended in mouse Differentiation medium. The human myoblasts were then added to the primary mouse myoblast culture right after the latter was changed to Differentiation medium (after 3 days of proliferation). 20,000 human cells were added per Fluorodish and cultures were normally induced to differentiate.

3.3 Whole muscle isolation and cryosectioning

For cryosectioning the gastrocnemius from 3-week old C57BL/6 was isolated and immediately frozen in 2-methylbutane for 1 minute. The samples then were kept in dry ice or at -80°C until the following step. Cryosections longitudinal to the muscle axis with a thickness of 8 µm were performed and immediately fixed in 3.7% Formaldehyde (Sigma-Aldrich #F8775).

3.4 Transfection of plasmids and siRNAs

Primary mouse myoblast cultures were transfected always after 3 days of proliferation, before inducing differentiation. Lipid-nucleic acid complexes were formed by mixing for 1 µg of plasmid DNA or 20pmol of siRNA in 50 µl of Opti-MEM (Invitrogen #31985062) with 1 µl of Lipofectamine also in 50 µl of Opti-MEM. Lipofectamine 2000 and RNAiMAX (Invitrogen #11668027, #13778030) were used for plasmid and siRNA transfection respectively. After 30 min incubation, 500 µl of Transfection Medium was added to the 100 µl of Lipid complexes and then added to the cells. After 5 h of transfection, cells were washed once and left in Differentiation Medium. For all siRNAs tested, the phenotype specificity was confirmed with a second siRNA sequence.

Table 2 – Plasmids transfected for overexpression

Plasmid	Purpose	Source
DsRed-p150$^{217–548}$	Dynactin complex disruption	Addgene #51146
pcDNA3.1/hChR2-EYFP	Sarcolemma depolarization	Addgene #20939
VG60	Binds microtubule growing plus ends	Edgar Gomes Lab
P179 pEGFP	Expression of cytoplasmic GFP	Edgar Gomes Lab

Table 3 – Silencer select siRNAs from Ambion

siRNA	ID
Dynactin2 #1	s88045
Dynactin2 #2	s88046
Kif5a #1	s68780
Kif5a #2	s68779
Kif5b #1	s68781
Kif5b# 2	s68782
Kif5c #1	s68786
Kif5c #2	s68784
Kif3a #1	s68767
Kif3a #2	s68768
Kif3c #1	s68773
Kif3c #2	s68772
Kif11 #1	s68730
Kif11 #2	s68732
Kif1b #1	s68751
Kif1b #2	s68753
Dync1h1 #1	s65056
Dync1h1 #2	s65057
siRNA control	4390843

3.5 RNA extraction and RT-qPCR

RNA was extracted from myofibers at differentiation day 6 grown in one 35 mm culture dish using an RNeasy Micro kit (Qiagen #50974004). Eluted RNA was quantified using a Qubit RNA HS Assay Kit (Life Technologies #Q32852) and the same amount of RNA per sample, typically 200ng, was reverse transcribed using High-Capacity RNA-to-cDNA Kit (Life technologies #4387406). The qPCR was performed in a StepOnePlus system with Power SYBR Green PCR MasterMix (Applied Biosystems # 4367659). Primers were designed with Primer-BLAST and are listed in Table 4 – Primers. Relative gene expression was calculated using the ΔCt method.

Table 4 – Primers used for RT-qPCR

Primer	Sequence	Gene ID
Dctn2 FP	CCCTAAATACGCCGATCTCCC	69654
Dctn2 RP	GTGCAAACGCATCAAACTCTGC	69654
Hprt FP	GTTAAGCAGTACAGCCCCAAA	15452
Hprt RP	AGGGCATATCCAACAACAAACTT	15452

3.6 Drug treatments

Latrunculin A (Sigma #L5163) was added at 5uM from a 10mM DMSO stock as previously described (Falcone et al., 2014). Colchicine was gift from Carmo Fonseca's lab and was added at 1ug/ml from a 1mg/ml DMSO stock. Ciliobrevin D (Merck #250401) was added at 50uM from a stock of 6.37mM in DMSO as previously described (Vilmont et al., 2016b). All drugs were added at day 5 and incubated overnight. As a control, the same volume of DMSO was added to an independent Fluorodish or ibidi well and incubated for the same period of time. The following day the cells were fixed for smFISH.

3.7 Immunofluorescence staining and image acquisition

For immunostaining at the time-point of interest, cells in Fluorodishes were washed once with PBS and fixed with 4% PFA (Science Services GmbH #E15710) at RT for 10 min. After two PBS washes, cells were permeabilized with 0.5% Triton X-100 for 5 min at RT and washed again twice with PBS. Blocking was performed with 10% Goat Serum and 5% BSA (Sigma-Aldrich #G9023 and #A7906) in PBS for 30 min at RT. Subsequently cells were incubated in 10% Goat Serum and 5% BSA 0.1% Saponine (Sigma-Aldrich #47036) in PBS containing the primary antibodies (Table 3.4) at 4 °C overnight. The following day cells were washed three times with PBS for 5 min with agitation before incubation with secondary antibodies or phalloidin (ThermoFisher # A12379) for 40 min at RT. DAPI was also added in this step at 1:10.000 (Sigma-Aldrich #D9542). After other three washes Fluoromount-G (Southern Biotech #0100-01) was added as antifade. For microtubule imaging, soluble tubulin was extracted immediately before fixation using 1% Triton X-100 in PHEM buffer (PIPES 60mM, HEPES 21mM, EGTA 10mM, $MgCl_2$ 2mM) for 30 seconds.

Table 5 - Antibodies used for immunofluorescence

Epitope	Antibody	Dilution	Source
SpectrinB1	SPEC1-CE	1:100	Leica
Lam A/C	ab40567	1:400	Abcam
Puromycin	EQ0001	1:1000	Kerafast
Mouse IgG (H+L)	A-11029	1:400	Life Technologies
Rabbit IgG (H+L)	A-21429	1:400	Life Technologies
DYNC1I2	HPA040619	1:200	Sigma
Ribosome P	126MD-14-0506	1:200	Ray Biotech
Alpha-tubulin	YL1/2	1:50	Edgar Gomes Lab

Wide-field immunofluorescence and live-cell image acquisition was performed on a Zeiss Cell Observer inverted microscope equipped with a 37ºC 5% CO_2 chamber and automated stage using a 40x or 63x Plan-Apochromat Oil objective (NA=1.4). Digital images were acquired by sCMOS camera Hamamatsu ORCA-flash4.0 V2 for 10ms/frame streaming acquisition upon excitation with Colibri2 (Zeiss) LED light source.

Spinning disk microscopy was performed on a Zeiss Cell Observer inverted microscope equipped with a Yokogawa CSU-x1 confocal scanner, a 37ºC 5% CO_2 chamber and automated stage for live-cell image acquisition. Digital images were acquired by an Evolve 512 EMCCD through a 40x or 63x Plan-Apochromat Oil objective (NA=1.4).

Confocal point-scanning microscopy was performed on a Zeiss LSM 880 inverted microscope equipped with GaAsP detector for increased sensitivity using a 63x Plan-Apochromat Oil objective (NA=1.4).

3.8 Active ribosome labelling (Puromycilation)

Myofibers were treated with 100µM Puromycin and 200µm Cycloheximide (Sigma-Aldrich #P9620 #C1988) for 30 min in a cell culture incubator (37 °C and 5% CO2). Subsequently unbound Puromycin was extracted for 5 min on ice with 0.015% w/v Digitonin in PBS, followed by immediate fixation and immunostaining.

3.9 smFISH and total mRNA FISH

smFISH was performed similarly to as originally described (Raj et al., 2008). Probes were designed to align in the mRNA coding sequence using the Stellaris probe designer (https://www.biosearchtech.com/stellaris-designer). Probe sequences are listed in Appendix 6.1. Probes were then either ordered to Stellaris coupled to Quasar570/670 at 12.5µM or ordered as thirty-five individual oligos containing a TEG-Amino modification for in-house labeling (Batish et al., 2011). After resuspending each oligo in TE buffer pH 8.0 (VWR # VWRCE112), 5 nmol of each oligo was pooled together and precipitated overnight at -20 °C using 0.1x 3M Sodium Acetate (Sigma-Aldrich #S2889) and 3x 100% cold Ethanol. Oligos were

then resuspended in 0.1M Sodium Tetraborate pH 9.0 and mixed with an equal volume of reactive dye (Quasar 570/670 Carboxylic Acid, Succinimidyl Ester, Biosearch #FC-1063S or FC-1065S) also in Sodium Tetraborate. The reaction occurred at 37 °C for 6h and probes were again precipitated overnight. After one ethanol wash, probes were resuspended in 0.1M Triethylammonium pH 6.5 and separated by Liquid chromatography–mass spectrometry using a XBridge OST C18 2.5 µm 4.6x50mm Column (Waters #186003953). The run of 30 min consisted in a gradient of 0.1M Triethylammonium in 75% acetonitrile at a 1 mL/min flow. The labeled oligos were collected and ethanol precipitated for final resuspension in TE buffer at 100ng/ul.

For smFISH at the time point of interest, cells were washed once in RNase free PBS (Ambion #AM9624) and fixed in 3.7% Formaldehyde (Sigma-Aldrich #F8775) for 10 min at RT. Cells were washed twice with PBS and permeabilized in 70% Ethanol overnight. The following evening cells were washed once in Wash buffer (10% Formamide (Ambion #AM9342) in 2x SSC (Sigma-Aldrich #S6639)). Incubation with the probes diluted 100x in Wash buffer containing 1% Dextran Sulfate (Sigma-Aldrich #D8906) occurred overnight in a cell culture incubator at 37 °C. The following day, after two washes of 30 min with 2x SSC at 37 °C and DAPI staining, cells were covered with Vectashield Antifade Mounting Medium (Vector Laboratories #H-1000). Image acquisition was for performed as soon as possible on a Zeiss Cell Observer wide-field inverted microscope using a 63x Plan-Apochromat Oil objective (NA=1.4). Digital images were acquired by a cooled Axiocam 506m camera upon excitation with a Zeiss HXP 120 metal halide light source using 1000ms exposure time.

For total mRNA staining, FITC labeled polyT(25) LNA oligos (Exiqon #300510) were used as in the same smFISH protocol. Final probe concentration was 5nmol from a 25µM stock. Imaging was performed on Zeiss Cell Observer Spinning disk inverted microscope equipped with a Yokogawa CSU-x1 confocal scanner. Digital images were acquired by an Evolve 512 EMCCD through a 40x or 63x Plan-Apochromat Oil objective (NA=1.4). Imaging of acta1 detected by smFISH was equally performed in the spinning disk.

3.10 SYTO14 live imaging

For SYTO14 RNA staining, 5µM of reagent was added to cells for 30 minutes followed by one medium wash and imaged consecutively (Thermo-Fisher #S7576). Spinning disk microscopy was performed on a Zeiss Cell Observer inverted microscope equipped with a Yokogawa CSU-x1 confocal scanner, a 37ºC 5% CO_2 chamber and automated stage for live-cell image acquisition. Digital images were acquired by an Evolve 512 EMCCD through a 40x or 63x Plan-Apochromat Oil objective (NA=1.4).

3.11 Nuclear movement imaging

For nuclear movement quantification, wide-field live-cell image acquisition was performed on a Zeiss Cell Observer inverted microscope equipped with a 37ºC 5% CO_2 chamber and automated stage using a 40x or 63x Plan-Apochromat Oil objective (NA=1.4). Cells were imaged with transmitted light overnight every 15 minutes at day 3 and 6 of differentiation. Digital images were acquired by sCMOS camera Hamamatsu ORCA-flash4.0 V2. Nuclear velocity and displacement were measured using the MtrackJ plugin in Fiji.

3.12 Light-induced contraction

Contraction was induced in cells transfected with hChR2-EYFP at differentiation day6. For stimulation close and away from nucleus, the fluorescence shutter was closed to minimum size (D=35µm) and the target area was positioned at the corresponding center of the field of view using transmitted light. Wide-field live-cell image acquisition was performed on a Zeiss Cell Observer inverted microscope equipped with a 37ºC 5% CO_2 chamber and automated stage using a 63x Plan-Apochromat Oil objective (NA=1.4). Digital images were acquired by sCMOS camera Hamamatsu ORCA-flash4.0 V2 for 10ms/frame streaming acquisition upon excitation with Colibri2 (Zeiss) LED light source. Immediately after starting the streaming, the fluorescence shutter was open to capture the initial cell response that otherwise is omitted by the camera acquisition delay. Per cell area 100 frames were acquired corresponding to 1 second of streaming.

3.13 Image analysis and quantification

Except for day 3 cells or stated otherwise, all quantified cells displayed maturation characteristics by transmitted light (peripheral nuclei and striations). Image processing was performed on Fiji except when specified. Intensity color map was obtained by applying the “royal” lookup table (LUT). Depth color-coding was applied by converting Z-slices into T-frames and using the temporal-color code plugin. All scale bars correspond to 10μm.

For mRNA distribution analysis, each image was cropped and rotated in order to have two nuclei at the edges and the myofiber portion in between parallel to the X axis. For smFISH images a maximum intensity projection (MIP) was applied and a MATLAB script was developed for background reduction, nuclei and mRNA spot detection and distance calculation to the nearest nucleus (see Appendix 6.2). The counts in each 5 μm bin were normalized to total counts in order to compare different cells and mRNA species. For total mRNA and acta1 mRNA a sum projection was applied and intensity was measured by doing a rectangular intensity profile from one nucleus to the center (Metamorph).

An mRNA clustering index (MCI) was developed in order to compare numerically the distribution of different species of mRNA. For this purpose, the mRNA intensity or count in the 5μm closest to the nucleus (nucleus not included) was divided by the corresponding 5μm value at the fiber center (in between two nuclei). All quantified myofiber fragments had a nuclear distance in the 80-148μm range in order to avoid outliers (see Figure 14A).

Since the puromycilation images contain heterogeneous puncta, intensity was measured doing a rectangular intensity profile (on Metamorph software) after applying a MIP. This profile was set to sum all the intensities in Y for each X in the rectangle drawn from one nucleus to the other.

3.14 Statistics

Statistical tests were performed using GraphPad Prism and are further described in figure legends. Statistical significance is represented as follows: **** $p<0.0001$; *** $p<0.001$; ** $p<0.01$, *$p<0.05$; n.s. not statistically significant. Unpaired and

paired student’s t-tests were 2 tailed. All experiments were performed with at least 3 biological replicates. For each set of results, n represents the number of cells. For mRNA distribution histograms, a one-way analysis of covariance (ANOVA) was performed and the significance of each column was compared to the first value (closest to nuclei) by applying a Bonferroni test. The p value in the graph represents the minimum significance common to all points contained in the grey area.

3.15 Protein size and GO term analysis

Biomart was used for transcriptome wide mRNA size analysis (http://www.ensembl.org/biomart/). The human transcriptome was utilized since it is generally believed to be best annotated. The CDS was used as a proxy for transcript size, given the high variability of UTR lengths in different isoforms as well as potential for the lack of annotation. Protein mass was estimated using the formula MW (in KD) = (CDS length (bp) / 3) x 110 x 1000. GO term enrichment analysis was performed for the top 10 longest CDS compared to all CDSs, using DAVID (https://david.ncifcrf.gov/ (Huang et al., 2009a, 2009b).

4 Results

4.1 Nuclear positioning in myofibers differentiated *in vitro*

In order to better understand mRNA localization in skeletal muscle, we took advantage of an *in vitro* system capable of differentiating mouse myofibers with mature muscle qualities – shape, myofibril alignment, peripheral nuclei, and triads (Falcone et al., 2014). In addition to the imaging and genetic manipulation advantages, the developmental perspective provides a dynamic insight that might lead to a better understanding of mRNA biology in these cells (Pimentel et al., 2017).

To ensure that nuclear anchoring – the last step of nuclear positioning *in vivo* – was recapitulated *in vitro*, we time-lapse imaged immature and mature cells (differentiated for 3 and 6 days respectively, Figure 14C). Nuclear anchoring has particular relevance given that longitudinal nuclear movement would greatly impact mRNA distribution. Although some peripheral nuclei still displayed residual longitudinal movements, overall the nuclear motility was reduced by 6-fold in matured cells (Figure 14B).

Importantly, nuclear spacing was normally distributed with 50% of the nuclei separated by 80 to 148 μm (Figure 14A). This variation could be attributed to non-anchored nuclei or possibly to the lack of a defined NMJ in the system. Considering a mean nuclear distancing of 102.9 μm in these cells, this is 3 times bigger than the reported for EDL and Soleus muscles (Bruusgaard et al., 2003). In contrast, given the *in vitro* myofiber average cross sectional area of 97.1 μm^2 ± 0.16 SD, the number of nuclei per surface area and volume is about 2 times smaller than *in vivo* (Bruusgaard et al., 2006). Thus, given the small diameter of *in vitro* differentiated myofibers there is a bigger spatial resolution between nuclei which could be beneficial to map mRNA localization.

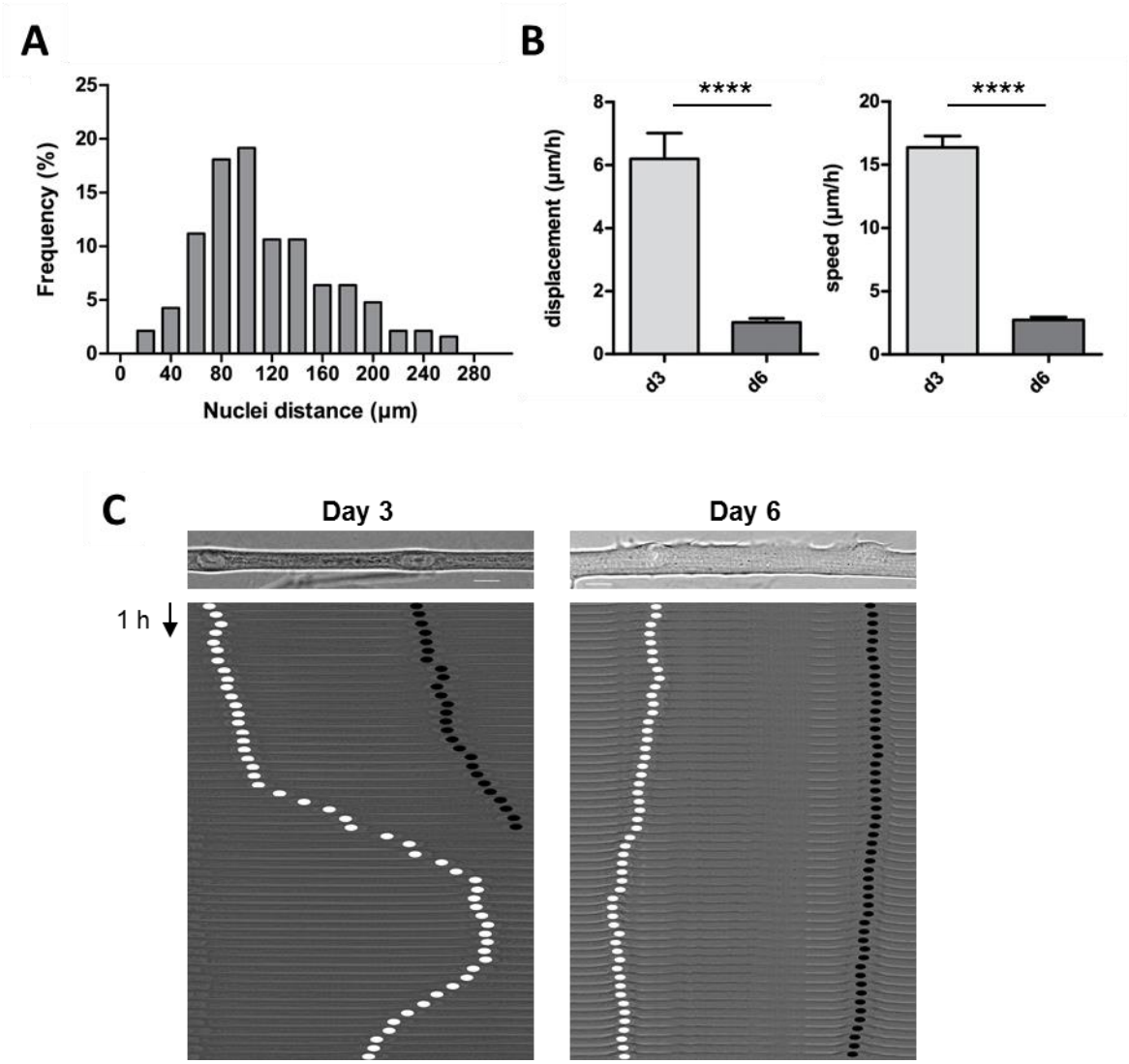

Figure 14 – Nuclear movement and positioning are recapitulated *in vitro*.

A) Nuclear distance has a median of 102.9 µm with Q_1=80.0 and Q_3=147.95 in myofibers differentiated for 6 days *in vitro* (n=188). B) Both nuclear speed and displacement have a 6-fold reduction with myofiber maturation, due to nucleus anchoring (day3 n=42; day6 n=47). C) Kymograph exemplifying the nuclear dynamics of day 3 (left) and 6 (right) over the course of 13 hours. White and black dot mark left and right nucleus respectively. Scale bar is 10 µm.

4.2 Perinuclear mRNA localization in mature myofibers

Having confirmed that nuclei stopped longitudinal movements, we looked at the overall mRNA distribution in these myofibers. For this purpose we started by performing a Fluorescence in situ hybridization (FISH) using polyT(25) LNA probes. Total mRNA concentration was highest in the nucleus and in its surrounding region (Figure 15A). The perinuclear region had on average twice more polyA mRNA than the central portion of the myofiber (Figure 15C). We deployed an index – mRNA clustering index (MCI) – in order to be able to compare perinuclear enrichment levels across different experiments (Figure 15A, see figure legend). This total mRNA localization pattern was further confirmed by staining live cells with SYTO14 (Figure 15B). Enrichment under the sarcolemma was observed in some cells but not all, being most times asymmetric (e.g. in Figure 15B). Altogether, these results are in accordance with previous *in vivo* reports (Nevalainen et al., 2013; Ralston et al., 1997).

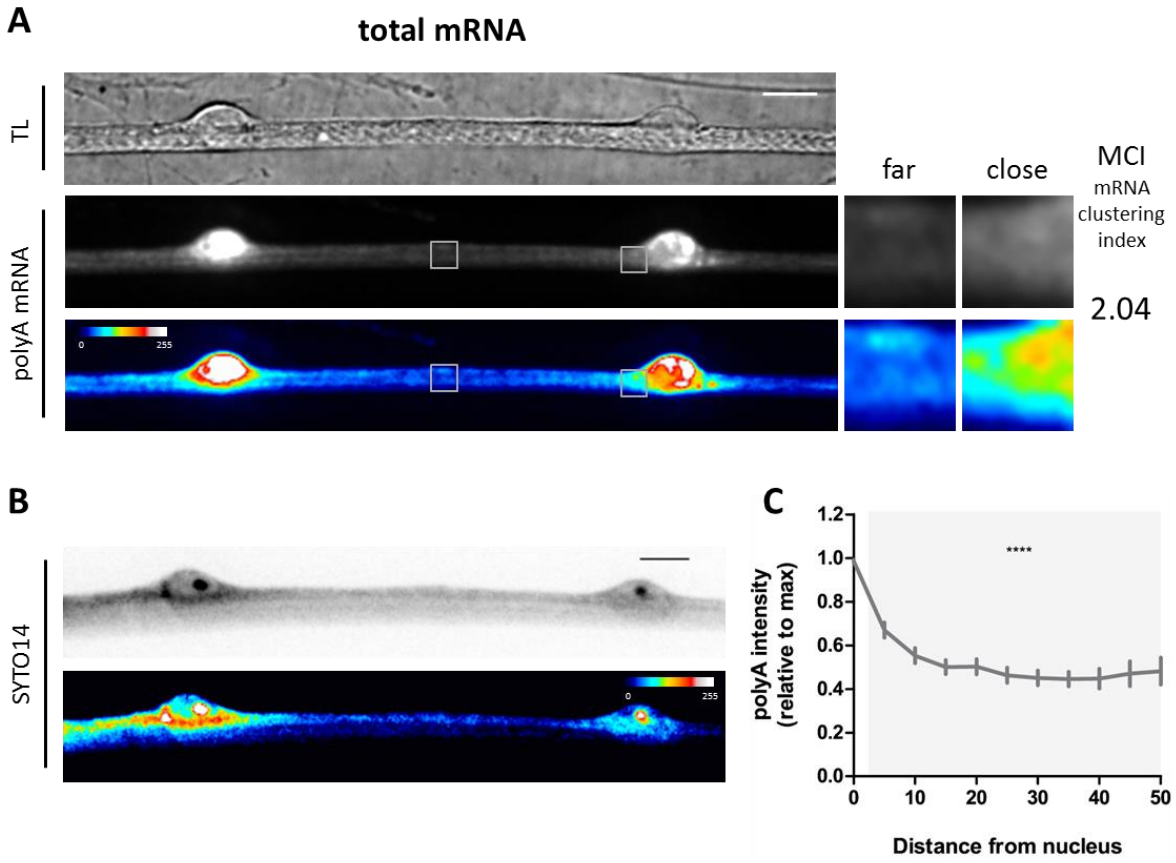

Figure 15 – Total mRNA is enriched perinuclearly.

A) PolyA mRNA detected by FISH using polyT(25) LNA FITC-oligos. Fluorescence signal is shown as a SUM projection of a confocal Z-stack (middle panel) and also as an Intensity color coded image of the SUM (bottom panel). Close and far insets correspond to the 5 µm sections closest and farthest to the right nucleus in the image. B) Total RNA stained in live cells with SYTO14. Fluorescence signal is shown as a SUM projection of a confocal Z-stack (top panel) and also as an Intensity color coded image of the SUM (bottom panel). C) Quantification of polyA signal from nucleus edge (0) to cell center normalized to background intensity. P-value corresponds to the points in the gray area of the graph relative to the first bin of 5 µm (closest to nucleus) in ANOVA (n=24). Bars indicate SEM. Scale bar is 10 µm.

We next sought to understand which mRNAs were contributing to this total mRNA perinuclear clustering. This distribution could reflect the localization of few but abundantly expressed mRNA species or it could be a general phenomenon. We used single molecule FISH (smFISH) to detect mRNAs important for muscle structure and function. The high resolution and specificity of this technique make it the gold standard to observe the subcellular localization of mRNAs (Gaspar and Ephrussi, 2015; Raj et al., 2008).

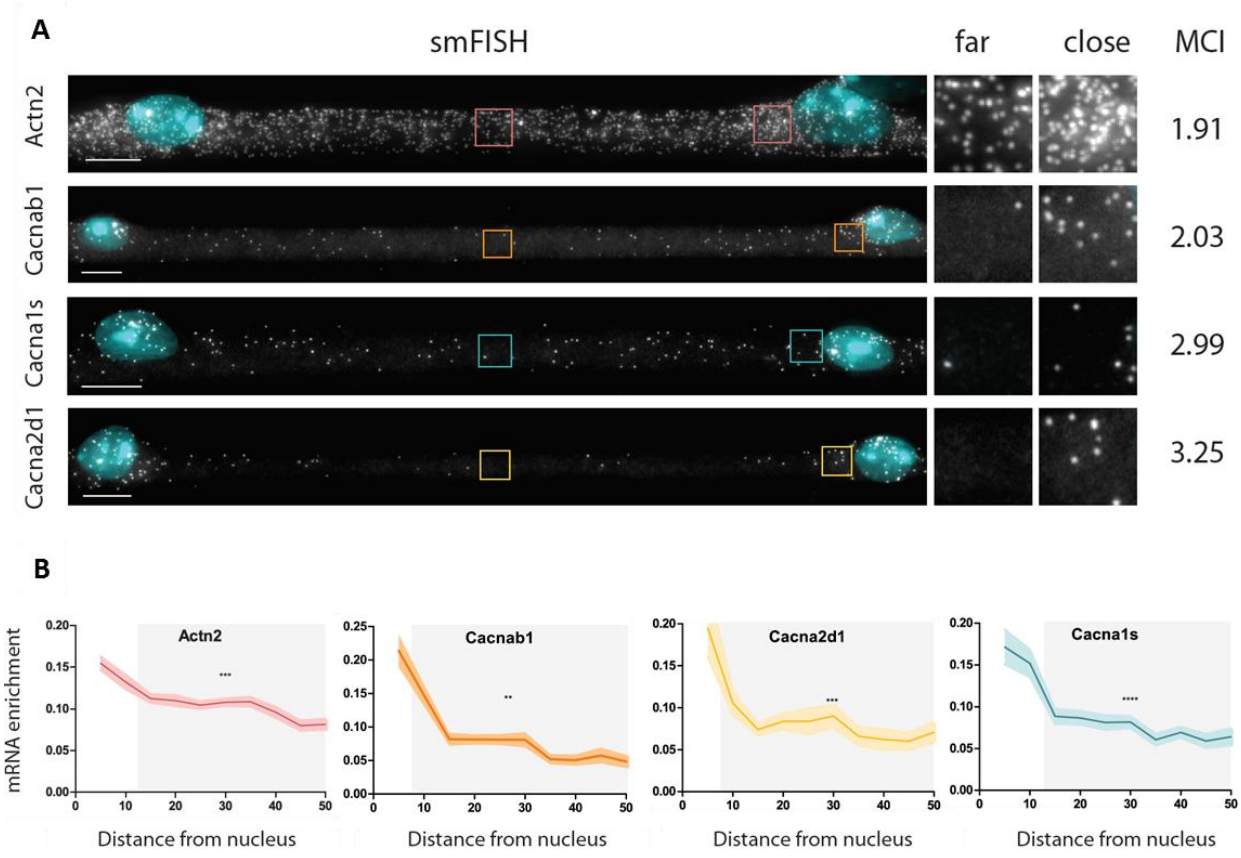

Figure 16 – Individual mRNAs detected by smFISH are enriched perinuclearly

A) smFISH of mRNAs important for muscle structure and function. Fluorescence signal is shown in grey as a MIP of a widefield Z-stack. Close and far insets correspond to the 5 µm sections closest and farthest to the right nucleus in the image. DAPI is shown in blue. MCI: mRNA count index. B) Quantification of mRNA distribution from nucleus edge (0) to cell center normalized to total counts. n=20, 34, 12 and 34 respectively. P-value corresponds to the points in the gray area of the graph relative to the first bin of 5 µm (closest to nucleus) in ANOVA. Colored shade indicates SEM. Scale bar 10 µm.

Similarly to the total mRNA, individual mRNAs also displayed a concentration gradient with its highest at the perinuclear region and lowest at the regions in between nuclei (Figure 16). The muscle specific mRNAs (e.g. Actn2) were only detected in myofibers and not in the fibroblasts present in the culture, demonstrating probe specificity. Some mRNAs were expressed in levels that hindered accurate single molecule quantification (e.g. actin alpha1), but the intensity of signal also followed the general trend (Figure 17). Given the elevated expression levels, confocal spinning disk imaging was used for quantification. Overall, the mRNAs analyzed had a MCI similar to the one obtained from the polyA results.

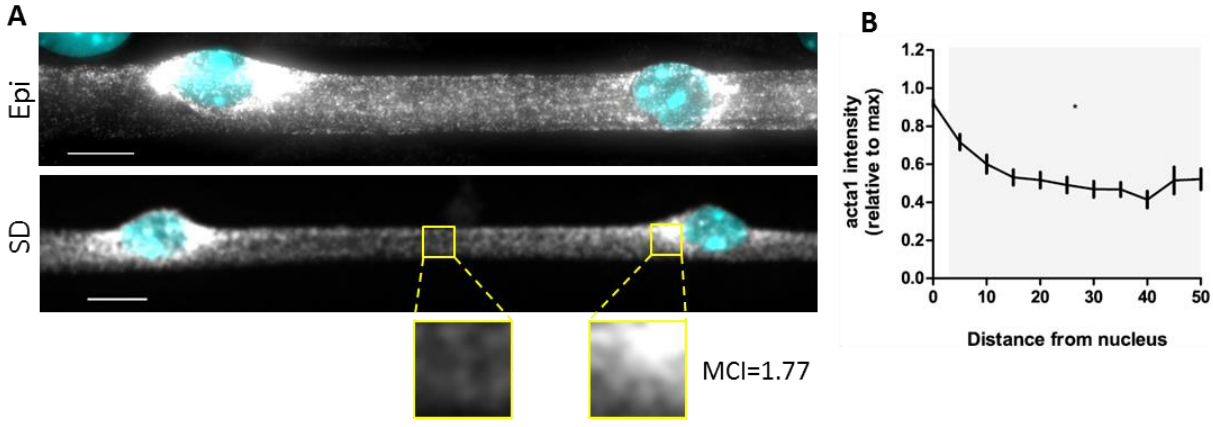

Figure 17 – Acta1 is a highly expressed mRNA clustered around the nucleus

A) smFISH of actin alpha1 mRNA (grey). Top panel: MIP of high magnification (100x) epifluorescence stack. Bottom panel: SUM of spinning disk confocal stack (63x). B) Quantification of mRNA distribution from nucleus edge (0) to cell center normalized to total counts. P-value corresponds to the points in the gray area of the graph relative to the first bin of 5 µm (closest to nucleus) in ANOVA. n=14. Bars indicate SEM. Scale bar 10 µm.

Although it seems reasonable to hypothesize, we wanted to confirm that gradients were created by mRNAs transcribed in the nearest nucleus. For this purpose we adapted the heterokaryon strategy used by Pavlath *et al.* in 1989. By having only one nucleus in the myofiber with a different genetic background it is possible to precisely determine the origin of its specific products. We fused C8820 human immortalized myoblasts with primary mouse myoblasts in a ratio that favored the differentiation of myofibers containing one single human nucleus. Human nuclei can be distinguished from their mouse counterpart by their homogenous DAPI staining (Ralston and Hall, 1989b). Using smFISH probes specific to human and mouse transcripts we could detect an mRNA gradient that was highest closer to the nucleus of origin (Figure 18).

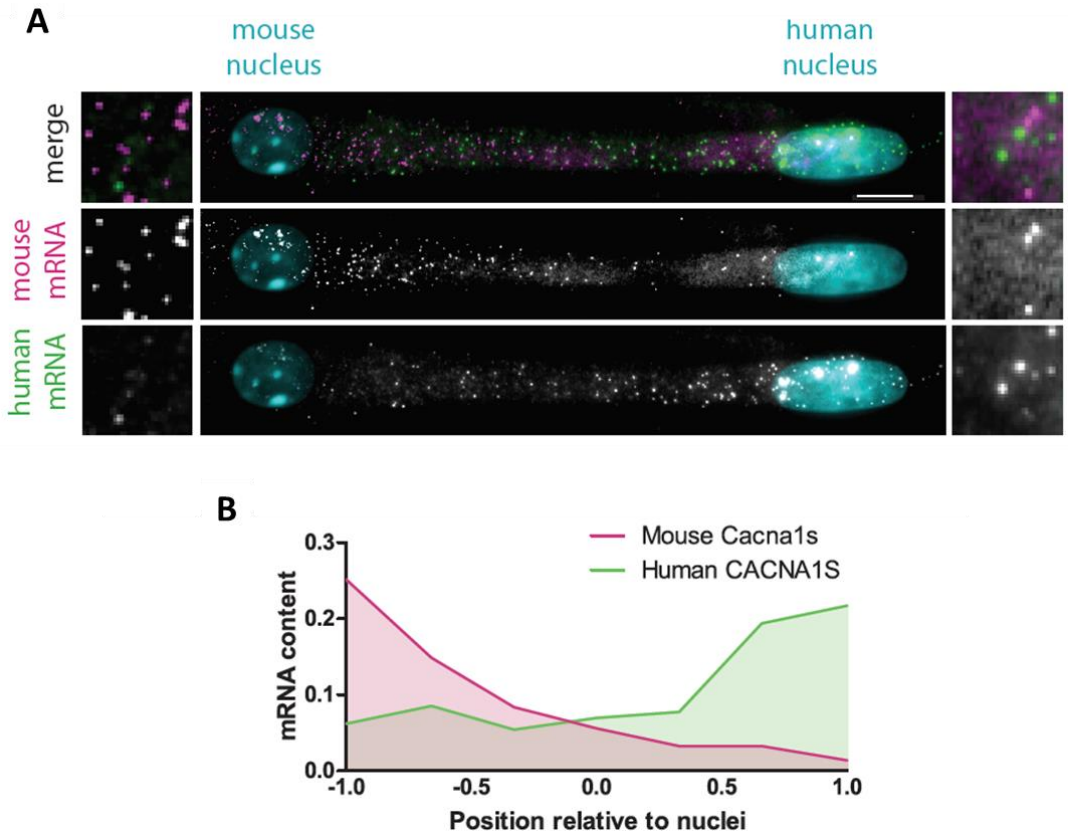

Figure 18 – Nuclear enrichment and origin of mRNAs in a heterokaryon

A) smFISH of mouse (green) and human (magenta) Cacna1s mRNAs in a myofiber containing one single human nucleus. Fluorescence signal is shown as a MIP of a widefield Z-stack. Left and right insets correspond to the 5 µm sections closest to the mouse and human nucleus in the image. DAPI is shown in blue, scale bar 10 µm. B) Quantification of mRNA distribution from the mouse nucleus (-1) to the human nucleus (1) normalized to total counts.

Subsarcolemmal mRNA accumulation was not evident in MIP images for most mRNAs, compared to what has been reported previously (Nevalainen et al., 2013; Nissinen et al., 2005). However, an asymmetric mRNA distribution in the transversal axis towards the side where both nuclei were located was sometimes observed for abundant transcripts in very mature myofibers (e.g. αActinin2, Figure 16; Figure 19, top panel). Given that the same asymmetry was detected for total mRNA accumulation (usually at the sarcolemma) we analyzed the distribution of individual mRNA molecules in 3D. Subsarcolemmal mRNA enrichment became more obvious either in the orthogonal view or depth color coded images (Figure 19A).

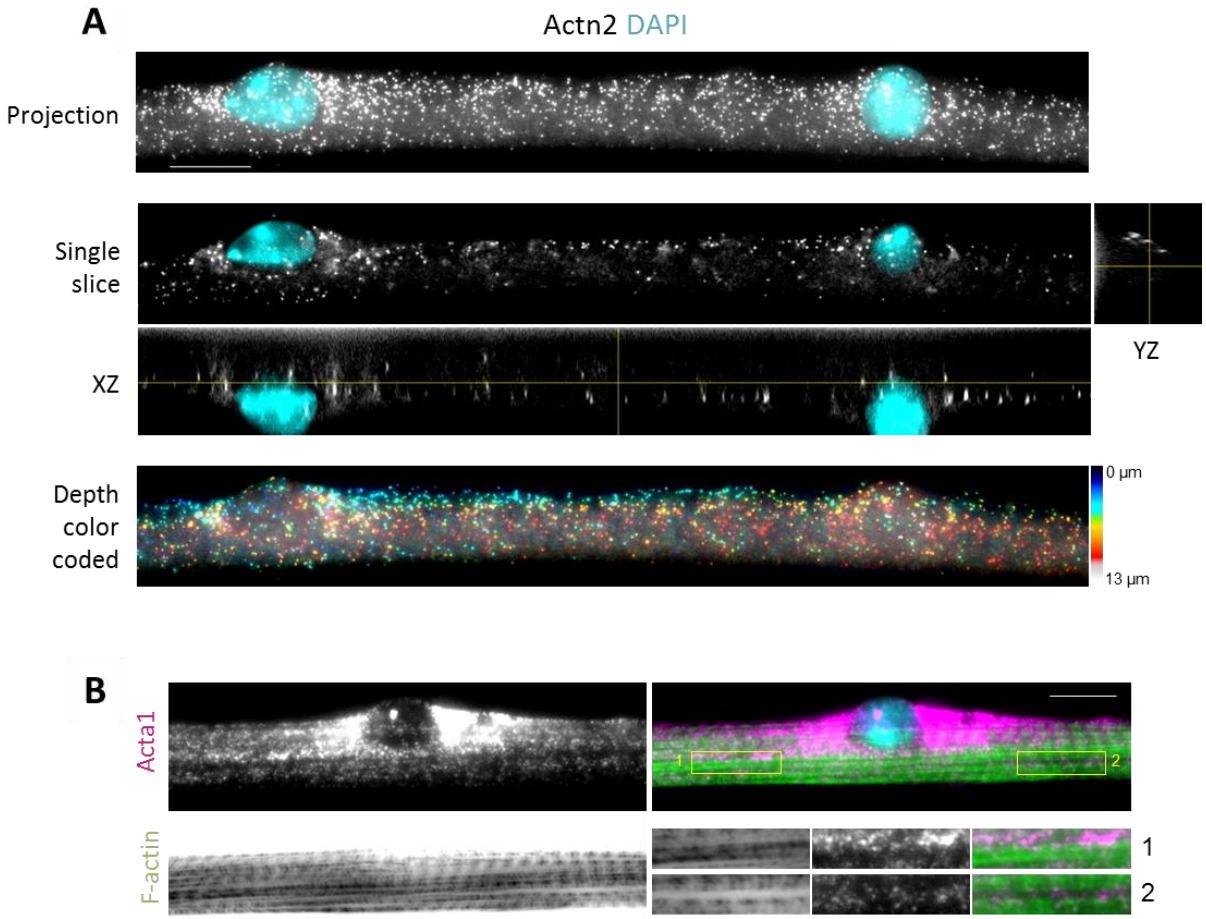

Figure 19 – mRNAs are excluded from cell center to sarcolemma by myofibrils

A) smFISH of mouse Actn2 mRNA (grey). Fluorescence signal is shown as a MIP (top panel) orthogonal view (middle panels) and depth color coded (bottom panel) originally from a widefield Z-stack. B) Representative image (single slice) of a myofiber containing Acta1 mRNAs (magenta) accumulated in myofibrillar gaps (green). Location of insets 1 and 2 is shown in the image composite. Scale bar 10 µm.

Since mRNA concentration at the membrane was only observed in some cells, we wondered if it could be related to different levels of myofiber maturity. By staining the actin filaments we could observe an accumulation of mRNAs at myofibril gaps (Figure 19B). These data suggest that once myofibrils are crosslinked and the space between them disappears, mRNAs are pushed towards the cell periphery due to physical constrains.

In order to understand if this localization pattern was specific to muscle transcripts, we looked at a housekeeping mRNAs. The mRNA encoding for Gapdh was not only equally enriched at the sarcolemma but also perinuclearly (Figure 20). Thus, accumulation at the perinuclear and subsarcolemmal regions seems to be the default distribution of mRNA in skeletal muscle.

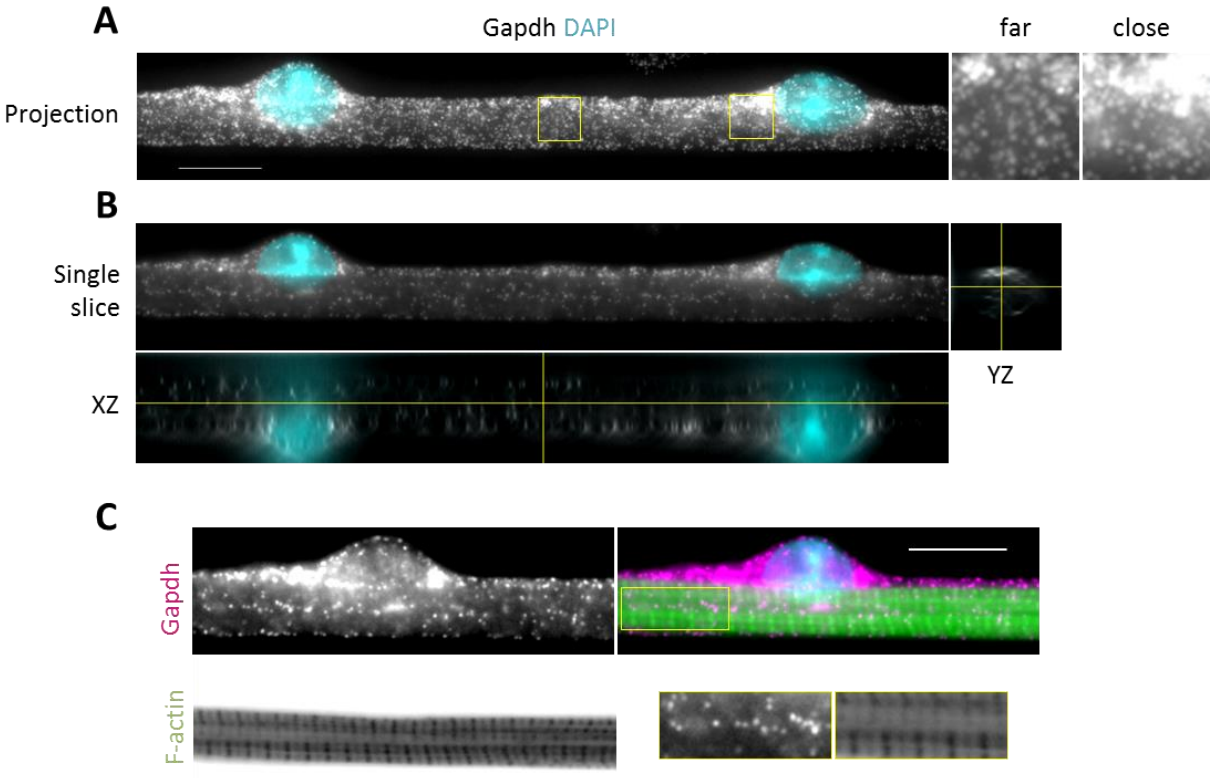

Figure 20 – Non-muscle mRNAs also accumulate perinuclearly by default

A) smFISH of mouse Gapdh mRNA (grey). Fluorescence signal is shown a MIP of a widefield Z-stack. Close and far insets correspond to the 5 µm sections closest and farthest to the right nucleus in the image. B) Fluorescence signal is shown as orthogonal view and depth color coded (bottom panel) originally from a widefield Z-stack. C) Representative image (single slice) of a myofiber containing Gapdh mRNAs (magenta) accumulated in myofibrillar gaps (green). Location of inset is shown in the image composite. DAPI is shown in blue, scale bar 10 µm.

4.3 Giant muscle mRNAs have a particular distribution

While checking which mRNAs followed the localization of polyA transcripts, we questioned if the observed localization patterns would be related to the mRNA properties and functions. Thus, we chose mRNA candidates encoding for both membrane and soluble proteins with structural and triad functions, as well as differently expressed transcripts (Table 6). Curiously, the biggest protein encoded in the human genome – Titin – is 4000 kD and is expressed specifically in muscle (www.proteinatlas.org). In fact, three out the five biggest proteins are muscle enriched (Table 7, see GO term analysis in Appendix 6.3) and the location of their respective mRNAs in myofibers has not been addressed to date.

Surprisingly, “giant” mRNAs detected by smFISH did not accumulate near the nucleus in contrast to normal transcripts and total mRNA (Figure 21A, B). Their homogenous distribution is reflected in the respective MCIs, which are significantly different from average mRNAs (Figure 21C). These results suggest that a different mechanism is responsible localization of these two types of muscle mRNAs.

Table 6 – Characteristics of mRNAs studied by smFISH

Different skeletal muscle specific mRNAs were chosen in order to cover the following criteria: encoding membrane and soluble proteins; encoding proteins important for muscle structure and triads; transcripts that are highly and lowly expressed; “giant” mRNAs and normal sized mRNAs (thick line separates the two).

Protein name	MCI	mRNA (bp)	Protein (kD)	Type	Function	Counts
Titin	1.01	100.404	3.959	Cytoplasm	Sarcomere	319
Obscurin	1.05	26.778	982	Cytoplasm	Sarcomere	23
Nebulin	1.31	25.683	942	Cytoplasm	Sarcomere	235
Ryanodine receptor1	0.99	15.358	554	TM	Triad (SR)	160
Ca (V) channel α1β	2.03	7.020	257	Cytoplasm	Triad (TT)	35
Ca (V) channel α1s	2.93	6.018	206	TM	Triad (TT)	52
Ca (V) channel α2δ1	3.25	3.276	120	TM	Triad (TT)	51
α-Actinin 2	1.91	3.013	98	Cytoplasm	Sarcomere	325

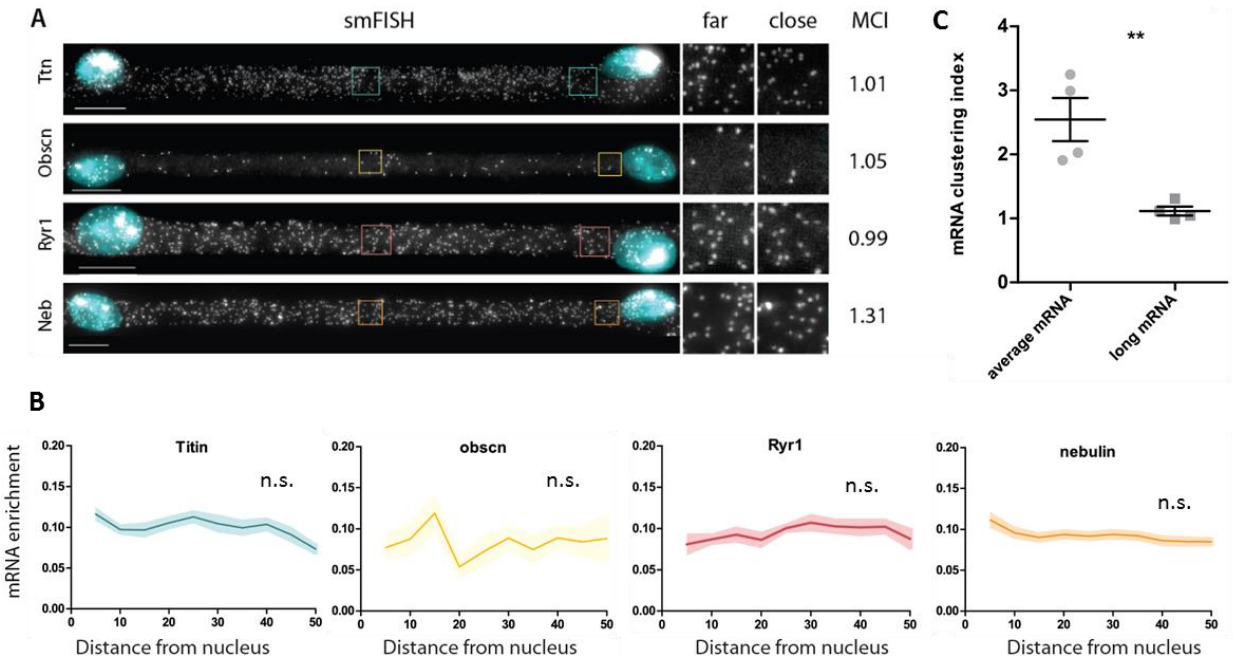

Figure 21 – Giant mRNAs are spread and do not accumulate perinuclearly

A) smFISH of giant muscle enriched mRNAs. Fluorescence signal is shown in grey as a MIP of a widefield Z-stack. Close and far insets correspond to the 5 µm sections closest and farthest to the right nucleus in the image. MCI: mRNA count index. DAPI is shown in blue, scale bar 10 µm. B) Quantification of mRNA distribution from nucleus (0) to cell center normalized to total counts. n=14, 14, 26 and 18. P-value is non-significant and relative to the first bin of 5 µm in ANOVA. Shade indicates SEM. C) MCI of long and average size mRNAs is significantly different in a t-test.

Table 7 – Top 10 biggest proteins are muscle enriched

mRNAs encoded in the human genome ranked by CDS and estimated protein size. Muscle enriched gene products are highlighted in bold. GO term analysis of this set in Appendix 6.3.

Gene symbol	Description	CDS Length (bp)	Protein (kD)	Transcript ID
TTN	**Titin**	**107976**	**3959**	**ENST00000589042**
MUC16	Mucin 16	43524	1596	ENST00000397910
OBSCN	**Obscurin**	**26778**	**982**	**ENST00000366707**
SYNE1	Nesprin1	26394	968	ENST00000367255
NEB	**Nebulin**	**25683**	**942**	**ENST00000618972**
MACF1	microtubule-actin crosslinking factor 1	22779	835	ENST00000567887
DST	Dystonin	22386	821	ENST00000361203
CCDC168	coiled-coil domain containing 168	21246	779	ENST00000322527
FSIP2	fibrous sheath interacting protein 2	20991	770	ENST00000343098
SYNE2	Nesprin2	20724	760	ENST00000358025

In order to confirm that this differential mRNA distribution is also happening *in vivo*, we isolated whole muscles and stained longitudinal cryosections for giant and normal mRNAs (Figure 22). In agreement, mRNA enrichment in the areas surrounding nuclei was observed for normal transcripts but not for giant ones. Overall, these results point to the existence of an active mRNA localization mechanism for at least one of these two mRNA types.

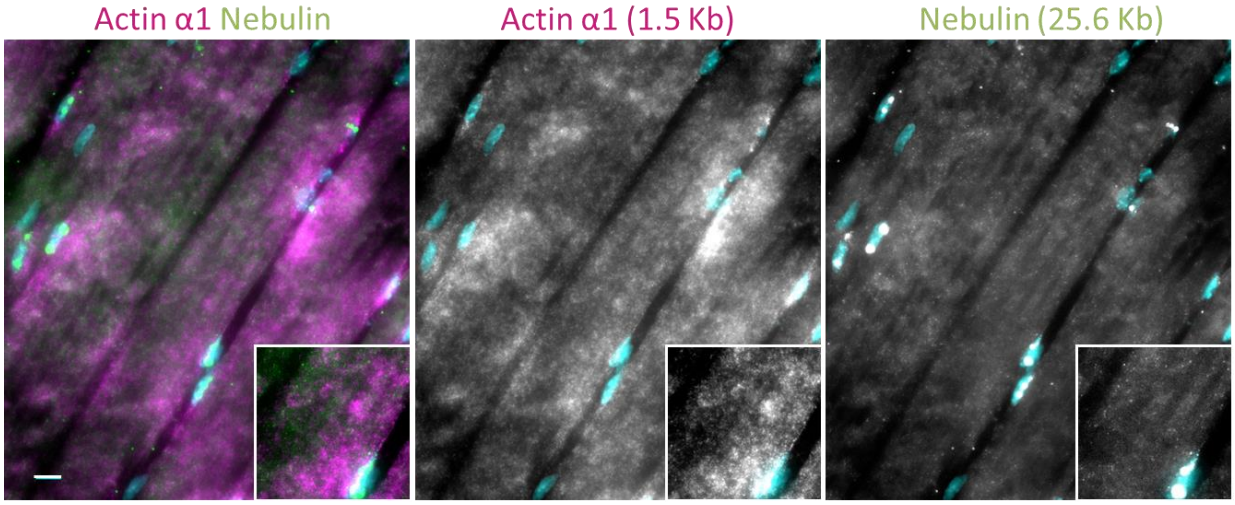

Figure 22 – Differential mRNA distribution is also observed *in vivo*

smFISH of Actinα1 (magenta and middle panel) and Nebulin (green and right panel) mRNAs in muscle cryosection. Fluorescence signal shows a MIP of a small widefield Z-stack. Inset is a zoom in. Actinα1 mRNA is increased in areas surrounding myonuclei, distinguishable by the high intensity of Nebulin signal. Nuclei are stained with DAPI (blue). Scale bar 10 µm.

4.4 mRNA localization is cytoskeleton dependent

In order to understand how these two sets of mRNAs were localized, we inhibited microtubule and actin polymerization with colchicine and latrunculin A respectively (Figure 23). Although latrunculin A did not have an effect, colchicine treatment led to increased mRNA clustering in the perinuclear region. Moreover, the homogenous distribution of giant mRNAs (e.g. Ryr1) was lost. Interestingly, this accumulation was accompanied by changes of transcript levels – Actn2 was increased whereas Ryr1 was decreased. Nevertheless, these results suggest that microtubules are likely to be involved in the localization of skeletal muscle mRNAs.

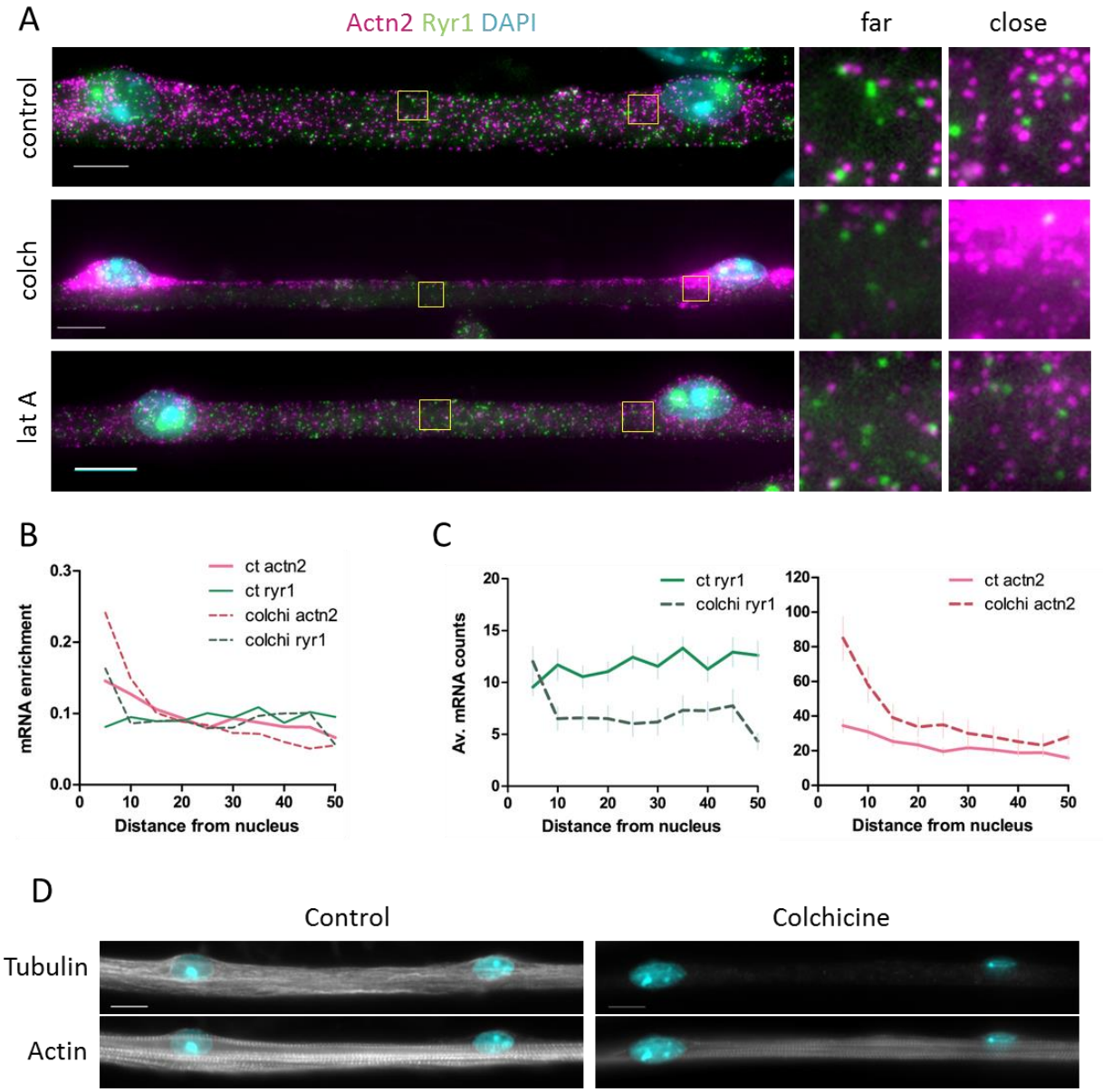

Figure 23 – mRNA localization and levels are affected by colchine treatment

A) smFISH of myofibers treated with colchicine (1ug/ml) and latrunculin A (5uM) overnight. B) Relative distribution of Actn2 (magenta) and Ryr1 (green) mRNA along the cell in control (solid) and colchicine (dashed) treated cells. Control: n=16, Colchicine n=10. C) Same distribution quantification as in B but showing absolute mRNA counts and error bars (SEM). MCI goes from 0.85 to 2.20 for Ryr1 and from 2.03 to 2.76 for Actn2. D) Microtubules are completely depolymerized when treated with colchicine (1ug/ml) overnight, but actin and myofibril (phalloidin) organization is not affected.

Assuming that both types of mRNAs are localized in a microtubule-dependent manner, different motors could potentially explain why normal and giant mRNAs are differently distributed. Given that Kinesin1 has been implicated in muscle function by still unknown causes (Metzger et al., 2012), we tested if this impact could be related with mRNA localization impairment. Nuclear positioning was completely hindered in cells depleted for Kif5b, yet mRNAs in general still accumulated close to the aggregated nuclei (Figure 24A). As a consequence, a portion of these cells (away from the nucleus) has a lower transcript density compared to myofibers with distributed nuclei. Surprisingly, giant mRNAs were still spread in the absence of this kinesin, being even enriched at the cell tips (Figure 24B). In fact, giant mRNA enrichment at myofiber tips was observed also in *wt* cells, but to a less extent (Figure 24C). Although the kif5b phenotype did not affect mRNA localization relative to the nucleus, it exacerbated the spatial difference between normal and giant transcripts.

Since in muscle the major microtubule nucleator is the nucleus, there is a plus end bias away from the nuclei and towards cell tips (Bugnard et al., 2005). In the absence of Kif5b, the growing ends of microtubules are specially polarized towards the cell tip (Figure 24E). Thus, giant mRNA in particular could potentially be transported by other kinesins given their similar directional bias. Several kinesins have been implicated in mRNA transport in other systems but to the date they have not been investigated in muscle (Hirokawa et al., 2009).

A caveat of this *in vitro* myofiber system is that liposome transfection and lentivirus transfection are limited to the day preceding differentiation. As a consequence, depletion of proteins important for development hinders phenotype observation at mature stages. This was the case for 3 out the 6 kinesins tested (Kif3c, Kif11 and Kif1b), whereas the remaining ones (Kif5a, Kif5c and Kif3a) did not affect mRNA localization (Figure 24C). We cannot exclude the possibility that Kif3c, Kif11 or Kif1b transport mRNAs in skeletal muscle and that their toxicity is a consequence of that, but it remains to be demonstrated.

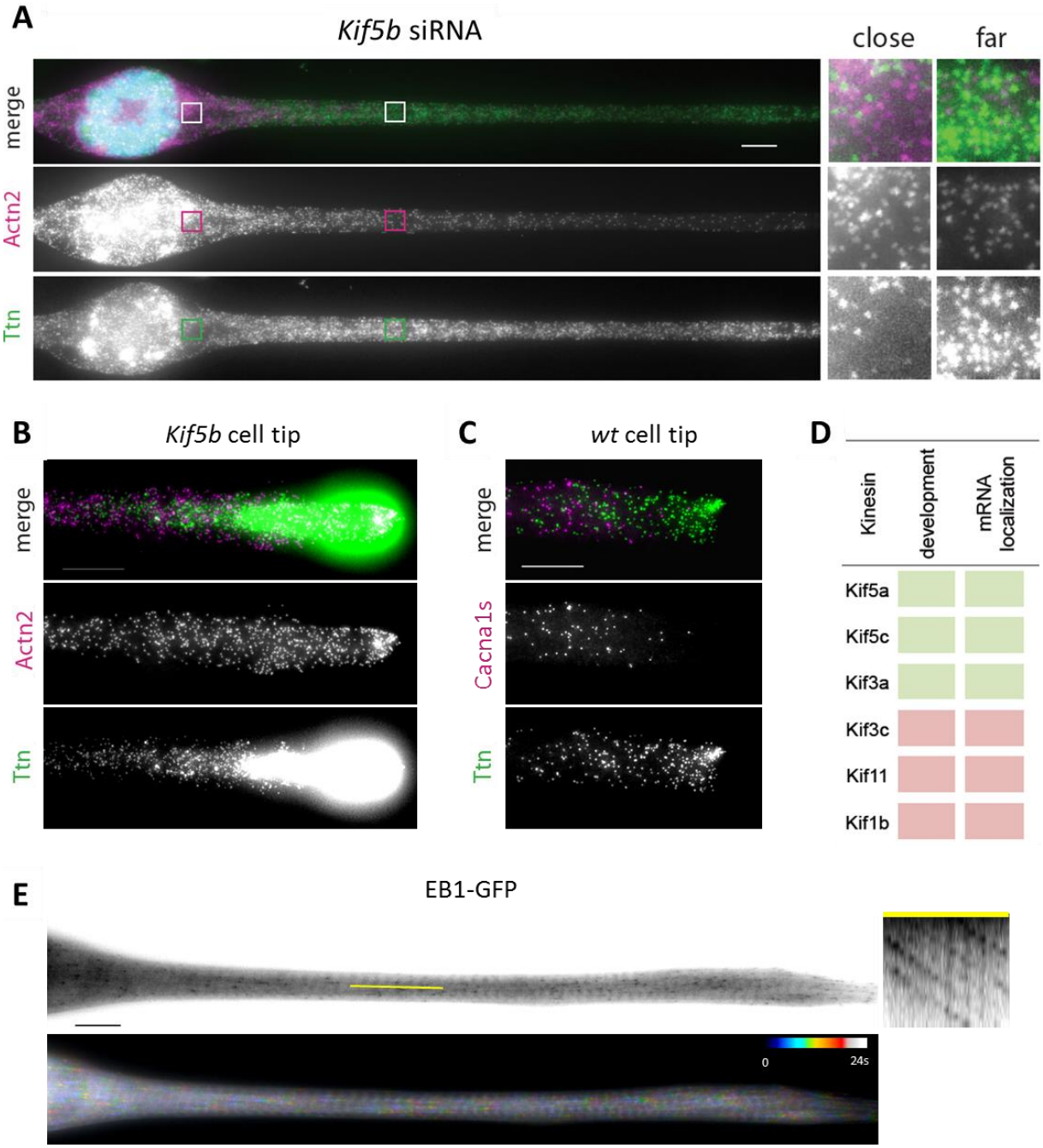

Figure 24 – Kinesin 1 (Kif5b) affects nuclear but not mRNA distribution

A) smFISH of αActinin2 (magenta) and Titin (green) mRNAs in a cell depleted for Kif5b. Close inset corresponds to the 5 µm section closest to the nuclei, far inset corresponds to the 5 µm section at a 50 µm distance from nuclei (mean distance between 2 nuclei in control cells). Fluorescence signals are shown as a MIP of a widefield Z-stack. B) Same smFISH as in A, at the tip of a cell depleted for Kif5b. C) Cell tip of a wild type cell stained for Cacna1s (magenta) and Titin (green) mRNAs. D) Impact of Kinesin depletion in muscle development and mRNA localization (green – not affected; red – affected). E) Growing microtubule (EB1-GFP) orientation is away from the nuclei in *Kif5b* depleted cells. Top: single widefield frame (inverted LUT); Left: kymograph of yellow line; Bottom: Temporal color coded time-lapse (3s/frame). Scale bar 10 µm

Given that regular-sized mRNAs were accumulated at the minus end microtubule ends in the perinuclear region, we tested if Dynein driven transport was important for their accumulation. Dync1h1 depletion severely affected myofiber development thus we took advantage of Ciliobrevin D, a highly specific inhibitor of the dynein complex ATPase activity (Firestone et al., 2012; Ye et al., 2001). After overnight inhibition of the Dynein motor, mRNA was completely dispersed compared to the control (Figure 25). Contrarily to colchicine treatment, Ciliobrevin D induced a slight decrease in the number of ACtn2 transcripts. No impact was observed on the localization or expression of giant mRNAs.

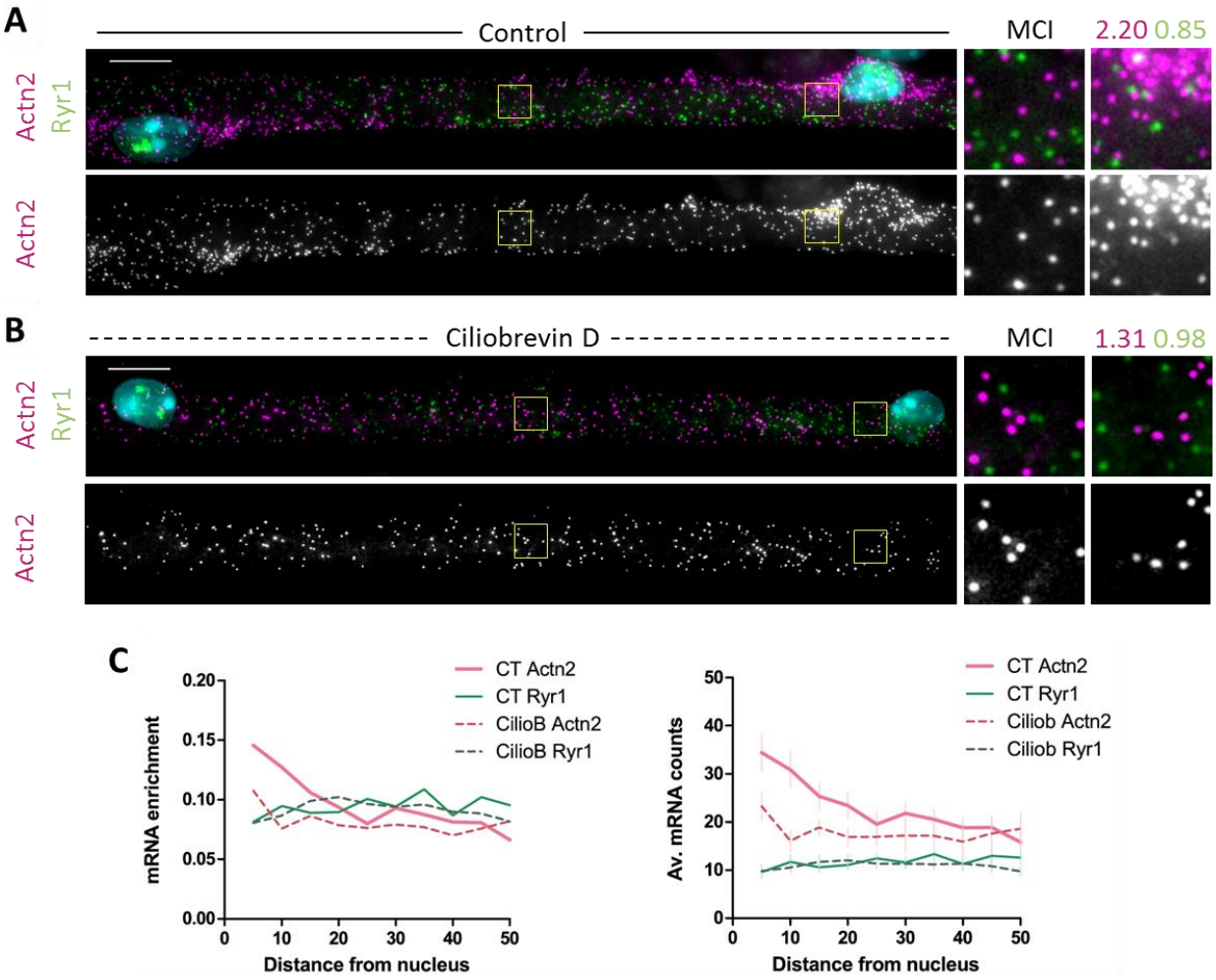

Figure 25 – Inhibition of dynein disperses perinuclear mRNA

A-B) Treatment of myofibers with 50 µM of Ciliobrevin D overnight (B) leads to dispersion of perinuclear transcripts (Actn2, magenta) compared to control (A), without affecting giant mRNAs (Ryr1, green). Fluorescence signal is shown as a MIP of a widefield Z-stack. DAPI is in blue, scale bar 10 µm. C) Quantification of relative and absolute distribution of Actn2 (magenta) and Ryr1 (green) mRNA along the cell in control (solid) and ciliobrevin (dashed) treated cells. Control: n=16, CIliobrevin D: n=14. Error bars indicate SEM.

Spreading of perinuclear mRNA could be a consequence of increased nuclear movement. To confirm that Ciliobrevin D was not inducing nuclear uncaging we performed time-lapse imaging of control and drug treated cells side by side. In fact, dynein inhibition decreased residual nuclear movements (Figure 26 A and B). Furthermore, staining of the dynein intermediate chain 2 subunit showed a slight increased concentration in the perinuclear area (Figure 26C). These data suggest that dynein might be actively anchoring normal-sized mRNAs in the perinuclear region.

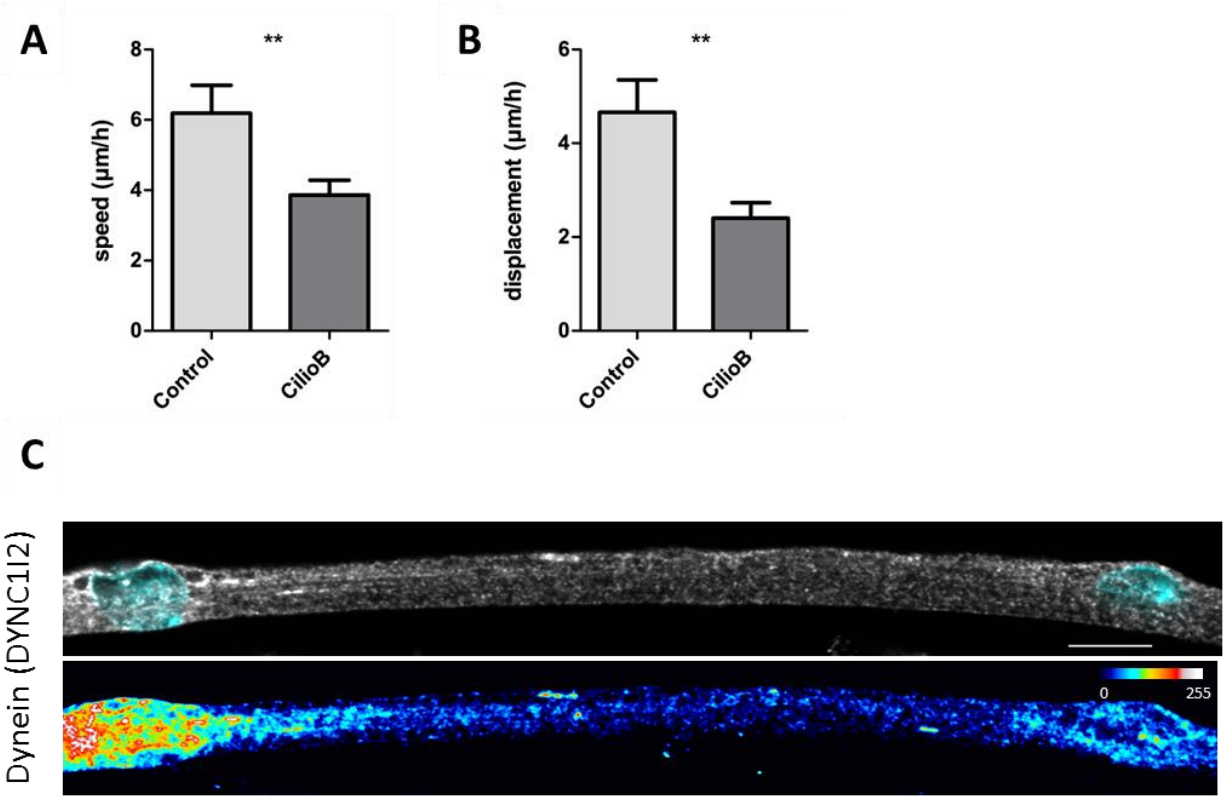

Figure 26 – Dynein is enriched perinuclearly and does not anchor the nucleus

A-B) Time-lapse imaging shows that Ciliobrevin D treatment overnight does not increase nuclear movements, measure by speed (in A) and average displacement (in B) in micrometers per hour. C) Top: Point-scan confocal slice of myofiber stained for dynein intermediate chain 2 (DYNC1I2, grey) and nuclei (blue); Bottom: Intensity color coded SUM of Z stack. Scale bar 10 µm

To further confirm the involvement of the Dynein complex in the localization of these mRNAs, we selectively targeted components of the Dynactin complex. The latter is necessary for virtually all Dynein functions, generally by augmenting its processivity (Kardon and Vale, 2009). Moreover, the Dynactin complex has been recently implicated in the localization of several mRNAs (Amrute-Nayak and Bullock, 2012; Herbert et al., 2017; Nieuwburg et al., 2017; Vendra et al., 2007). To address the involvement of Dynactin, we expressed a dominant negative of Dynactin1 (p150) and independently also depleted Dynactin2 (p50) by siRNA (Quintyne and Schroer, 2002). Only the silencing of Dctn2 decreased the degree of clustering around nucleus compared to the cell center (Figure 27). Curiously, the mRNA levels were increased in both silenced cells and in dominant negative expressing cells. Despite the absence of phenotype in cells expressing the dominant negative, the depletion results suggest that mRNAs are kept in the nuclear proximity in a Dynein-Dynactin dependent manner.

To confirm that the observed alterations in mRNA distribution were not a consequence of overall MT architectural changes, we stained triton extracted cells for alpha-tubulin (Figure 27E and F). We did not see any evident difference in microtubule organization and density, with clear membrane enrichment in both conditions. Interestingly myofibers depleted for Dctn2 were often thicker. This could possibly be a consequence of the observed gene expression alterations.

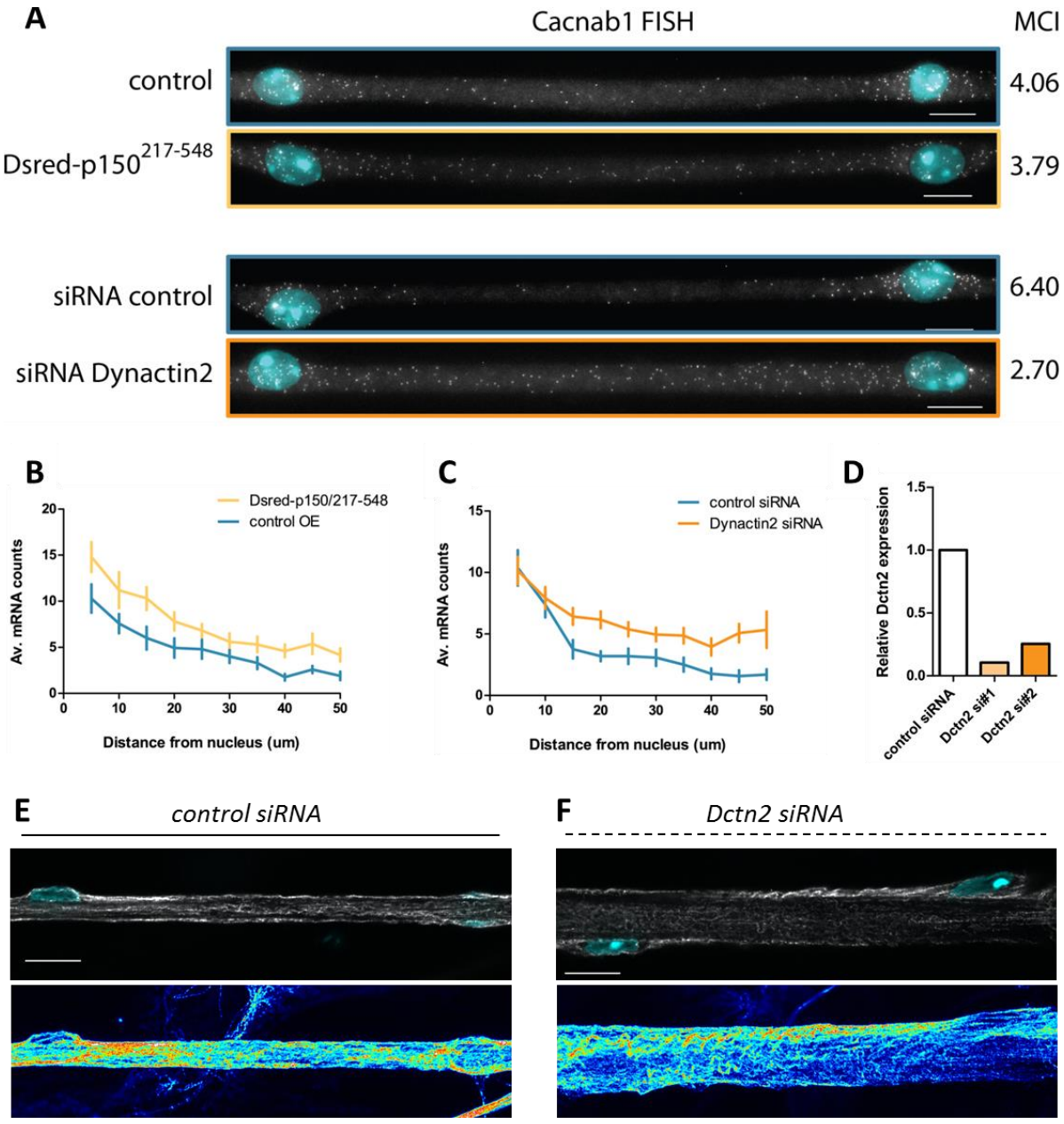

Figure 27 – Dynactin complex contributes to perinuclear mRNA accumulation

A) Top: Overexpression of a dominant negative of Dynactin1 does not affect mRNA distribution; Bottom: depletion of Dynactin2 reduces the relative enrichment of mRNA at the perinuclear region (cacnab1, gray). Fluorescence signal is shown as a MIP of a widefield Z-stack. B-C) Quantification of mRNA distribution from nucleus (0) to cell center in the conditions in (A). Bars indicate SEM. D) Relative expression of Dctn2 levels in cells transfected with *control* and *Dctn2* siRNA, detected by qPCR. EF) Alpha-tubulin staining of control and Dctn2 siRNA cells. Top panels show single confocal slice and bottom panels show intensity color coded MIP. DAPI is in blue, scale bar 10 µm.

4.5 Translation correlates with regular mRNA distribution

In order to understand the implications of mRNA localization in muscle function, we decided to investigate if translation was also localized in myofibers. Similarly to messenger RNA, ribosomal RNA was also enriched around the nucleus (Figure 28A). Of note, the 18S concentration was so high in the cytoplasm that single molecule signal could not be resolved. As expected, rRNA was also detected in the nucleoli. These results suggest that ribosome content is higher close to the nucleus. Ribosomes detected by immunostaining of P proteins were also increased at the nuclear vincinity (Figure 28B), corroborating the rRNA observations.

To test if the enrichment of ribosomes close to nuclei was not a consequence of increased cytoplasmic space, we expressed soluble eGFP (Figure 28C,E). This protein showed no perinuclear enrichment, suggesting that the localization of ribosomes is not a passive event. To check if ribosome clustering is also dependent on the Dynein-Dynactin complex, we analyzed ribosome distribution is cells depleted for Dynactin2 (Figure 28D). The localization of ribosomes was unaltered, suggesting that it is mediated by a mechanism different of mRNA localization.

To determine if translation levels were proportional to this perinuclear ribosomal enrichment, we performed a puromycilation assay (David et al., 2012). By incubating myofibers with the tRNA analogue Puromycin, this becomes incorporated in the nascent peptide chain. The addition of Cyclohexamide is also necessary to avoid chain releasing, enabling a snap shot of the translation in space for short periods of time. In comparison to the results above, translation levels were also higher at the perinuclear region (Figure 29).

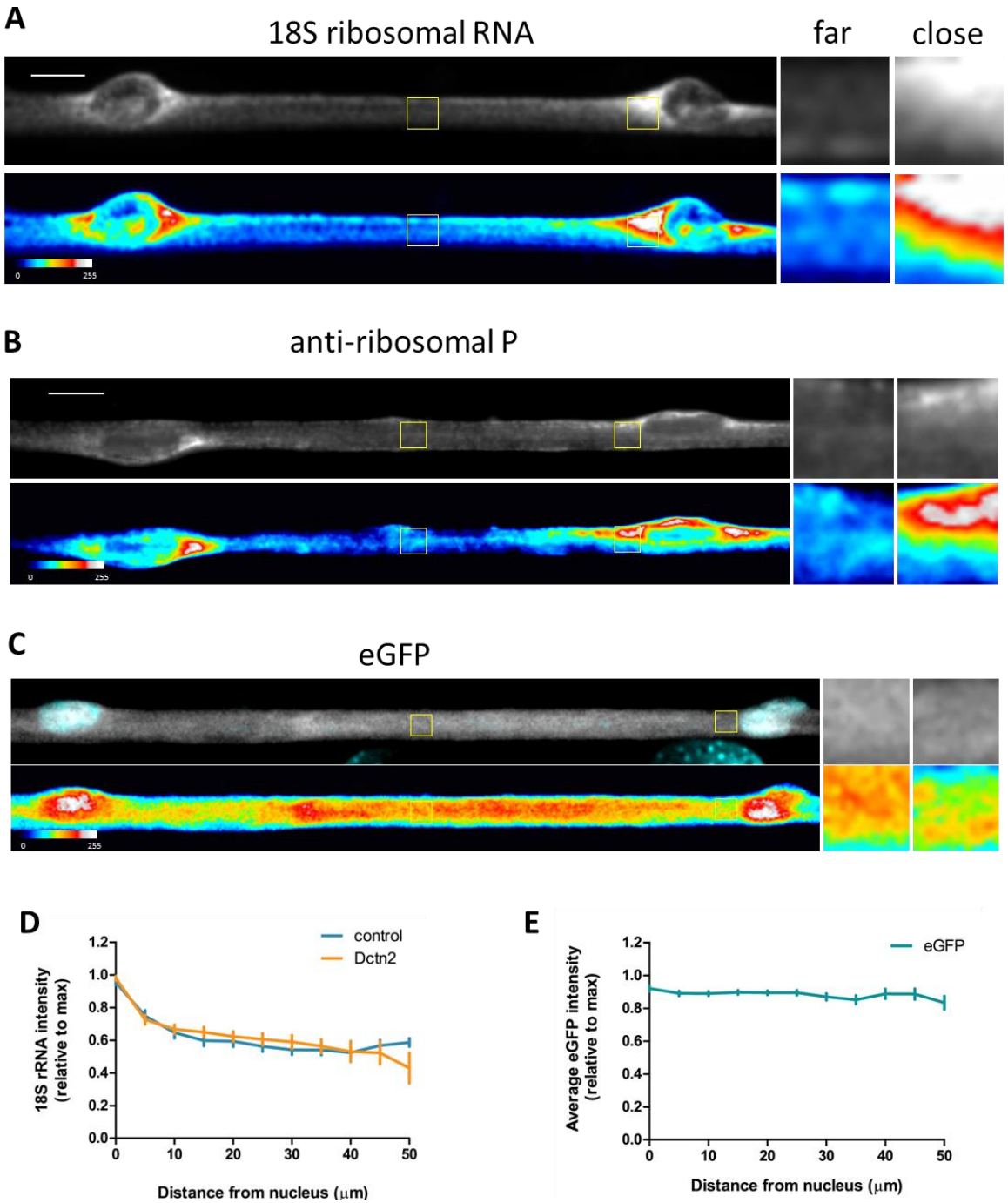

Figure 28 – Ribosome content is increased in the nuclear proximity

A) smFISH of 18S rRNA as a proxy for ribosome content. Fluorescence is shown as a SUM (top) and as Intensity color map (bottom) of a SD confocal Z-stack. B) Immunofluorescence of ribosomal P proteins. Fluorescence is shown as single slice (top) and as SUM Intensity color map (bottom) of a widefield Z-stack. C) Expression of eGFP shown as a SUM (top) and as Intensity color map (bottom) of a SD confocal Z-stack. D) Distribution of relative intensity of 18S rRNA smFISH in siRNA control and Dctn2 depleted myofibers, from the nucleus (0) to cell center (n=24 in each condition, MCI=1.68 and 1.87 respectively). E) Distribution of relative intensity of eGFP expression levels along myofibers, from the nucleus (0) to cell center (n=22, MCI=1.10). Scale bar is 10 µm.

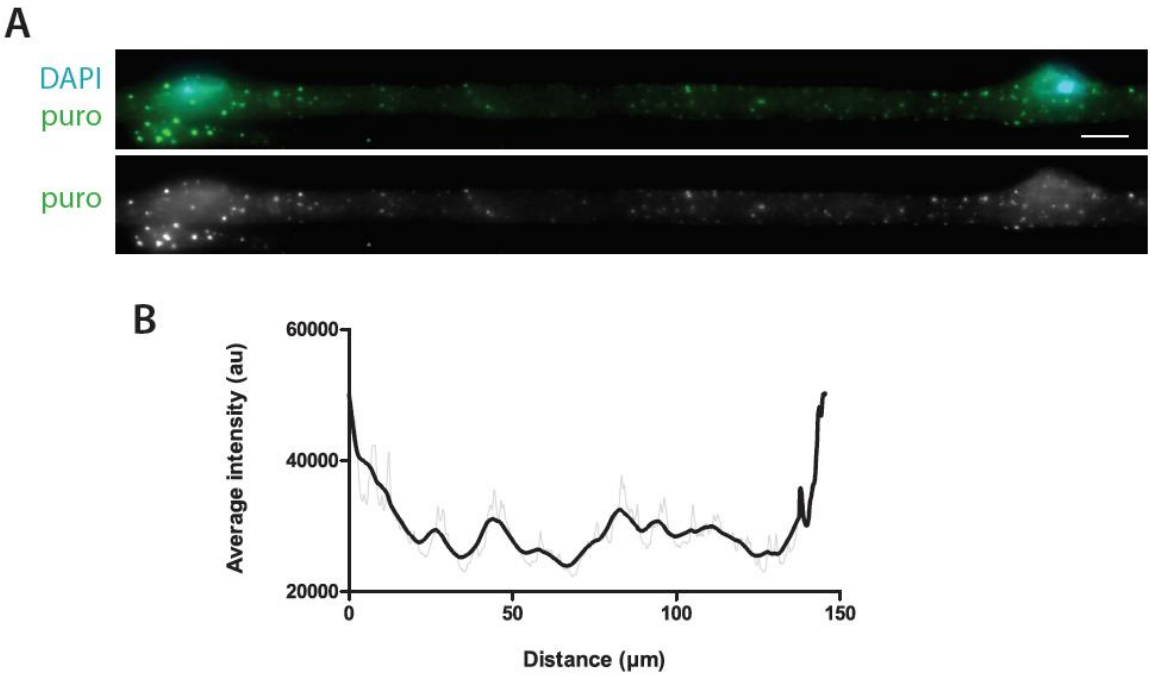

Figure 29 – Translation is increased at the perinuclear region

A) Representative image of puromycilation levels after 30 minutes of incubation. Puromycin incorporated by ribosomes is detected with an anti-puromycin antibody (green). Fluorescence signal is shown as a MIP. DAPI is shown in blue, scale bar 10 µm. B) Quantification of puromycin intensity measured on Metamorph over the X axis in between two nuclei. a.u. arbitrary units.

To further confirm if translation is localized to the perinuclear region, we investigated the localization of human proteins in heterokaryons containing a single human nucleus. Using an antibody specific for human Lamin A/C (hLamA/C) we detected protein levels at the highest in the human nucleus (Figure 30A). A very faint signal was observed in the immediately neighboring nuclei but it was completely faded beyond those. Even non-nuclear proteins were enriched close to the nucleus of origin, as observed by staining for human Spectrin α1 (Figure 3030B). Overall, these results suggest that the area surrounding skeletal muscle nuclei is a privileged site for mRNA translation and the underlying regulation of this process.

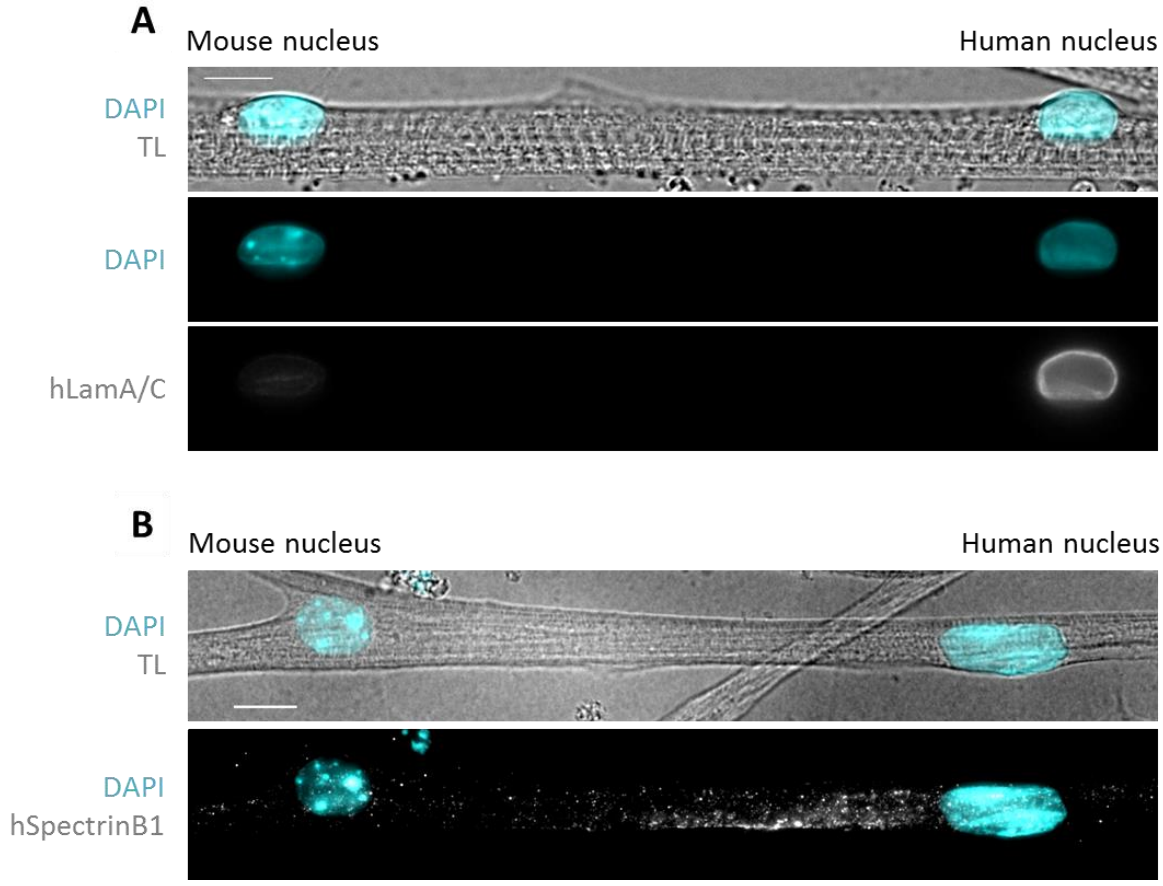

Figure 30 – Protein localization is dependent on nuclear position

A) Immunofluorescence of human Lamin A/C in a myofiber containing one single human nucleus (on the right). B) Immunofluorescence of human Spectrin α1 also in a heterokaryon (single human nucleus on the right). Fluorescence signal is shown as a MIP of a widefield Z-stack. TL, transmitted light. DAPI is shown in blue, scale bar 10 µm.

4.6 mRNA localization correlates with muscle function

Having observed increased mRNA translation closer to its nucleus of origin, we questioned if this could have an impact on muscle function. For this purpose, we expressed a humanized version of Channelrhodopsin-2 fused to YFP (Zhang et al., 2007a). This protein is a blue-light sensitive cation channel, and its activation at the myofibers membrane can induce contraction (Roman et al., 2017). To test the contractility of the myofibers close to the nucleus compared to regions away from it, we first confirmed that ChR2 expression itself did not differ with nuclear distance (Figure 31A, B, E). We next emitted blue light only specifically close and

away from the nucleus to depolarize the membrane and induce contraction. Contraction was induced faster and at a higher rate closed to the nucleus than away from it (Figure 31C, D). These results suggest that proper nuclear positioning might be necessary in order to have mRNAs minimally distributed in myofibers and consequently have protein levels that propagate contraction thoroughly along the myofiber.

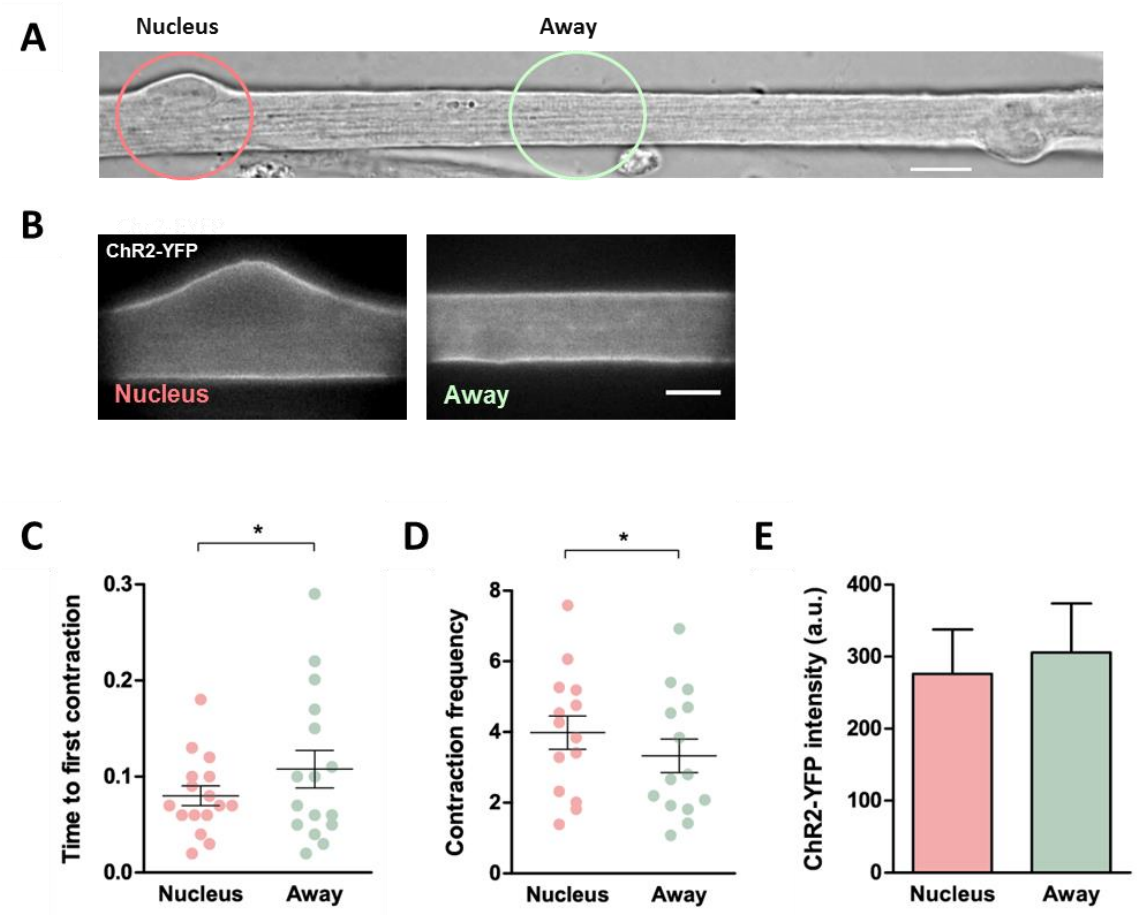

Figure 31 – Sensitivity to contraction is highest at the perinuclear region

A) Transmitted light representative image of a mature myofiber expressing ChR2-YFP with the areas stimulated by blue light depicted in pink and green. Scale bar 10 µm. B) Same myofibers areas as in panel A seen during stimulation with blue light. Emission of green light from a single focal plane is shown. Scale bar 5 µm. C) Time in milliseconds for first induced contraction to take place close and away from the nucleus measured by streaming acquisition. D) Contraction frequency was measured and normalized to the acquisition period of 1 second. E) ChR2-YFP emission at the myofibers membrane was similar between the regions close and away from the nucleus. a.u. arbitrary units.

4.7 Contributions

All results were obtained by the candidate except for the following in the specified sections:

4.3 – Collection of adult muscle and cryosectioning was performed by Sara Ferreira and smFISH of sections was performed and acquired by Helena Pinheiro.

4.5 – Puromycilation was optimized and performed by Graciano Leal, except for image analysis which was done by the candidate.

4.6 – Contraction experiments were optimized by the candidate and image acquisition, analysis and quantification was performed by Graciano Leal.

5 Discussion

During skeletal muscle formation, the numerous nuclei arising from myocyte fusion undergo several complex movements until they reach their final destination in the myofiber. In mature myofibers, the multiple non-synaptic nuclei stop their longitudinal movements and become anchored at the cell periphery. These nuclei are positioned so that the distance between them is maximized, in a non-random manner (Bruusgaard et al., 2003). This distribution and localization is highly conserved across mammals, suggesting an underlying functional relevance (Liu et al., 2009). Moreover, the number of nuclei present in the cell is increased with hypertrophy so that a proportion is actively maintained between the number of nuclei and cell size (Bruusgaard et al., 2010). Disruption of muscle nuclear positioning has been shown to affect Drosophila larval motility (Metzger et al., 2012). Yet, so far the molecular consequences of affecting the location of nuclei in myofibers have not been established.

Here we used in vitro differentiated myofibers as a system to study the biology of peripherally anchored nuclei (Figure 14). We hypothesized that nuclei have to be properly localized because their range of influence in the cell is limited. Under conditions of improper nuclear distribution, there would be an abnormal concentration of proteins important for muscle function and homeostasis in certain cellular locations. This is in accordance with the nuclear domain theory from Pavlath in 1989, stating that gene products are limited to the region surrounding their nucleus of origin. Although some experimental data exists supporting this theory, it is either in very artificial and immature muscle in vitro systems or in the context of satellite cell supplementation for treatment of muscle disorders (Hall and Ralston, 1989; Karpati et al., 1989; Pavlath et al., 1989; Ralston and Hall, 1989a, 1989b, 1992).

In this work we show with high resolution that mRNAs in general (both muscle enriched and housekeeping) cluster in the perinuclear region (Figure 15Figure 16Figure 17 Figure 20). A similar observation had been made for total mRNA in isolated fibers but if this pattern was due to particularly abundant types of mRNA had not been addressed (Nevalainen et al., 2013). We have also confirmed that mRNAs accumulate around their nucleus of origin by introducing a different

nucleus in these cells and tracking its specific products (Figure 18). Importantly, a couple of studies in isolated and sections of myofibers had reported enrichment of mRNAs under the sarcolemma (Nevalainen et al., 2013; Nissinen et al., 2005). Given the continuous developmental aspect of these myofibers, we could observe that this enrichment only occurs upon myofibril alignment and crosslinking (Figure 19). Thus, it seems that subsarcolemmal mRNA enrichment is only a consequence of cytoplasmic volume constrains at the center of these cells.

During significant skeletal muscle activity, microinjuries are constantly being exerted and repaired on the myofiber, particularly at the cell membrane (Lovering and De Deyne, 2004; Proske and Morgan, 2001). Whether mRNA enrichment at the sarcolemma facilitates the sustainment of muscle activity has not yet been tested. It is also a possibility that local translation is regulated by such local stimuli. When extensively damaged, the myofiber undergoes regeneration and the nuclei originated from newly fused myoblasts are maintained at the center of for up to 94 weeks (Bischoff, 1975; Grounds, 2014; Meyer, 2018). Although it is still not understood if central nuclei are actually necessary or just a recapitulation of the normal differentiation process, where and how mRNAs are localized throughout the regeneration process *in vivo* could be suggestive of its relevance.

Given that the foundations of muscle architecture are built with the biggest proteins encoded in the genome, we wondered where the respectively big mRNAs were located in these cells. Surprisingly, these mRNAs showed a different localization to what seemed to be the default in these cells, without accumulation at the perinuclear region (Figure 21). This result was very consistent, being also the case for *in vivo* muscle sections and in myofibers with affected nuclear positioning (Figure 22, 24). In fact, these mRNAs were even enriched at cell tips away from any nuclei suggesting some form of active transport. Under an evolutionary perspective this would be reasonable given that: 1) energetically it would be more efficient to transport one big mRNA and locally translate multiple proteins; 2) with the lengthy translation periods of giant proteins, having transcripts already available at a local of sudden need would at reduce significantly any delay in stimulus response; 3) the extremely compact cytoplasm in these cells (sarcoplasm) is not a compliant environment for transport of giant proteins with complex topologies.

The most common dystrophy (DMD) is caused by a mutation in the Dystrophin gene and absence of the respective protein (Ahn and Kunkel, 1993). This also giant 427 kD protein is encoded by a 14kb mRNA. On a scenario in which mRNA transport is necessary for protein spreading, Dystrophin would possibly be one of those cases. In fact, the rescue of Dystrophin expression in DMD patients using satellite cells transplantation leads to protein expression very limited in space (Gussoni et al., 1997). This contrasts with the broad soluble GFP expression used as a control in a similar study in mouse (Chretien et al., 2005). This clinical limitation could be due to the low number of Dystrophin expressing nuclei in the myofiber. Although the Dystrophin mRNA would be expected to spread, in such low proportion it would be unlikely to cover the extent of the cell. Thus a correlation between mRNA and protein localization in such transplantation studies would support the hypothesis that the transport of giant mRNAs facilitates protein spreading.

In order to better understand what would be the role of the two types of mRNA localization in skeletal muscle, we tried to dissect the underlying molecular mechanisms. Disruption of microtubule polymerization but not of actin led to altered mRNA localization (Figure 23). Interestingly, this effect was accompanied by alteration of mRNA levels. This could be due to impairment of the skeletal mechanosensing machinery, recently reported to be linked to microtubules (Kerr et al., 2015). In accordance, a global increase in transcription has been linked to mechanical load *in vivo* (Kirby et al., 2016). Another possibility is that microtubule disruption in myofibers affects the means by which cells control transcriptional rates (Padovan-Merhar et al., 2015).

Given that most of the reported cases of mRNA transport in mammalian cells are performed by kinesins, we studied the impact of their respective knock-down in myofibers. Four out of six kinesins did not have any type of mRNA localization phenotype and the remaining affected differentiation deeply (Figure 24). The latter group (Kif3c, Kif11 and Kif1b) might thus have a role in the transport of essential mRNAs in early myogenesis. However, given the lack of methodologies to induce the depletion of these proteins at later *in vitro* time points, their role remains to be demonstrated. An alternative approach to test the function of these kinesins would be silencing of these kinesins in adult muscles by electroporation. Remarkably,

Kif5b siRNA led to nuclear aggregation (as reported in Metzger et al., 2012) leaving a large portion of the cell devoid of nuclei. Even so, the pattern of mRNA localization was maintained with giant transcripts being independent of nuclear position. Although normal-sized mRNAs were found at lower concentrations away from the nuclei, we did not see any difference in the overall muscle structure. However, we noticed that Kif5b depleted cells have MT growing ends almost exclusively oriented away from the nuclei, probably as a direct consequence of nuclear aggregation. In normal myofibers microtubule orientation is mixed (Oddoux et al., 2013).

Given that the nuclear envelope is the main microtubule nucleator in these cells we sought to determine a role for the Dynein complex in keeping mRNAs at the perinuclear region. This motor has been implicated in the transport and anchoring of several mRNAs, particularly during the Drosophila development (Bullock and Ish-Horowicz, 2001; Clark et al., 2007; Dienstbier et al., 2009; St Johnston, 2005). Blocking of the ATPase function of the Dynein complex or depletion of proteins of its activating complex Dynactin resulted in decreased clustering of mRNAs in the perinuclear region relative to the region in-between nuclei (Figure 25Figure 27). Somehow consistently, the mRNA levels were once again altered when the dynein-dynactin complex was affected. Although the relevance of this expression alteration remains elusive, it would be interesting to test if it would be reversible upon for instance drug release. Strangely the expression of a p150 fragment with reported dominant negative effects did not have a distribution phenotype, although the mRNA expression levels were altered. Perhaps after one week of dominant negative expression, the myofiber eventually compensates by overexpressing the functional p150 subunit, although we did not test this hypothesis.

Interestingly, Dynein has been shown to be important for nuclear position and muscle function in Drosophila larvae, in a CLIP-190 dependent manner (Folker et al., 2012). The authors of this study found microtubules to be differently organized in CLIP-190 mutant larvae and suggest that nuclear mispositioning might be a consequence of these alterations. In our Dctn2 depleted cells we did not observe evident changes in microtubule organization (Figure 26). Recently, the mammalian CLIP-170 has been shown shift to the nuclear envelope upon centrosome relocalization (Gimpel et al., 2017). It is thus possible that the dynein phenotype

observed by Folker and colleagues is a consequence of deficiencies at the nuclear envelope MTOC which *per se* organizes the MT network and not the other way around. Thus, attention must be taken when studying the effects of the Dynein complex given that they might be upstream enough to alter the overall MT organization. A classic example of this duality is the complex nuclear positioning in the drosophila oocyte, with a mechanistic model that has been updated over the years (Bernard et al., 2018; Tissot et al., 2017). As a control, we confirmed that myofibers treated with Ciliobrevin D do not show increased nuclear movement compared to controls (Figure 26).

In parallel, MT dynamics might be hindered instead of motored transport when the dynein-dynactin complex is affected (e.g. Arp1 subunit), eventually leading to mRNA mislocalization (Nieuwburg et al., 2017; Yogev et al., 2017). In fact, dynein has only been recently associated with mammalian mRNA transport although it's biochemical interaction had been observed almost two decades ago (Epstein et al., 2000; Herbert et al., 2017). Herbert and colleagues found dynein to be important for anterograde transport of Mbp by identifying Arpc11 in a myelination mutant screen. The Arpc11 mutant phenotypes were highly comparable with the Kif1b results obtained in a similar study (Lyons et al., 2009). It remains to be confirmed that the dynein phenotype is not an indirect consequence of impaired kinesin transport and vice-versa, as shown for kinesin-1 (Twelvetrees et al., 2016). This distinction would be facilitated by the identification of a mammalian mRNA adaptor homologous to Egalitarian in Drosophila. Only the adaptor protein BicD2 is known in mammals but this also has also multiple important roles (Hoogenraad and Akhmanova, 2016; Jha et al., 2017).

In DMD patients the subsarcollema region is highly dysfunctional, in part because of the role of Dystrophin as MT organizer (García-Pelagio et al., 2011; Goldstein and McNally, 2010). How mRNAs are localized in these patients has not been studied to date. However, the levels of microtubule detyrosination have been shown to be increased in DMD (Belanto et al., 2016). Interestingly, tyrosination of microtubules have been shown to modulate dynein activity and processivity (Barbosa et al., 2017; McKenney et al., 2016). In light of the recent implications of detyrosinated MTs in muscle mechanotransduction, it would be interesting to test if this PTM has a role on mRNA localization (Kerr et al., 2015).

After establishing that mRNA perinuclear accumulation is an active process we wondered how this could impact translation in these cells. Accordingly, ribosome localization assessed by 18S rRNA localization showed preferential enrichment close to the nuclear or origin (Figure 28). Importantly, ribosome localization was independent of Dynactin2 expression which suggests that these are localized independently of mRNAs. By performing a puromycilation assay that can be used to provide the local translation levels in a short period of time, we also observed that protein production rate was higher in the perinuclear area (Figure 29). In skeletal muscle the Sarcoplasmic Reticulum is a highly specialized form of the Endoplasmic Reticulum. Whether the canonical ER, more specifically rough ER exists in muscle remains unclear. One particular study has shown enrichment of resident ER proteins around the nucleus (Kaisto and Metsikkö, 2003). Since secretory and transmembrane encoding mRNAs have been shown to localize to the ER in a translation dependent and independent manner, it would be relevant to understand what is the role of this organelle in skeletal muscle transcript localization (Blobel and Dobberstein, 1975; Cui et al., 2012). In accordance, the perinuclear localization of transferrin mRNA in myotubes has been shown to be translation dependent (Ralston et al., 1997).

Although mRNAs and ribosomes are clustered around the nuclei in these cells, we would not expect proteins in general to be so, given the highly repetitive nature of muscle architecture along the cell. In fact, nuclear distribution is probably necessary to ensure that disequilibrium of important proteins does not take place. In order to understand how far the gene products of each nucleus go, we made use of heterokaryons to look at the localization of human proteins in a myofiber containing one single human nucleus among mouse nuclei. By using human specific antibodies we confirmed that proteins are also kept within a broad area surrounding the nucleus of origin (Figure 30). Unfortunately, no human specific antibody for Giant proteins was found and overexpression of tagged versions of such long CDSs is extremely challenging. As an alternative it would be interesting to use a mixture of myoblasts from Dystrophin-eGFP and wt mice in order to understand giant protein spreading in myofibers (Petkova et al., 2016).

These heterokaryon results suggest that nuclear localization might indeed affect the levels of specific proteins that might ultimately impact muscle contraction.

Given the smaller caliber of these myofibers compared to isolated myofibers, and the bigger spatial resolution in between two nuclei (discussed in section 4.1), we compared the contractility of regions close and away from the nucleus. This was possible through the expression of an optogenetic cation channel that locally depolarizes the sarcolemma and induces contraction (Roman et al., 2017). We observed that the regions closer to the nucleus are more prone to contraction than regions devoid of nuclei (Figure 31). These results are in line with the mRNA and translation results mentioned above, and might be the reason underlying the necessity for nuclear spreading for proper muscle function (Metzger et al., 2012). It is possible that the higher excitability of the perinuclear region helps signal propagation in the presence of a NMJ *in vivo*.

In this work, we clearly establish the dependency of mRNA localization on nuclear positioning. We determined that this is an active process, dependent on the microtubule Dynein motor. We show that translation and certain protein levels follow this general trend, pointing out to a necessity for nuclear distribution in myofibers for homogenous protein concentration through the cell. We also show for the first time that contraction might be affected by the position of the nucleus inside the cell. Moreover, we uncover a different distribution for a specific set of mRNAs and speculate on its relevance.

6 Appendix

6.1 smFISH probes

Gene: Rn18s - 18S ribosomal RNA; species: mouse; stringency level 2

1 gagacaagcatatgctacct 2 acttagacatgcatggctta 3 cattcgcagtttcactgtac 4 gagcgaccaaaggaaccata 5 accacagttatccaagtagg 6 tcggcatgtattagctctag 7 gggttggttttgatctgata 8 gttatctagagtcaccaagc 9 gatagggcagacgttcgaat 10 acggcgactaccatcgaaag 11 tatttttcgtcactacctcc 12 cctcgaaagagtcctgtatt 13 gtggactcattccaattaca 14 tccaatggatcctcgttaaa 15 tacgctattggagctggaat 16 acgagctttttaactgcagc 17 acactcagctaagagcatcg 18 tcaaagtaaacgcttcgggc 19 gcctgctttgaacactctaa 20 attattcctagctgcggtat 21 acaaaatagaaccgcggtcc 22 cttaatcatggcctcagttc 23 gtccaagaatttcacctcta 24 ttcttggcaaatgctttcgc 25 ccgactttcgttcttgatta 26 ggtatctgatcgtcttcgaa 27 catcgtttatggtcggaact 28 ggaacccaaagactttggtt 29 tcagctttgcaaccatactc 30 cttccgtcaattccttttaag 31 tcccgtgttgagtcaaatta 32 atcaatctgtcaatcctgtc 33 cacccacggaatcgagaaag 34 aactaagaacggccatgcac 35 taaccagacaaatcgctcca 36 cagagtctcgttcgttatcg 37 gtcgcgtaactagttagcat 38 cttgtccctctaagaagttg 39 tgttattgctcaatctcggg 40 catctaagggcatcacaga 41 aatggggttcaacgggttac 42 tggggaataattgcaatccc 43 cacttactgggaattcctcg 44 atcaacgcaagcttatgacc 45 tgtgtacaaagggcagggac 46 cactaaaccatccaatcggt 47 agatagtcaagttcgaccgt 48 cacctacggaaaccttgtta

Gene: Acta1 - actin alpha1 skeletal muscle; species: mouse; stringency level 4

1 ctcgtcttcgtcgcacat 2 gtcacacacaagagcggt 3 gctttcaccaggccagag 4 catcatccccggcaaagc 5 cccacgatggatgggaac 6 atgacaccctggtgacgg 7 ccttctgacccataccta 8 ctcatcacccacgtagga 9 gatacctcgcttgctctg 10 atggggtacttcagggtc 11 gtcccagttggtgatgat 12 cacacgcagctcattgta 13 tagctttggggttcaggg 14 ttgagtcatcttctcccg 15 gcacgttgaaggtctcaa 16 gatagccacatacatggc 17 tagagggacagcaccgcc 18 cggtggtacggccggaag 19 tccccagaatccaacacg 20 gcacgttgtgggtgacac 21 ggcatagccctcatagat 22 agacgcatgatggcgtgt 23 atcaggtagtcagtgagg 24 ccacgctcagtgaggatt 25 cagctgtggtcacgaagg 26 gtcgcgcacaatctcacg 27 ggccatctcattctcgaa 28 gcagctcatagctcttct 29 cgatggtgatgacctgcc 30 cgggcaacggaaacgctc 31 ggaaggctggaagagcgt 32 gcagactccataccgata 33 aggtggtctcatggatcc 34 cgcacttcatgatgctgt 35 gtccttcctgatgtcgat 36 gacatgacgttgttggca 37 agggtacatggtggtgcc 38 tgcatgcggtcagcgata 39 ccagagctgtgatctcct 40 gatcttcatggtgctggg 41 tcagggggggcgatgatc 42 caccgatccacactgagt 43 gacagcgaggccaggatg 44 tccacatctgctggaagg 45 tcgtcgtactcctgcttg 46 tgcggtgcacaatggagg

Gene: Actn2 - actinin alpha2; species: mouse; stringency level 5

1 gacatagttgtactgcacgc 2 tcatatactcatcttcgtcg 3tgaaatcctcctcgatgttc
4 ccctgagatgacttctagaa 5 gacattcgcaatcttgtgga 6 ctatgtaatccagagccttg
7 tcatcttcacattgccatcg 8 ggatgatggtccagatcata 9 agatgtcctgaatggcgaag
10 tttctgtatggagctgtctt 11 gtggaagttctggatattca 12 gtcatccttgttaagctttg
13 gggagtgttgacaatgtctt 14 cgtaagtcatgatggctctt 15 ccgcgaaagcatggtagaag
16 atattctgttagctgctgtc 17 cattctcttgattcacagca 18 ctctcatattcttccatcag
19 gcttatgcttacgacggtaa 20 caatgtccgacaccatcttg 21 ccagtcttcgaatctcattc
22 ctgaacttctcagccaagtg 23 cagcaagatctgttctttgc 24 cgaagtagggctcgaacttc
25 gtgatagtccagttcattga 26 gatcattgacgttcacagca 27 actggtcgcaaattttctgg
28 aacttctcagttctctccaa 29 tgcagttggtcgattgtttc 30 agtgatcagactctggatct
31 atgctgtagctctggatcac 32 catggtgacagtgctgtagg 33 agacgctcattagcatgttg
34 tgatgttgtgttcgtactgc 35 gtcgatgttgttcttgtagt 36 gtgtgcttgttgtcgaagac
37 gatatgctccatggtgtagt 38 atagttgtcagcagcaactc 39 cacctcattgatggttctgg
40 catctcttgtcaggatctgg 41 tgaactcattcatctgctcc 42 aatcctcatgatccatcagg
43 catggaaatgaggcaggctc 44 aaattcagcttcacccaagt 45 ttggggtcaaccaaagtcat
46 aagccagaatccggaaggag 47 ctgccaagatgtaaggctta 48 ttctcttgatgcagtactgg

Gene: ACTN2 - Actinin alpha2; species: human; stringency level 5

1 acacgtagttgtactgcacg 2 atcatgtactcatcctcgtc 3 agttacaccaggcagtgaag
4 cgatgttctcaatctgggtg 5 ttaaggccattcctgaagtc 6 ccctgagatgacttccaaaa
7 tagcaattttgtggaaccgc 8 ttgctggctatgtaatccaa 9 caatggacaccagtttcacc
10 attttcacgttgccatcaac 11 cgaaggatgatggtccagat 12 tctttggcagatgtttcttc
13 gttttcctctgacaccaaag 14 tctttccagctagtatggaa 15 atgagggcacagagtccaag
16 agtagtcaatgaggtcaggc 17 tttccatggccaggttaata 18 ttaggaatatccaggtgctt
19 ttcacgatgtcttcagcatc 20 tacgtcatgatggctctttc 21 ccgcaaaagcgtggtagaag
22 gcaagaaccttacatatcct 23 tgcgacgaatccattccaaa 24 caatatccgacaccatcttg
25 ctccgaatctcattgagcaa 26 cttctgcctgaacttctcag 27 gatctgctctttgccataag
28 gactcgtaatccttctgcag 29 gatagtccagttcattgagc 30 tcattgacattcacagcgtc
31 gtcacaaattttctggcacc 32 cctccatccaattgttgaaa 33 gaacatatcttgcagatcct
34 agtgatcagactctggatct 35 tgtagctctgaatcaccttc 36 ttgcttgagctgattctgat
37 catggtgacagtgctgtacg 38 cgtgtgcttgttgtcaaaga 39 caacacgaatgtgctccatc
40 cattgatggttctggcgatg 41 atctctcgtcaggatctgag 42 ctcctgtcaaagtggttgaa
43 ggtcataatgcgggcaaatt 44 aaggattggaaggtgacggt 45 cgtctctctagtcatgaagt
46 tatggcttatcagaagccag 47 atcctcttgatgcagtactg 48 cggaagagaacgcagcgtaa

Gene: Cacna1b - calcium channel, voltage-dependent, N type, alpha 1B subunit; species: mouse; stringency level 5

1 gaagacctccatagggatc 2 tttcctcttgctgtacttg 3 cgtctgacctttgaaccg 4 gttgtatccgaggacgtac 5 ctggcggacgaagctgttg 6 cgtgtaggactctgctgag 7 atcagagtctgatggtcgg 8 tttctcgagctgggctaag 9 aaagccactggtttggtct 10 gccaacatttgtccgaaca 11 atcccctggagacggattg 12 tcaaaggtgatggccactc 13 ccaatccaccagtcattat 14 gatgaagccaacctcgcag 15 gaaggctgtccagtttgac 16 tggagctgaggcggttctg 17 tttcattaccactggcagg 18 gggtctagctcaaaggcaa 19 actgctcacgctagtcttg 20 atgatgggcctcatggaag 21 tcatagcccttgagcgacg 22 ttctgcatcatgtctgtca 23 tgccatcaaaccgatgctt 24 aaatgtcagctgttacccg 25 gttgaggacggagcgtttg 26 gatgatgtgtttgctgggg 27 tggaacgcgtgttggagcg 28 tttcactctgtacctcagc 29 ccagctcgaagatcctctc 30 caaggcgaccagctgcaag 31 gttttagagagctgggctg 32 atttgatgagcctctgcag 33 tttggattgagacttccct 34 gaggctgctatttggacat 35 acatttcgggggggacactg 36 tctcgtccaggattatgtc 37 cgcaggcatcttccaattg 38 gtaggcttccaagtactca 39 ttcagcagcggattgggtg 40 ctggaggttggagacgggg 41 tgagcgaggtgagcacctg 42 cccagaagctgagatttct

Gene: Cacna1s - calcium channel, voltage-dependent, L type, alpha 1S; species: mouse; stringency level 5

1 tctcaggaacaggtttcttc 2 ctgtagagtcaggcagaaca 3 gagcaagatgatggtctcga 4 gttcagagtgttgttgtcat 5 tgcatcctgatggaatagga 6 gccttgaagatggagttgag 7 cccaatgaagtagcaagtct 8 agttgtcgaagtgggtgatg 9 gcattgatacacagtgagca 10 tgacaaagtagatccagggc 11 tgtgatccagctcatgtaac 12 ttcatccaaagacagcttgc 13 agccaatagaagaccttgga 14 aatggacagggtgtttaggg 15 cttgcaaatgggtcaaccag 16 tttcgatggtgaagagggtc 17 aagcagtcgaagcggttgaa 18 tcgtacttctgtgtcttcaa 19 ctgggggaagttgtcaaagt 20 cctggaagacactgatgagg 21 atgatcccattgtacatcac 22 atgtagttgccacagacgaa 23 agccaggaagacgttgagaa 24 agcaggatgaagagcaggat 25 aggtggtcatcttaaggaca 26 ggatgttgaagtagttgcgg 27 cactctcagaacccttaaga 28 tgtatatgtagtagtagccc 29 ggaagtcattgtgtatccac 30 gagtgacatcatagcggaga 31 aggtaacgatgacaaagccc 32 gctcacagttcttatactca 33 gtttttggggatgtaacacc 34 ggaggaagtgacgacatacc 35 actggttgtaatgctgcatg 36 gagatgtggttcatctgttc 37 ggcttgaaagctatgagctt 38 aaggatctccaaaatagccc 39 gatgacgtcaatgatgctgc 40 ccgcgtagatgaagaagagc 41 agtagtaggcgaagttggtg 42 aggttgatgatcaggaaggc 43 gggcaaatagtgtggcatta 44 ttctgtcttgatcttgaggg 45 tgtatctgaactgtgtcctt 46 tttcagcaaattggaggggt 47 ttcagtttgtccacatgaga 48 gacgaagttagcatctgctg

Gene: CACNA1S - calcium channel, voltage-dependent, L type, alpha 1S; species: human; stringency level 5

1 gagcaagatgatcgtctcga 2 ctggtggaataagaagccgt 3 cccaggaagacaatggtgaa 4 cgttaacctgttccagaatc 5 tgtgaaagaggggagcatg 6 accataaagaggaccagcag 7 atggagaagccgaagttgtc 8 taatgcactggtacacggtg 9 attgacccagtaaaggacgt 10 gacaaaatagatccagggcc 11 aggatcccagcaaaatgagg 12 ttgttcaagcctgcaatttc 13 ccaatgtcggatgaactgga 14 cttggacttcacgatgtcat 15 ggcaacgatgagaatcacca 16 tggcaatgtcttgcaaacgg 17 aagcagtcgaagcggttgaa 18 cgacgtccaatatttggtga 19 gagggcgaagatgacgatga 20 tgtacatcattgaggtccag 21 aaatgcacacaagcatgcca 22 atgtagttgccacagacgaa 23 atggccaggaagacattgag 24 gacacaggacacggatctta 25 taaaccaggtggcattgacg 26 agcaggatgaagagcaggat 27 tgaggacaatctccacagtg 28 ccgatgcaggcaaacatgaa 29 gaagaacttccccttgaaga 30 ctgtcatcttggacaagtcg 31 tccttgtacacgtagtagta 32 attgtcgaagtggaagtcgc 33 tcacagttcttgtactcagt 34 cagggcatactgtacacatt 35 tgggtttttgggaatgtagc 36 aggaggtgacaatgtaccac 37 gatgagggcaaacatcaggt 38 gacatcaatgatgctgccaa 39 acggaacaggcggaagaagg 40 aggacttgatgaacgtccac 41 aaacatctgcatgccgatga 42 aggtctggaagttgttgttc 43 tagtatgcaaagttggtgcc 44 gatgacagccacaaagaggt 45 tggcattgaaggtgactgtg 46 cgatagccataatactcctc 47 gatctgtacaatgtccttct 48 attgttggtattggcacgag

Gene: Cacna2d1 - calcium channel, voltage-dependent, alpha2/delta subunit 1; species: mouse; stringency level 5

1 tcagcccagattggaaaagt 2 acccatgacttgatagtgac 3 tgacaaggtcttcttgcatc 4 gggctccacagtatacaaat 5 aatttcaaccagttggcgtg 6 ccttagatctgttgcttaga 7 attgcttgcaaaatcttccc 8 gataggatatctgacgtcca 9 tcatagatgtccgtgggaat 10 cttcatctaaggcacttgtc 11 tcttcgtctcgatttctttt 12 gagttctactattatccacc 13 gtcttctgcgtacatcatat 14 tcggatgagtttcagagtca 15 ctggaaacagcttacatcct 16 tcttacattcgcttgaacca 17 gctgtaatgttattcacggc 18 agcctttcttgtaatctgtg 19 tagctgttcgaaggcaaagc 20 ttattttcacaagccatcca 21 ttgtccattgaacttgcttc 22 gactggtagagttccagtaa 23 tcttatttttcagattggcca 24 cccatcacaccaagaatcaa 25 agccattaggatcaattgca 26 tggctgaagatttggatgca 27 gtatacctacaccaataggc 28 ggtctccttttccttaaatt 29 agatttggggttctgaacgt 30 aaaatccagtgtgactggct 31 tctcatcttgagacttgacc 32 actgtaatctgtgccattga 33 ctgtaggttggcaataccaa 34 aaaacctgcatccagcaaga 35 agggcgcagtgaaaacgtag 36 ccaggtccacttttgttaaa 37 agttctactgctttgcttac 38 caactgcgggcttaagaagt 39 ccctgattgaagttttggta 40 gtaatcatcgtgatttgcca 41 taaccaggtgtctcatcatg 42 tctgcaatcgatggcacata 43 ggagccgtggaaatgtcaaa 44 tagacagggaggctgtgaag 45 aagatcctggaacagtttcc 46 gatctggaccatcagaagtc 47 caccacagtcagtataatcc 48 agataccagccaaaggagta

Gene: Neb - nebulin; species: mouse; stringency level 5

1 aaactgtctcctctgtgtag 2 atcctggactttcttgattc 3 tgctttttcatccacatgac
4 tgcgacactttcttagcatg 5 aaacaatgccttgtctgctt 6 attctggctgttgcaatttc
7 gtagatctggtctttcatgt 8 ggggtctcacagtaattgat 9 acgtagtgtcccaagatatt
10 tacagtgtgtgtgatacggg 11 tcactttcatgtttggcttt 12 tctgtgctggataaaggcag
13 cacttaggttataggcgttc 14 tccttcttgtacatcacatc 15 gtgtgatctttacactggtc
16 gtcttatcaggatgcacttt 17 tccttcttgtacatcacatc 18 cacattgatgctgtcaggag
19 atgttggcggtatttttct 20 ttgtaagcaatatcgctcct 21 tcaagtcagccttgtacata
22 cttggagactttggaatccg 23 cttggccacattcatgtaat 24 cgaacatgtcgtgaggtgta
25 ctggtgaacttgagtgtgtc 26 tttggctattaagtcatgcc 27 ataatggaccaacttggggt
28 ttttcttgtattctcggtct 29 gtaacttgtcttggtgttct 30 ggttgtttgtagttgacgtt
31 gttgtactcgtctttgtaca 32 gtgaacttgatggtgtctgg 33 tcactcatgttgatggcatt
34 gaatggcatctggtctcaag 35 atttgcagtcactagcgatg 36 ttttggccacattcatgtag
37 cattcaaggcatcaggcaag 38 tcttatccatagtcagcttg 39 gagagcaagatgtctggagt
40 tcactcattgtgatctggtt 41 attgttcataggcttgcttg 42 aagctcatggcatcaggaag
43 cttcatgaagtcggcatagt 44 atatctcttgatgctttggc 45 tagttggtgttggtgatgtt
46 cggcatcacatgaatcttgg 47 gggatgctggtgaacttatt 48 gtttgctttagccagaatga

Gene: Obsc - obscurin; species: mouse; stringency level 5

1 gtagaacaggctgctgatga 2 tctcaaaggagggtgtcttg 3 ctctgacactggaactaggt
4 ggaacaggagttgttccttg 5 agtggtttcatgagtcaacc 6 ggacagactcctgcaagaac
7 tcaccactcataggtggaaa 8 tacaactgtcctgggatgat 9 tcagagtgacaggaagaggc
10 gccaagcgattgagatgatg 11 ctgaaaagagtgggccacag 12 ggcttacttgagttgggaat
13 ctgaggttccttctcagaac 14 aactggcccttcagatagag 15 ctggagaactggagggaact
16 gaggcgtgaagtcacatgtg 17 gggactccagagagaacttc 18 cgccaaaggcaaaagtacca
19 caagctctccagaggttgag 20 aaggggtgaggcttggagag 21 agggaaacctgctcaacttc
22 aaggagatagtgtcagctgc 23 gcaggatcgacctcagaaat 24 gtcatatagatccgagaggt
25 gacccttctgaagatcatga 26 ctctgtaatctccagaccag 27 ctcccagggaattggaagag
28 ttgaggatcctggagatgtg 29 gtggaggagatgaggaggtg 30 ctcacacagcaggtatatgt
31 atagcttgccagtgaggtag 32 cggaagatatacatgccacc 33 tgctttgctgacacatgctg
34 tagggaacgatcttagcagc 35 cttagtacagctgtcttgtc 36 tctcttaagtgcctcgtatt
37 caaagagggtagcagctcag 38 cttcacatcagactctgagt 39 tactcagtgaccatcatgtt
40 ttctcttggtcgagactctg 41 ccaggtagtctttgaagttc 42 tgttacaccaatagcccaaa
43 cgccactcagcataatgaag 44 gcgactcaaccgaatgagtc 45 ctcctgataatcctgcatag
46 ccagggttgagcacataatg 47 cattgcaagcaggtggaagc 48 tatgcttcttgtagaggagc

Gene: Ryr1 - ryanodine receptor 1; species: mouse; stringency level 5

1 cagaaagcaaaggcggttgc 2 caggatgaagcagcagatgg 3 atacaagagtgtcctgtgtc 4 ctgcataaaggaggcgtcaa 5 agagcagatgggattcatgt 6 cattcatccatatgtccatg 7 atcatcactgtcagaagggg 8 ctcgtagtagacaagtctgc 9 tggtcacatgtctgattctt 10 aaaggaagtagccttggtgt 11 gtacaaagcagagcgactct 12 aagctatcgagacccтttat 13 ggttcacaatctctttccaa 14 aggacacagtacaacacctc 15 cccatcaaagccgtaagaat 16 gctcacgacagggaagaaga 17 ctttgatgggttggagatgg 18 ccacaggacagggtacaaag 19 ttcacaagacatgggtgcag 20 aagttgtaattccgctcagg 21 ttgtatccattgctcatcat 22 tggtgactgcttcaaactcg 23 cgatgcccattgaagacata 24 aatgtcacggaaggctgttt 25 gcaaaaaacctcagggagct 26 ttgatggcgaacggctcaaa 27ggtgttgaggatgatctcag 28 tccgggactcacaaaatctc 29 ccaatgacaaggtctgtgtg 30 ggaagaaggtgttgctttct 31 aggaaacagcttcgtgttgg 32 ctcagatagctctaggatgt 33 cacgatgtactcagagagca 34 aggtgggaaaagcgtgatgg 35 gagaaatggtgtggaggtct 36gagggtagacacaagcttga 37 tgcatcttgtccacataaca 38 gcaatagcatgttgatctgc 39 catctgcacaatgagcagtg 40 cataacctccatgactgttt 41 tagctcaggtggtcaaacat 42 caatgacagaagcagcagct 43 tcttgtaatgccaaggctag 44 gtatgacacaacctttтcca 45 caccgttgacaaagacagca 46 ggcagcatagaaggacatga 47 aaggatgcagacatcttcgg 48 agcacatgcagcaagaagtc

Gene: Ttn – titin; species: mouse; stringency level 5

1 ctcaaaggttgcggtactac 2 ggaactggggaaccactaac 3 ggaagttgaaatcacctggc 4 cgctaaaggagatctgcacg 5 ggaaatcaagggagctctgg 6 gaggtctccttcttgagaaa 7 cttcggcaatcagtaagctg 8 ggcatttacagaataggtcc 9 ttgaaccaccaattctgcag 10 tctttgtctttttagcaggt 11 aatctgagcagtcgacacga 12 ctttttttcaatccgggttt 13 tgatctggcatcaaagtggg 14 accatctatgaccatctcaa 15 tttggcagcaatggaaggtg 16 cttattggtgatggggactg 17 gtctgagtcttgcgaatgag 18 tgaatgacgagctgaccgac 19 ccatatcaacagcagcaacg 20 cttgagcaggttgtatatgc 21 ctttatcggcagcaactaca 22 ctctggttcgtgattttagt 23 aatttctcccgtgattctag 24 tgagttattcgcttttgctc 25 ctctagttttgtggacttgg 26 cgtggcaactatgactttgg 27 tagtgatggcttctctactt 28 tcagaactgtttcttgctct 29 cacagcagctacaactgttg 30 agtctgctgagaatgcgatt 31 ttctttgtagccatactcta 32 ggacctttgtggtggaaatg 33 cagaaggagcctgaatcaca 34 gacctgtgacgatatatgca 35 cactccaaggtgacagattc 36 cgatttggtagtcttctctg 37 tcatgagacgagcaattcca 38 cagagttgtttccttgtcaa 39 ttctcttcggtggcaaattt 40 catctcttgactccacgaag 41 ccaccggctttgaaatgaag 42 tatccagtggtgagaggaac 43 atagtgtattctccagcatc 44 atttcttgctgagtcttcac 45 tgctcatttgtgtctggtaa 46 atgcaaatccaggtgctatt 47 tttcttcctaattaaggcct 48 gaccatcacagtatctttgg

6.2 MATLAB script for spatial analysis of smFISH

```
function smFISH(input1)

%Input is the Composite of Maximum intensity projection (MIP) of RNA and Nuclei. It assumes 2 nuclei per image. If there are more modify n.
%Returns peaks positions, index for clustering and distances of each particle to the nucleus.

    n=2;
    Im=bfOpen3DVolume(input1);
    Im=Im{1};Im=Im{1};
    prompt={'Enter Nuclei channel','Enter Rna channels (space separated)','Enter the name of file to save'};
    dlgtitle='Input';

    answers = inputdlg(prompt,dlgtitle);
    Nuc=str2num(answers{1,:});
    rna=str2num(answers{2,:});
    filename=answers{3};
    Nuclei=Im(:,:,Nuc);

    %creates BW image of the nuclei and calculates the centroids
    BW=im2bw(Nuclei,graythresh(Nuclei)); BW=bwareaopen(BW,50);
    S=regionprops(BW,'Area','Centroid');

        if size (S,1)>2
            A=[S.Area];
            B=sort(A,'descend');
            ind= A==B(1) | A==B(2);
            S=S(ind);
        end

    c=cat(1,S.Centroid);

        %Cycles through the rna images
        for kp=1:size(rna,2)
            Rna=Im(:,:,rna(1,kp));
            Name=['Rna_' num2str(rna(1,kp))];
            pk=[];pk1=[];pk2=[];
%bandpass filter of the Rna image and finds the peaks in the image
            bpn=15;pkn=80;
            Rna1=bpass(Rna,1,bpn); pk=pkfnd(Rna1,pkn,1);
            figure;imshow(mat2gray(Rna));hold on; plot(pk(:,1),pk(:,2),'yo');
            prompt = 'Is the threshold correct? Y/N [Y]: ';

            str = input(prompt,'s');

             while str~= 'Y'
                if isempty(str)| str=='Y'
```

```
            str = 'Y';

        else if str=='N'
            prompt={'Enter bpn','Enter pkn'};
            dlgt='Threshold';
            ans = inputdlg(prompt,dlgt);
            bpn=str2num(ans{1,:});
            pkn=str2num(ans{2,:});
            Rna1=bpass(Rna,1,bpn); pk=pkfnd(Rna1,pkn,1);
            figure;imshow(mat2gray(Rna));hold on; plot(pk(:,1),pk(:,2),'yo');
            prompt = 'Is the threshold correct? Y/N [Y]: ';

      str = input(prompt,'s');
        end
        end
      end
%%Removing pks that are not in between the nuclei or within one nucleus
   B=bwboundaries(BW);
   for z=1:length(B)
      B1=B{z};
      in=inpolygon(pk(:,1),pk(:,2),B1(:,2),B1(:,1));
      pk=pk(in==0,:);
   end

   ind= pk(:,1)>c(1,1)&pk(:,1)<c(2,1);
   pk=pk(ind,:);

  figure; imshow(mat2gray(Rna));hold on; plot(c(:,1),c(:,2),'rX');

   dNuclei=(sqrt((c(1,1)-c(2,1))^2+(c(1,2)-c(2,2))^2));
   count1=1;
   d1=[];
      for j=1:length(pk)
   d01=sqrt((c(1,1)-pk(j,1))^2+(c(1,2)-pk(j,2))^2);
   if d01<=dNuclei/2
      pk1(count1,1)=pk(j,1);
      pk1(count1,2)=pk(j,2);
      d1(count1)=d01;
      count1=count1+1;
   end
      end
   count2=1;
   d2=[];
   for k=1:length(pk)
   d02=sqrt((c(2,1)-pk(k,1))^2+(c(2,2)-pk(k,2))^2);
   if d02<=dNuclei/2
      pk2(count2,1)=pk(k,1);
      pk2(count2,2)=pk(k,2);
      d2(count2)=d02;
      count2=count2+1;
```

```
    end
    end
    plot(pk1(:,1),pk1(:,2),'ob')
    plot(pk2(:,1),pk2(:,2),'or')

    figure
    %distances in um. It assumes a pixel size of 0.072 um/pxl.
    dNuclei=dNuclei*0.072;
    d1=d1*0.072;
    d2=d2*0.072;
    %%Makes a histogram of the particles in each cluster. It bins every 5um
    %%up to half the distance between the nuclei
    [H2,x2]=histcounts(d2,0:5:dNuclei/2);
    [H1,x1]=histcounts(d1,0:5:dNuclei/2);
    bar(x1(1:length(H1)),H1);hold;bar(x2(1:length(H2)),H2,'FaceColor',[1                0
1],'FaceAlpha',0.5); xlabel('Distance from the nucleus (\mum)');ylabel('# Rna');
    figure
    %%Ccalculate the radial distribution function g(r)
      %calculate the density of particles in a rectangular box
    % of size L(x,y)
     L1=(max(pk1)-min(pk1))*0.072;
     L2=(max(pk2)-min(pk2))*0.072;
    % Density in the box
     Rho1=size(pk1,1)/(L1(1)*L1(2));
     Rho2=size(pk2,1)/(L2(1)*L2(2));
    %  Gr1=[];
    %  Gr2=[];
       for i=1:(size(x1,2)-1)
        Ar1=pi*(x1(i+1)^2-x1(i)^2);
        N1=Rho1*Ar1;
        Gr1(i)=2*(H1(i)/N1)/(size(pk1,1)-1);
        Ar2=pi*(x2(i+1)^2-x2(i)^2);
        N2=Rho2*Ar2;
        Gr2(i)=2*(H2(i)/N2)/(size(pk2,1)-1);
        end
        plot(x1(:,1:size(Gr1,2)),Gr1);hold
     plot(x2(:,1:size(Gr2,2)),Gr2);xlabel('Distance                from                the
nucleus(\mum)');ylabel('g(r)')

      Sheet=['Sheet' num2str(rna(1,kp))];

        x1=x1(1:length(H1));x2=x2(1:length(H2));
     Hist=[x1',H1',x2',H2'];
     header={'Bins','Hist1','Bins','Hist2'};
     data=num2cell(Hist);
     output=[header;data];
     xlswrite(filename,output,Sheet);
     Gr=[Gr1',Gr2'];
     header2={'Gr1','Gr2'};
     output2=[header2;num2cell(Gr)];
```

```
        xlswrite(filename,output2,Sheet,'E')
        header3={'d1'};
        output3=[header3;num2cell(d1')];
        xlswrite(filename,output3,Sheet,'G')
        header4={'d2'};
        output4=[header4;num2cell(d2')];
        xlswrite(filename,output4,Sheet,'H')
       header5={'Distance'};
       output5=[header5;num2cell(dNuclei)];
       xlswrite(filename,output5,Sheet,'J');
%     A={pk1,pk2,x1',H1',x2',H2',Gr1',Gr2'};
   end
```

6.3 GO term analysis of top10 biggest CDSs in the genome

Muscle related GO terms are significantly enriched when comparing the mRNAs encoding the top 10 biggest proteins to entire human transcriptome (TTN, MUC16, OBSCN, SYNE1, NEB, MACF1, DST, CCDC168, FSIP2, SYNE2, see Table 7 in section 4.3). GO terms are ranked by significance.

Term	Background frequency	Sample frequency	Expected	P-value
muscle structure development (GO:0061061)	408	4	1.68E+02	1.003e-04
sarcomere organization (GO:0045214)	24	2	9.91E+00	3.038e-04
muscle cell differentiation (GO:0042692)	224	3	9.25E+01	6.087e-04
actin-myosin filament sliding (GO:0033275)	37	2	1.53E+01	7.199e-04
muscle filament sliding (GO:0030049)	37	2	1.53E+01	7.199e-04
myofibril assembly (GO:0030239)	40	2	1.65E+01	8.409e-04
cytoskeleton organization (GO:0007010)	707	4	2.92E+02	8.552e-04
actin-mediated cell contraction (GO:0070252)	45	2	1.86E+01	1.063e-03
actomyosin structure organization (GO:0031032)	56	2	2.31E+01	1.642e-03
actin filament-based movement (GO:0030048)	61	2	2.52E+01	1.947e-03
cellular localization (GO:0051641)	1817	5	7.50E+02	2.660e-03
forward locomotion (GO:0043056)	1	1	4.13E-01	2.889e-03
actin filament-based process (GO:0030029)	386	3	1.59E+02	3.011e-03
striated muscle cell development (GO:0055002)	89	2	3.67E+01	4.119e-03
protein localization to organelle (GO:0033365)	444	3	1.83E+02	4.528e-03
muscle cell development (GO:0055001)	100	2	4.13E+01	5.188e-03
protein localization to M-band (GO:0036309)	2	1	8.26E-01	5.777e-03
establishment or maintenance of cell polarity (GO:0007163)	112	2	4.62E+01	6.492e-03
regulation of microtubule-based process (GO:0032886)	116	2	4.79E+01	6.958e-03
cellular component movement (GO:0006928)	1228	4	5.07E+02	7.054e-03
striated muscle myosin thick	3	1	1.24E+00	8.663e-03

filament assembly (GO:0071688)				
nuclear matrix anchoring at nuclear membrane (GO:0090292)	3	1	1.24E+00	8.663e-03
sarcomerogenesis (GO:0048769)	3	1	1.24E+00	8.663e-03
detection of muscle stretch (GO:0035995)	3	1	1.24E+00	8.663e-03
skeletal muscle myosin thick filament assembly (GO:0030241)	3	1	1.24E+00	8.663e-03
cell cycle arrest (GO:0007050)	135	2	5.57E+01	9.385e-03
striated muscle cell differentiation (GO:0051146)	147	2	6.07E+01	1.110e-02
peptidyl-tyrosine phosphorylation (GO:0018108)	149	2	6.15E+01	1.140e-02
directional locomotion (GO:0033058)	4	1	1.65E+00	1.155e-02
response to muscle stretch (GO:0035994)	4	1	1.65E+00	1.155e-02
nuclear matrix organization (GO:0043578)	4	1	1.65E+00	1.155e-02
somatic muscle development (GO:0007525)	4	1	1.65E+00	1.155e-02
peptidyl-tyrosine modification (GO:0018212)	151	2	6.23E+01	1.170e-02
single-organism organelle organization (GO:1902589)	1431	4	5.91E+02	1.251e-02
anatomical structure development (GO:0048856)	4047	6	1.67E+03	1.433e-02
posttranslational protein targeting to membrane (GO:0006620)	5	1	2.06E+00	1.443e-02
cytoskeletal anchoring at nuclear membrane (GO:0090286)	5	1	2.06E+00	1.443e-02
myosin filament assembly (GO:0031034)	5	1	2.06E+00	1.443e-02
myosin filament organization (GO:0031033)	5	1	2.06E+00	1.443e-02
skeletal muscle thin filament assembly (GO:0030240)	5	1	2.06E+00	1.443e-02
retrograde axon cargo transport (GO:0008090)	5	1	2.06E+00	1.443e-02
response to wounding (GO:0009611)	675	3	2.79E+02	1.516e-02
cellular component assembly involved in morphogenesis (GO:0010927)	173	2	7.14E+01	1.529e-02
maintenance of cell polarity (GO:0030011)	6	1	2.48E+00	1.732e-02
cellular component organization (GO:0016043)	4248	6	1.75E+03	1.863e-02
muscle contraction (GO:0006936)	198	2	8.17E+01	1.992e-02
cardiac muscle fiber development	7	1	2.89E+00	2.020e-02

(GO:0048739)				
skeletal myofibril assembly (GO:0014866)	7	1	2.89E+00	2.020e-02
cellular component organization or biogenesis (GO:0071840)	4354	6	1.80E+03	2.128e-02
anatomical structure formation involved in morphogenesis (GO:0048646)	781	3	3.22E+02	2.297e-02
single-organism developmental process (GO:0044767)	4587	6	1.89E+03	2.816e-02
muscle system process (GO:0003012)	237	2	9.78E+01	2.830e-02
developmental process (GO:0032502)	4634	6	1.91E+03	2.973e-02
negative regulation of cell cycle (GO:0045786)	252	2	1.04E+02	3.189e-02
muscle organ development (GO:0007517)	252	2	1.04E+02	3.189e-02
cellular component morphogenesis (GO:0032989)	878	3	3.62E+02	3.197e-02
hemidesmosome assembly (GO:0031581)	12	1	4.95E+00	3.460e-02
cellular protein localization (GO:0034613)	919	3	3.79E+02	3.635e-02
cellular macromolecule localization (GO:0070727)	924	3	3.81E+02	3.691e-02
anatomical structure morphogenesis (GO:0009653)	1926	4	7.95E+02	3.731e-02
mitotic chromosome condensation (GO:0007076)	13	1	5.37E+00	3.747e-02
cell cycle process (GO:0022402)	947	3	3.91E+02	3.954e-02
organelle assembly (GO:0070925)	283	2	1.17E+02	3.995e-02
adult heart development (GO:0007512)	14	1	5.78E+00	4.035e-02
endomembrane system organization (GO:0010256)	292	2	1.21E+02	4.245e-02
maintenance of protein location in nucleus (GO:0051457)	15	1	6.19E+00	4.322e-02
cardiac myofibril assembly (GO:0055003)	15	1	6.19E+00	4.322e-02
cardiac muscle hypertrophy (GO:0003300)	17	1	7.02E+00	4.897e-02

6.4 Publications

jove Journal of Visualized Experiments www.jove.com

Video Article

In Vitro Differentiation of Mature Myofibers for Live Imaging

Mafalda R. Pimentel[1], Sestina Falcone[2], Bruno Cadot[2], Edgar R. Gomes[1,2]

[1]Instituto de Medicina Molecular, Faculdade de Medicina, Universidade de Lisboa

[2]Myology Research Center, UM76-INSERM U974-CNRS FRE 361, Sorbonne University, UPMC University of Paris 6

Correspondence to: Edgar R. Gomes at edgargomes@medicina.ulisboa.pt

URL: https://www.jove.com/video/55141
DOI: doi:10.3791/55141

Keywords: Developmental Biology, Issue 119, muscle, myofiber, differentiation, *in vitro*, microscopy, development

Date Published: 1/7/2017

Citation: Pimentel, M.R., Falcone, S., Cadot, B., Gomes, E.R. *In Vitro* Differentiation of Mature Myofibers for Live Imaging. *J. Vis. Exp.* (119), e55141, doi:10.3791/55141 (2017).

Abstract

Skeletal muscles are composed of myofibers, the biggest cells in the mammalian body and one of the few syncytia. How the complex and evolutionarily conserved structures that compose it are assembled remains under investigation. Their size and physiological features often constrain manipulation and imaging applications. The culture of immortalized cell lines is widely used, but it can only replicate the early steps of differentiation.

Here, we describe a protocol that enables easy genetic manipulation of myofibers originating from primary mouse myoblasts. After one week of differentiation, the myofibers display contractility, aligned sarcomeres and triads, as well as peripheral nuclei. The entire differentiation process can be followed by live imaging or immunofluorescence. This system combines the advantages of the existing *ex vivo* and *in vitro* protocols. The possibility of easy and efficient transfection as well as the ease of access to all differentiation stages broadens the potential applications. Myofibers can subsequently be used not only to address relevant developmental and cell biology questions, but also to reproduce muscle disease phenotypes for clinical applications.

Video Link

The video component of this article can be found at https://www.jove.com/video/55141/

Introduction

Skeletal muscle composes up to 40% of the human body weight[1]. Muscle-associated disorders represent an immense health and economic burden[2]. How this highly complex and organized tissue is formed, maintained, and regenerated constitutes an extensive and well-established research field. Depending on the specific scientific interest, the most suited approach can range from simple myotube cultures to complex *in vivo* models[3-6].

The goal of this protocol is to provide an *in vitro* system that allows for the monitoring of myogenesis through live imaging and immunofluorescence. Compared to traditional approaches, this system offers a very complete and dynamic insight into the mouse myogenic process. Cells can be followed from the myoblast stage to the mature, multinucleated myofiber displaying transversal triads and peripheral nuclei[7]. This maturation level can be achieved using regular cell culture equipment, without the need for complex stimulatory or mechanical apparatuses. Although some successful *in vitro* systems have been reported[8,9], to our knowledge, this is the only protocol generating mature mouse myofibers with T-tubules transversally paired with Sarcoplasmic Reticulum (SR). Thus, this *in vitro* system can be used to study the molecular mechanisms of triad formation, which are still poorly understood[10].

A further advantage of using this system is the availability of validated mouse-targeted resources, such as antibodies, drugs, and RNAi tools. The relatively simple protocol does not require laborious steps, highly skilled manipulation, or expensive and dedicated equipment. Matured myofibers start appearing after 5 d of culture differentiation[7], displaying contractility coupled with calcium sparks (unpublished data). In one week, the different developmental stages of one of the most complex cells in the mammalian body can be studied in combination with a variety of *in vitro* assays.

Protocol

NOTE: One mouse yields sufficient myoblasts for approximately two 35 mm dishes or two live-imaging dishes, so plan mattings, dissection, and coating (step 2.6) accordingly. Since myoblasts are isolated through sequential centrifugations and preplating, the protocol should be done in batches of 5 - 10 animals.

All procedures involving animal subjects were approved by the Animal Ethics Committee at Instituto de Medicina Molecular and University Pierre et Marie Curie

1. Dissection of Neonatal Mice Hind-limb Muscles

1. Prepare all solutions in advance (**Materials Table**) and sterilize by filtration (0.22 µm filter). Make sure all media are at 37 °C before addition to the cells, except the formulations containing basement membrane matrix (*e.g.,* Matrigel).
2. Sterilize the dissection material (one each of: curved scissors, straight scissors, regular forceps, and fine-tip forceps) and the work bench by wiping them with 70% ethanol.
3. Prepare a 100 mm Petri dish with 5 mL of Dulbecco's Phosphate Buffered Saline (DPBS) for muscle collection and keep it on ice until the mincing step.
4. Decapitate P6 - P8 mice with straight scissors and sterilize the skin with 70% ethanol.
5. Make an incision in the back skin and pull it gently towards the hind limbs until it is removed, completely exposing the hind-limb musculature.
6. Use the forceps to remove fat tissue without damaging the muscles.
7. To remove the dorsal hind-limb muscles, keep the limb stretched and bend the paw to expose the heel tendons. Use the curved scissors to separate muscle from bone, starting from the tendons, by gently sliding and cutting upwards. Excise the muscles and place them in iced DPBS.
8. Isolate the quadriceps by pinching the muscle with fine-tip forceps and cutting around it without damaging the femur or the knee joint.
9. After dissecting all animals, proceed to a sterile laminar flow cell culture hood, where all the following steps should be performed.

2. Myoblast Isolation

1. Remove the excess of DPBS. Mince the tissue with sterilized curved scissors in order to obtain a uniform mass.
2. Collect the minced tissue in a 50 mL conical centrifuge tube using 5 mL of digestion mix and incubate it with agitation at 37 °C for 90 min.
3. Stop the digestion by adding 6 mL of dissection medium and centrifuge the suspension for 5 min at 75 x g to pellet the remaining tissue.
4. Carefully collect the supernatant. Make sure to not collect tissue debris. Centrifuge it at 350 x g for 5 min; resuspend it in 5 mL of dissection medium.
5. Filter the cell suspension through a 40 µm cell strainer. Add 25 mL of dissection medium and preplate it in a 150 mm dish for 4 h in a cell culture incubator (37 °C and 5% CO_2) to allow the fibroblasts to adhere.
6. While preplating, coat dishes with 500 µL of basement membrane matrix diluted 1:100 in cold IMDM for 1 h at RT. Wash once with DPBS and plate the cells immediately (step 2.8) or leave with growth medium until plating.
7. After preplating, collect the supernatant and centrifuge it at 350 x g for 10 min.
8. Resuspend it in growth medium and count the cells on a hemocytometer. Adjust the volume so that between 150,000 and 250,000 cells are plated per basement membrane matrix-coated dish. Keep the cells in a cell culture incubator.

3. Myofiber Differentiation

NOTE: After 3 d, the cells should start to fuse and form myotubes at around 70% confluency (**Figure 1B**).

1. At this point, transfect the cells, if desired, with a siRNA or DNA of interest. If the cells are not to be transfected, change directly to differentiation medium and skip to step 3.4.
2. Transfect with transfection reagents following the manufacturer's instructions. Incubate the cells for 5 h with siRNA-lipid complexes (20 nM + 1 µL of reagent) or DNA-lipid complexes (1 µg + 1 µL of reagent). Optimize the siRNA and DNA concentrations if necessary.
3. Wash them once with differentiation medium and then switch to new differentiation medium.
4. The following day, dilute the basement membrane matrix 1:2 in ice-cold differentiation medium. Remove the existing medium and add 200 µL of ice-cold matrix to each dish.
5. Incubate for 30 min in a cell culture incubator.
6. Supplement the differentiation medium with agrin (100 ng/mL) and carefully add 2 mL to the cells.
7. Carefully change half of the medium every 2 d, always supplementing with agrin to a final concentration of 100 ng/µL.
8. Monitor cell differentiation and viability. Depending on a variety of factors (such as FBS and chicken embryo extract origins), the cells might take between 5 - 10 differentiation d to reach full maturation (**Figure 2**).

4. Immunostaining in Glass-bottom Dishes

1. For immunostaining, at any time-point of interest, wash the cells once with DPBS and fix them with 4% PFA at RT for 10 min.
2. Wash them twice with DPBS. At this point, the cells can be stored at 4 °C.
3. Permeabilize them with 0.5% Triton X-100 for 5 min at RT.
4. Wash them twice with PBS and block with blocking solution for 30 min at RT.
5. Incubate them with primary antibody diluted in blocking solution O/N at 4 °C.
6. Wash 3x with DPBS for 5 min at RT.
7. Incubate them with the secondary antibody and 0.2 µg/mL of DAPI for 1 h at RT.
8. Wash 3x with DPBS for 5 min at RT.
9. Add 200 µL of mounting medium and proceed to imaging.

Representative Results

The extent of myofiber development is mostly determined by the purity and viability of the isolated myoblasts. The adhesion, proliferation, and fusion capacity can be used to empirically access those parameters (**Figure 1 A, B**). At proliferation D2, myoblasts should have adhered and should display the typical fusiform shape. Proliferation is expected to happen extensively at this stage, leading to spontaneous myotube formation the following day (**Figure 1B**).

Cell confluency might need slight adjustments. It should be increased if myoblasts take more than 3 d to proliferate and fuse. It should be decreased if myofibers are not allowed to grow and elongate relatively straight due to their density. Confluency typically decreases from the center to the periphery of the dish, so the best myofibers should be found towards the outer regions.

Myotubes will quickly elongate and display multiple centrally aligned nuclei (**Figure 1C**). By D5, some cells start acquiring striations and moving their nuclei to the periphery. The number of myofibers with mature characteristics will increase with time as well as with cell thickness (**Figure 1D**).

The degree of differentiation can be further observed by immunofluorescence. Myofibers fixed at differentiation D8 present transversal triads. This can be confirmed by imaging components of the T-tubules (DPHR) and the SR (triadin), which are expected to colocalize at the triads (**Figure 2**).

The functionality of myofibers can be addressed by live imaging. From differentiation D3 onwards, the cells display spontaneous twitching. By transfecting a calcium sensor (*e.g.,* GCaMP6f[11]), it is possible to observe that the contractions are coupled with calcium peaks (**Figure 3**).

Using this system, we were able to identify a novel molecular pathway that is disrupted in centronuclear myopathies and myotonic dystrophies, which can therefore be a novel target for innovative molecular therapies[7]. We have also adapted this method to study the development of the neuromuscular junction (NMJ)[12]. Through the coculture with rat spinal cord explants, we have described a role for dynein in NMJ formation[13].

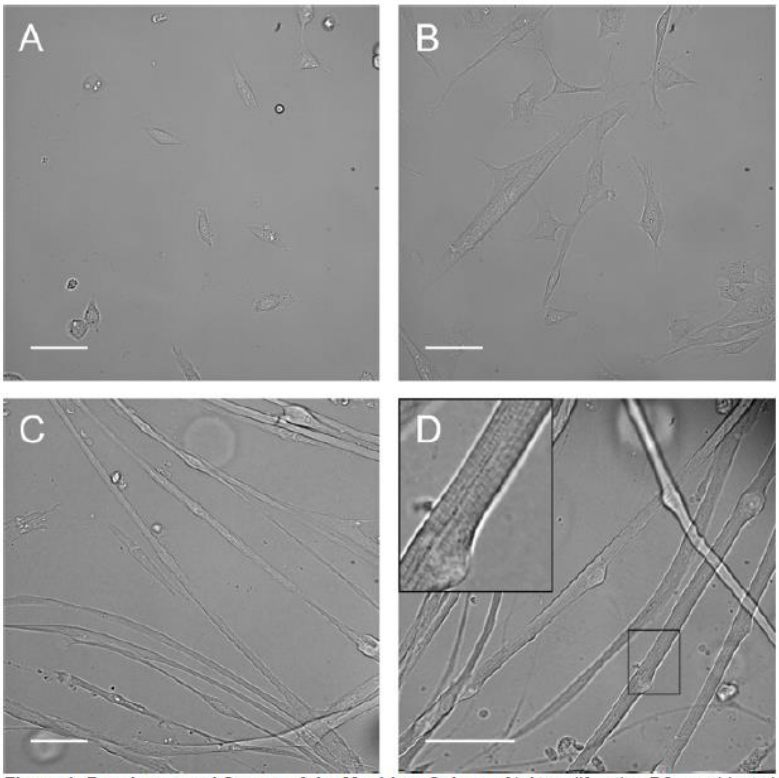

Figure 1: Developmental Stages of the Myoblast Culture. A) At proliferation D2, myoblasts have adhered and started proliferating. **B**) At proliferation D3, a confluency of 60 - 80% is reached, and myoblasts start fusing spontaneously. **C**) At differentiation D3, myotubes containing centrally located nuclei are predominant. **D**) From differentiation D5 onwards (*e.g.,* day 8), myofibers start exhibiting striations and peripheral nuclei and begin to thicken. Scale bar: 50 µm. Please click here to view a larger version of this figure.

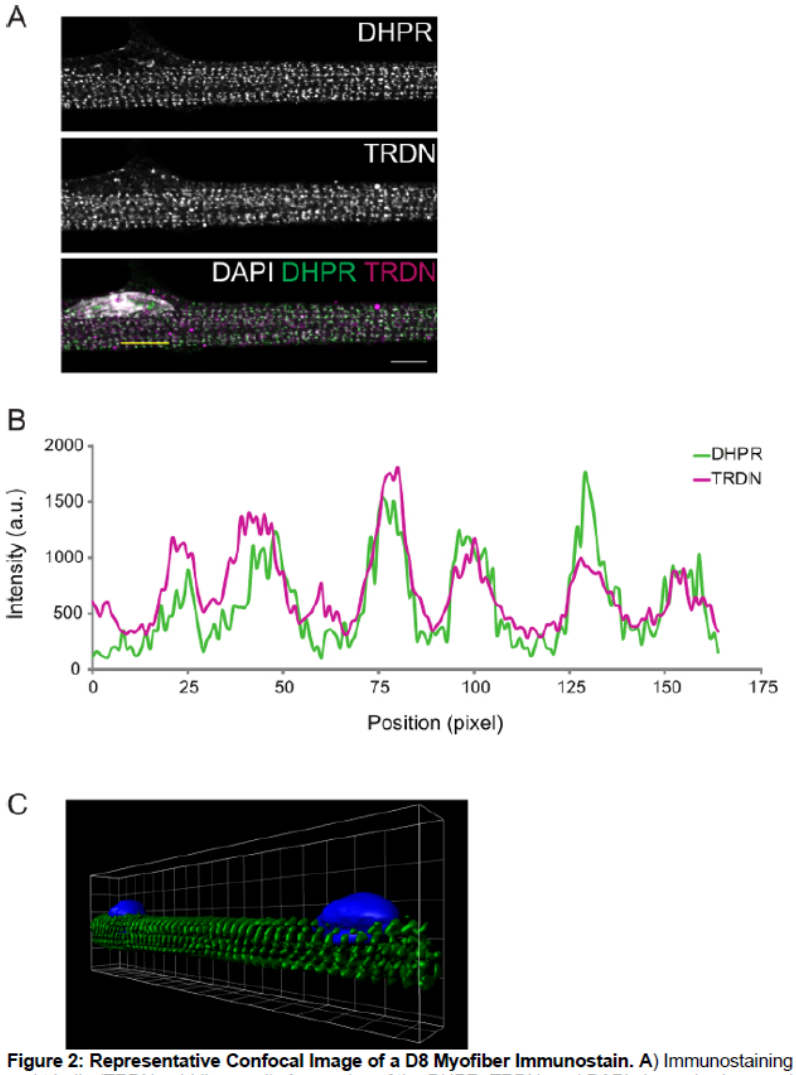

Figure 2: Representative Confocal Image of a D8 Myofiber Immunostain. A) Immunostaining for dihydropyridine receptor (DHPR, top panel) and triadin (TRDN, middle panel). An overlay of the DHPR, TRDN, and DAPI channels shows colocalization of the triad components. **B**) An intensity profile of the yellow line drawn in A. **C**) A 3D image of volume rendering of myofibers stained for α-actinin (green) and DAPI (blue). Scale bar and grid width: 5 µm. Please click here to view a larger version of this figure.

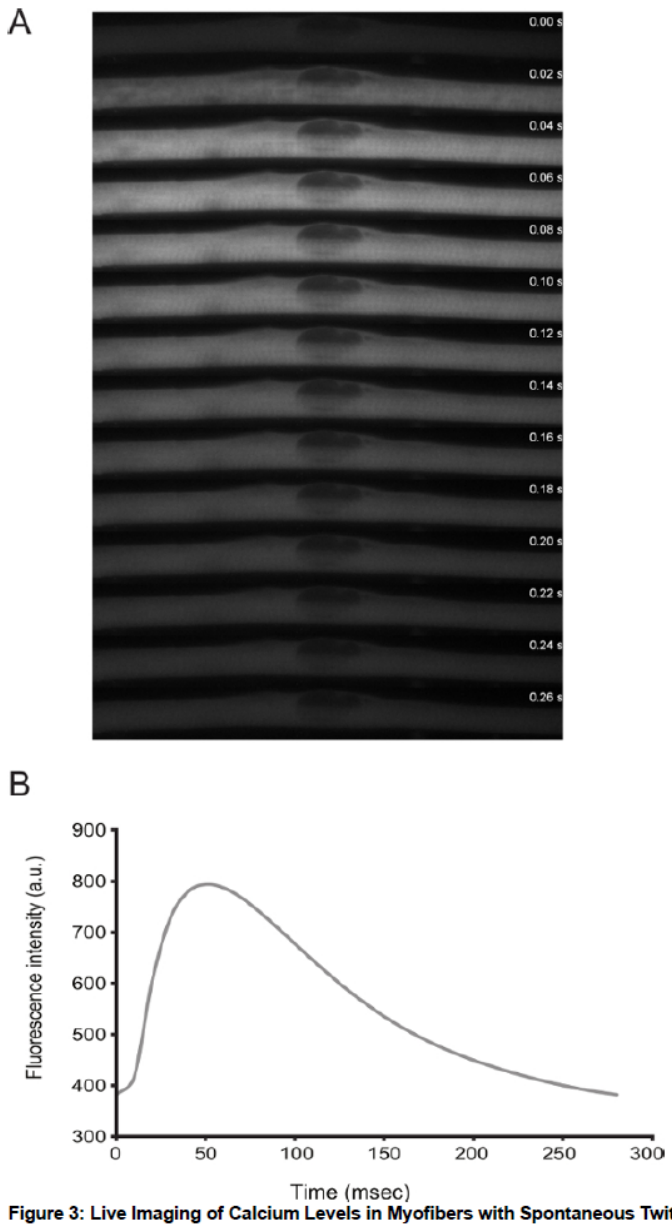

Figure 3: Live Imaging of Calcium Levels in Myofibers with Spontaneous Twitching. A) High-speed time-lapse (20 ms frames) microscopy of a calcium spark in a twitching myofiber. Calcium was detected through the expression of GCaMP6f (Addgene plasmid #40755). **B**) Quantification of the fluorescence intensity over time for the calcium sensor in panel A. Please click here to view a larger version of this figure.

Discussion

The use of this protocol for the cultivation of primary myoblasts gives rise to a special niche that greatly nurtures the development of myofibers. This is partially due to other cell types that are also present in very small numbers. A balance between myoblast concentration and culture purity must be achieved. A good cell culture also depends on the quality of the products used for the medium formulation. All products derived from animal sources should be thoroughly tested. In our experience, the digestion conditions should also be monitored.

As usual for primary cultures, experimental variability can be higher than in studies with isolated fibers or immortalized myoblasts. This variability can be diminished by the standardization of medium and digestion components, mice age and size, and the time points for culture manipulation

and results collection. Nevertheless, the advantage of scrutinizing in real time the intricate mechanisms necessary for myofiber development greatly surpasses the variability drawback.

This protocol confers the advantages of *in vitro* approaches without compromising cell differentiation. Myofibers mature until triads are formed and contractions are coupled to calcium sparks. These functional outputs can be accessed in different experimental conditions. Furthermore, there can be many technical variations made to the protocol. Myoblasts can be harvested from neonatal mice with mutations of interest relating to muscle development. Cells can be lysed for biochemical analysis at different differentiation time points. Calcium indicators can be added to the culture to follow its dynamics. Optogenetic constructs can be used to enforce certain signaling pathways or to induce specific local responses. Finally, the myofibers can be cocultured with other cells types to study their interactions.

Disclosures

The authors have nothing to disclose.

Acknowledgements

This work was supported by the European Research Council (ERG) and EMBO installation (ERG) and by a PhD fellowship from the Fundação para a Ciência e Tecnologia (MP).

References

1. Janssen, I., Heymsfield, S. B., Wang, Z., & Ross, R. Skeletal muscle mass and distribution in 468 men and women aged 18-88 yr. *J Appl Physiol.* **89** (1), 81-88 (2000).
2. Manring, H., Abreu, E., Brotto, L., Weisleder, N., & Brotto, M. Novel excitation-contraction coupling related genes reveal aspects of muscle weakness beyond atrophy-new hopes for treatment of musculoskeletal diseases. *Front Physiol.* **5**, 37 (2014).
3. Yaffe, D., & Saxel, O. Serial passaging and differentiation of myogenic cells isolated from dystrophic mouse muscle. *Nature.* **270** (5639), 725-727 (1977).
4. Pasut, A., Jones, A. E., & Rudnicki, M. A. Isolation and Culture of Individual Myofibers and their Satellite Cells from Adult Skeletal Muscle. *J Vis Exp.* (73) (2013).
5. Meng, H., Janssen, P. M. L., *et al.* Tissue Triage and Freezing for Models of Skeletal Muscle Disease. *J Vis Exp.* (89) (2014).
6. Demonbreun, A. R., & McNally, E. M. DNA Electroporation, Isolation and Imaging of Myofibers. *J Vis Exp.* (106) (2015).
7. Falcone, S., Roman, W., *et al.* N-WASP is required for Amphiphysin-2/BIN1-dependent nuclear positioning and triad organization in skeletal muscle and is involved in the pathophysiology of centronuclear myopathy. *EMBO Mol Med.* **6** (11), 1455-1475 (2014).
8. Flucher, B. E., Phillips, J. L., & Powell, J. A. Dihydropyridine receptor alpha subunits in normal and dysgenic muscle in vitro: expression of alpha 1 is required for proper targeting and distribution of alpha 2. *J Cell Biol.* **115** (5), 1345-1356 (1991).
9. Cooper, S. T., Maxwell, A. L., *et al.* C2C12 co-culture on a fibroblast substratum enables sustained survival of contractile, highly differentiated myotubes with peripheral nuclei and adult fast myosin expression. *Cell Motil Cytoskeleton.* **58** (3), 200-211 (2004).
10. Al-Qusairi, L., & Laporte, J. T-tubule biogenesis and triad formation in skeletal muscle and implication in human diseases. *Skelet Muscle.* **1**, 26 (2011).
11. Vilmont, V., Cadot, B., Ouanounou, G., & Gomes, E. R. A system to study mechanisms of neuromuscular junction development and maintenance. *Development.* (2016).
12. Vilmont, V., Cadot, B., Vezin, E., Le Grand, F., & Gomes, E. R. Dynein disruption perturbs post-synaptic components and contributes to impaired MuSK clustering at the NMJ: implication in ALS. *Sci Rep.* **6**, 27804 (2016).

7 Bibliography

Ahn, A.H., and Kunkel, L.M. (1993). The structural and functional diversity of dystrophin. Nat. Genet. *3*, 283–291.

Alami, N.H., Smith, R.B., Carrasco, M.A., Williams, L.A., Winborn, C.S., Han, S.S.W., Kiskinis, E., Winborn, B., Freibaum, B.D., Kanagaraj, A., et al. (2014). Axonal transport of TDP-43 mRNA granules is impaired by ALS-causing mutations. Neuron *81*, 536–543.

Allen, D.G., Lamb, G.D., and Westerblad, H. (2008). Skeletal Muscle Fatigue: Cellular Mechanisms. Physiol. Rev. *88*, 287–332.

Al-Qusairi, L., and Laporte, J. (2011). T-tubule biogenesis and triad formation in skeletal muscle and implication in human diseases. Skelet. Muscle *1*, 26.

Aminoff, M.J. (2005). Myology, Basic and Clincal, 3rd Edition, edited by Andrew G. Engel and Clara Franzini-Armstrong, 2 vols., 1960 pp., ill., New York, McGraw-Hill, 2004, $395. Muscle Nerve *31*, 531–531.

Amrute-Nayak, M., and Bullock, S.L. (2012). Single-molecule assays reveal that RNA localization signals regulate dynein–dynactin copy number on individual transcript cargoes. Nat. Cell Biol. *14*, 416.

Andersen, J.L. (2003). Muscle fibre type adaptation in the elderly human muscle. Scand. J. Med. Sci. Sports *13*, 40–47.

Arregui, C.O., Mas, C.R., Argaraña, C.E., and Barra, H.S. (1997). Tubulin tyrosine ligase: Protein and mRNA expression in developing rat skeletal muscle. Dev. Growth Differ. *39*, 167–178.

Barbosa, D.J., Duro, J., Prevo, B., Cheerambathur, D.K., Carvalho, A.X., and Gassmann, R. (2017). Dynactin binding to tyrosinated microtubules promotes centrosome centration in C. elegans by enhancing dynein-mediated organelle transport. PLoS Genet. *13*, e1006941.

Batish, M., Raj, A., and Tyagi, S. (2011). Single Molecule Imaging of RNA In Situ. In RNA Detection and Visualization, (Humana Press, Totowa, NJ), pp. 3–13.

Baumann, S., Pohlmann, T., Jungbluth, M., Brachmann, A., and Feldbrügge, M. (2012). Kinesin-3 and dynein mediate microtubule-dependent co-transport of mRNPs and endosomes. J Cell Sci *125*, 2740–2752.

Beard, N.A., Wei, L., and Dulhunty, A.F. (2009). Control of Muscle Ryanodine Receptor Calcium Release Channels by Proteins in the Sarcoplasmic Reticulum Lumen. Clin. Exp. Pharmacol. Physiol. *36*, 340–345.

Becalska, A.N., Kim, Y.R., Belletier, N.G., Lerit, D.A., Sinsimer, K.S., and Gavis, E.R. (2011). Aubergine is a component of a nanos mRNA localization complex. Dev. Biol. *349*, 46–52.

Becht, P., König, J., and Feldbrügge, M. (2006). The RNA-binding protein Rrm4 is essential for polarity in Ustilago maydis and shuttles along microtubules. J. Cell Sci. *119*, 4964–4973.

Belanto, J.J., Mader, T.L., Eckhoff, M.D., Strandjord, D.M., Banks, G.B., Gardner, M.K., Lowe, D.A., and Ervasti, J.M. (2014). Microtubule binding distinguishes dystrophin from utrophin. Proc. Natl. Acad. Sci. *111*, 5723–5728.

Belanto, J.J., Olthoff, J.T., Mader, T.L., Chamberlain, C.M., Nelson, D.M., McCourt, P.M., Talsness, D.M., Gundersen, G.G., Lowe, D.A., and Ervasti, J.M. (2016). Independent variability of microtubule perturbations associated with dystrophinopathy. Hum. Mol. Genet. *25*, 4951–4961.

Ben-Ari, Y., Brody, Y., Kinor, N., Mor, A., Tsukamoto, T., Spector, D.L., Singer, R.H., and Shav-Tal, Y. (2010). The life of an mRNA in space and time. J. Cell Sci. *123*, 1761–1774.

Bentzinger, C.F., Wang, Y.X., and Rudnicki, M.A. (2012). Building Muscle: Molecular Regulation of Myogenesis. Cold Spring Harb. Perspect. Biol. *4*, a008342.

Berezuk, M.A., and Schroer, T.A. (2007). Dynactin enhances the processivity of kinesin-2. Traffic Cph. Den. *8*, 124–129.

Bergsten, S.E., and Gavis, E.R. (1999). Role for mRNA localization in translational activation but not spatial restriction of nanos RNA. Dev. Camb. Engl. *126*, 659–669.

Berleth, T., Burri, M., Thoma, G., Bopp, D., Richstein, S., Frigerio, G., Noll, M., and Nüsslein-Volhard, C. (1988). The role of localization of bicoid RNA in organizing the anterior pattern of the Drosophila embryo. EMBO J. *7*, 1749–1756.

Bernard, F., Lepesant, J.-A., and Guichet, A. (2018). Nucleus positioning within Drosophila egg chamber. Semin. Cell Dev. Biol. *82*, 25–33.

Biancalana, V., Beggs, A.H., Das, S., Jungbluth, H., Kress, W., Nishino, I., North, K., Romero, N.B., and Laporte, J. (2012). Clinical utility gene card for: Centronuclear and myotubular myopathies. Eur. J. Hum. Genet. *20*.

Birsoy, B., Kofron, M., Schaible, K., Wylie, C., and Heasman, J. (2006). Vg 1 is an essential signaling molecule in Xenopus development. Dev. Camb. Engl. *133*, 15–20.

Bischoff, R. (1975). Regeneration of single skeletal muscle fibers in vitro. Anat. Rec. *182*, 215–235.

Blau, H.M., Chiu, C.P., and Webster, C. (1983). Cytoplasmic activation of human nuclear genes in stable heterocaryons. Cell *32*, 1171–1180.

Blobel, G., and Dobberstein, B. (1975). Transfer of proteins across membranes. II. Reconstitution of functional rough microsomes from heterologous components. J. Cell Biol. *67*, 852–862.

Bobola, N., Jansen, R.-P., Shin, T.H., and Nasmyth, K. (1996). Asymmetric Accumulation of Ash1p in Postanaphase Nuclei Depends on a Myosin and Restricts Yeast Mating-Type Switching to Mother Cells. Cell *84*, 699–709.

Brendza, R.P., Serbus, L.R., Duffy, J.B., and Saxton, W.M. (2000). A Function for Kinesin I in the Posterior Transport of oskar mRNA and Staufen Protein. Science *289*, 2120–2122.

Brinegar, A.E., and Cooper, T.A. (2016). Roles for RNA-binding proteins in development and disease. Brain Res. *1647*, 1–8.

Bruusgaard, J.C., and Gundersen, K. (2008). In vivo time-lapse microscopy reveals no loss of murine myonuclei during weeks of muscle atrophy. J. Clin. Invest. *118*, 1450–1457.

Bruusgaard, J.C., Liestøl, K., Ekmark, M., Kollstad, K., and Gundersen, K. (2003). Number and spatial distribution of nuclei in the muscle fibres of normal mice studied in vivo. J. Physiol. *551*, 467–478.

Bruusgaard, J.C., Liestøl, K., and Gundersen, K. (2006). Distribution of myonuclei and microtubules in live muscle fibers of young, middle-aged, and old mice. J. Appl. Physiol. *100*, 2024–2030.

Bruusgaard, J.C., Johansen, I.B., Egner, I.M., Rana, Z.A., and Gundersen, K. (2010). Myonuclei acquired by overload exercise precede hypertrophy and are not lost on detraining. Proc. Natl. Acad. Sci. *107*, 15111–15116.

Buckingham, M., and Relaix, F. (2015). PAX3 and PAX7 as upstream regulators of myogenesis. Semin. Cell Dev. Biol. *44*, 115–125.

Buckley, P.T., Lee, M.T., Sul, J.-Y., Miyashiro, K.Y., Bell, T.J., Fisher, S.A., Kim, J., and Eberwine, J. (2011). Cytoplasmic Intron Sequence-Retaining Transcripts Can Be Dendritically Targeted via ID Element Retrotransposons. Neuron *69*, 877–884.

Bugnard, E., Zaal, K.J.M., and Ralston, E. (2005). Reorganization of microtubule nucleation during muscle differentiation. Cell Motil. Cytoskeleton *60*, 1–13.

Bullock, S.L., and Ish-Horowicz, D. (2001). Conserved signals and machinery for RNA transport in Drosophila oogenesis and embryogenesis. Nature *414*, 611–616.

Bullock, S.L., Nicol, A., Gross, S.P., and Zicha, D. (2006). Guidance of Bidirectional Motor Complexes by mRNA Cargoes through Control of Dynein Number and Activity. Curr. Biol. *16*, 1447–1452.

Buxbaum, A.R., Wu, B., and Singer, R.H. (2014). Single β-Actin mRNA Detection in Neurons Reveals a Mechanism for Regulating Its Translatability. Science *343*, 419–422.

Buxbaum, A.R., Haimovich, G., and Singer, R.H. (2015). In the right place at the right time: visualizing and understanding mRNA localization. Nat. Rev. Mol. Cell Biol. *16*, 95–109.

Cadot, B., Gache, V., Vasyutina, E., Falcone, S., Birchmeier, C., and Gomes, E.R. (2012). Nuclear movement during myotube formation is microtubule and dynein dependent and is regulated by Cdc42, Par6 and Par3. EMBO Rep. *13*, 741–749.

Cadot, B., Gache, V., and Gomes, E.R. (2015). Moving and positioning the nucleus in skeletal muscle – one step at a time. Nucleus *6*, 01–09.

Cajigas, I.J., Tushev, G., Will, T.J., tom Dieck, S., Fuerst, N., and Schuman, E.M. (2012). The Local Transcriptome in the Synaptic Neuropil Revealed by Deep Sequencing and High-Resolution Imaging. Neuron *74*, 453–466.

Can, T., Faas, L., Ashford, D.A., Dowle, A., Thomas, J., O'Toole, P., and Blanco, G. (2014). Proteomic analysis of laser capture microscopy purified myotendinous junction regions from muscle sections. Proteome Sci. *12*, 25.

Capetanaki, Y., Bloch, R.J., Kouloumenta, A., Mavroidis, M., and Psarras, S. (2007). Muscle intermediate filaments and their links to membranes and membranous organelles. Exp. Cell Res. *313*, 2063–2076.

Cardamone, M., Darras, B.T., and Ryan, M.M. (2008). Inherited Myopathies and Muscular Dystrophies. Semin. Neurol. *28*, 250–259.

Cha, B.J., Koppetsch, B.S., and Theurkauf, W.E. (2001). In vivo analysis of Drosophila bicoid mRNA localization reveals a novel microtubule-dependent axis specification pathway. Cell *106*, 35–46.

Chang, W., Webster, D.R., Salam, A.A., Gruber, D., Prasad, A., Eiserich, J.P., and Bulinski, J.C. (2002). Alteration of the C-terminal Amino Acid of Tubulin Specifically Inhibits Myogenic Differentiation. J. Biol. Chem. *277*, 30690–30698.

Chapman, M.A., Zhang, J., Banerjee, I., Guo, L.T., Zhang, Z., Shelton, G.D., Ouyang, K., Lieber, R.L., and Chen, J. (2014). Disruption of both nesprin 1 and desmin results in nuclear anchorage defects and fibrosis in skeletal muscle. Hum. Mol. Genet. *23*, 5879–5892.

Chartrand, P., Meng, X.H., Huttelmaier, S., Donato, D., and Singer, R.H. (2002). Asymmetric sorting of ash1p in yeast results from inhibition of translation by localization elements in the mRNA. Mol. Cell *10*, 1319–1330.

Cheng, A.J., and Westerblad, H. (2017). Mechanical isolation, and measurement of force and myoplasmic free [Ca2+] in fully intact single skeletal muscle fibers. Nat. Protoc. *12*, 1763–1776.

Cherednichenko, G., Hurne, A.M., Fessenden, J.D., Lee, E.H., Allen, P.D., Beam, K.G., and Pessah, I.N. (2004). Conformational activation of Ca2+ entry by depolarization of skeletal myotubes. Proc. Natl. Acad. Sci. U. S. A. *101*, 15793–15798.

Chretien, F., Dreyfus, P.A., Christov, C., Caramelle, P., Lagrange, J.-L., Chazaud, B., and Gherardi, R.K. (2005). In Vivo Fusion of Circulating Fluorescent Cells with Dystrophin-Deficient Myofibers Results in Extensive Sarcoplasmic Fluorescence

Expression but Limited Dystrophin Sarcolemmal Expression. Am. J. Pathol. *166*, 1741–1748.

Cianfrocco, M.A., DeSantis, M.E., Leschziner, A.E., and Reck-Peterson, S.L. (2015). Mechanism and Regulation of Cytoplasmic Dynein. Annu. Rev. Cell Dev. Biol. *31*, 83–108.

Clark, A., Meignin, C., and Davis, I. (2007). A Dynein-dependent shortcut rapidly delivers axis determination transcripts into the Drosophila oocyte. Development *134*, 1955–1965.

Clark, K.A., McElhinny, A.S., Beckerle, M.C., and Gregorio, C.C. (2002). STRIATED MUSCLE CYTOARCHITECTURE: An Intricate Web of Form and Function. Annu. Rev. Cell Dev. Biol. *18*, 637–706.

Cohn, R.D., and Campbell, K.P. (2000). Molecular basis of muscular dystrophies. Muscle Nerve *23*, 1456–1471.

Cui, X.A., and Palazzo, A.F. (2014). Localization of mRNAs to the endoplasmic reticulum. Wiley Interdiscip. Rev. RNA n/a-n/a.

Cui, X.A., Zhang, H., and Palazzo, A.F. (2012). p180 Promotes the Ribosome-Independent Localization of a Subset of mRNA to the Endoplasmic Reticulum. PLoS Biol *10*, e1001336.

Dale, L., Matthews, G., and Colman, A. (1993). Secretion and mesoderm-inducing activity of the TGF-beta-related domain of Xenopus Vg1. EMBO J. *12*, 4471–4480.

Danoviz, M.E., and Yablonka-Reuveni, Z. (2012). Skeletal muscle satellite cells: background and methods for isolation and analysis in a primary culture system. Methods Mol. Biol. Clifton NJ *798*, 21–52.

David, A., Dolan, B.P., Hickman, H.D., Knowlton, J.J., Clavarino, G., Pierre, P., Bennink, J.R., and Yewdell, J.W. (2012). Nuclear translation visualized by ribosome-bound nascent chain puromycylation. J. Cell Biol. *197*, 45–57.

Davidovic, L., Jaglin, X.H., Lepagnol-Bestel, A.-M., Tremblay, S., Simonneau, M., Bardoni, B., and Khandjian, E.W. (2007). The fragile X mental retardation protein is a molecular adaptor between the neurospecific KIF3C kinesin and dendritic RNA granules. Hum. Mol. Genet. *16*, 3047–3058.

Deacon, S.W., Serpinskaya, A.S., Vaughan, P.S., Lopez Fanarraga, M., Vernos, I., Vaughan, K.T., and Gelfand, V.I. (2003). Dynactin is required for bidirectional organelle transport. J. Cell Biol. *160*, 297–301.

Delanoue, R., Herpers, B., Soetaert, J., Davis, I., and Rabouille, C. (2007). Drosophila Squid/hnRNP Helps Dynein Switch from a gurken mRNA Transport Motor to an Ultrastructural Static Anchor in Sponge Bodies. Dev. Cell *13*, 523–538.

Dictenberg, J.B., Swanger, S.A., Antar, L.N., Singer, R.H., and Bassell, G.J. (2008). A Direct Role for FMRP in Activity-Dependent Dendritic mRNA Transport

Links Filopodial-Spine Morphogenesis to Fragile X Syndrome. Dev. Cell *14*, 926–939.

Dienstbier, M., Boehl, F., Li, X., and Bullock, S.L. (2009). Egalitarian is a selective RNA-binding protein linking mRNA localization signals to the dynein motor. Genes Dev. *23*, 1546–1558.

Dix, D., and Eisenberg, B. (1988). Insitu Hybridization and Immunocytochemistry in Serial Sections of Rabbit Skeletal-Muscle to Detect Myosin Expression. J. Histochem. Cytochem. *36*, 1519–1526.

Dix, D.J., and Eisenberg, B.R. (1990). Myosin mRNA accumulation and myofibrillogenesis at the myotendinous junction of stretched muscle fibers. J. Cell Biol. *111*, 1885–1894.

Donnelly, C.J., Willis, D.E., Xu, M., Tep, C., Jiang, C., Yoo, S., Schanen, N.C., Kirn-Safran, C.B., van Minnen, J., English, A., et al. (2011). Limited availability of ZBP1 restricts axonal mRNA localization and nerve regeneration capacity. EMBO J. *30*, 4665–4677.

Doyle, M., and Kiebler, M.A. (2011). Mechanisms of dendritic mRNA transport and its role in synaptic tagging. EMBO J. *30*, 3540–3552.

Duncan, J.E., and Warrior, R. (2002). The cytoplasmic dynein and kinesin motors have interdependent roles in patterning the Drosophila oocyte. Curr. Biol. CB *12*, 1982–1991.

Egner, I.M., Bruusgaard, J.C., Eftestøl, E., and Gundersen, K. (2013). A cellular memory mechanism aids overload hypertrophy in muscle long after an episodic exposure to anabolic steroids. J. Physiol. *591*, 6221–6230.

Eliscovich, C., Peset, I., Vernos, I., and Méndez, R. (2008). Spindle-localized CPE-mediated translation controls meiotic chromosome segregation. Nat. Cell Biol. *10*, 858–865.

Englander, L.L., and Rubin, L.L. (1987). Acetylcholine receptor clustering and nuclear movement in muscle fibers in culture. J. Cell Biol. *104*, 87–95.

Eom, T., Antar, L.N., Singer, R.H., and Bassell, G.J. (2003). Localization of a beta-actin messenger ribonucleoprotein complex with zipcode-binding protein modulates the density of dendritic filopodia and filopodial synapses. J. Neurosci. Off. J. Soc. Neurosci. *23*, 10433–10444.

Ephrussi, A., and Lehmann, R. (1992). Induction of germ cell formation by oskar. Nature *358*, 387–392.

Epstein, E., Sela-Brown, A., Ringel, I., Kilav, R., King, S.M., Benashski, S.E., Yisraeli, J.K., Silver, J., and Naveh-Many, T. (2000). Dynein light chain binding to a 3′-untranslated sequence mediates parathyroid hormone mRNA association with microtubules. J. Clin. Invest. *105*, 505–512.

Erdélyi, M., Michon, A.M., Guichet, A., Glotzer, J.B., and Ephrussi, A. (1995). Requirement for Drosophila cytoplasmic tropomyosin in oskar mRNA localization. Nature *377*, 524–527.

Ervasti, J.M. (2003). Costameres: the Achilles' Heel of Herculean Muscle. J. Biol. Chem. *278*, 13591–13594.

Falcone, S., Roman, W., Hnia, K., Gache, V., Didier, N., Lainé, J., Auradé, F., Marty, I., Nishino, I., Charlet-Berguerand, N., et al. (2014). N-WASP is required for Amphiphysin-2/BIN1-dependent nuclear positioning and triad organization in skeletal muscle and is involved in the pathophysiology of centronuclear myopathy. EMBO Mol. Med. *6*, 1455–1475.

Farina, K.L., Hüttelmaier, S., Musunuru, K., Darnell, R., and Singer, R.H. (2003). Two ZBP1 KH domains facilitate β-actin mRNA localization, granule formation, and cytoskeletal attachment. J. Cell Biol. *160*, 77–87.

Ferrandon, D., Elphick, L., Nüsslein-Volhard, C., and St Johnston, D. (1994). Staufen protein associates with the 3'UTR of bicoid mRNA to form particles that move in a microtubule-dependent manner. Cell *79*, 1221–1232.

Ferrandon, D., Koch, I., Westhof, E., and Nüsslein-Volhard, C. (1997). RNA-RNA interaction is required for the formation of specific bicoid mRNA 3' UTR-STAUFEN ribonucleoprotein particles. EMBO J. *16*, 1751–1758.

Firestone, A.J., Weinger, J.S., Maldonado, M., Barlan, K., Langston, L.D., O'Donnell, M., Gelfand, V.I., Kapoor, T.M., and Chen, J.K. (2012). Small-molecule inhibitors of the AAA+ ATPase motor cytoplasmic dynein. Nature *484*, 125–129.

Flucher, B.E. (1992). Structural analysis of muscle development: Transverse tubules, sarcoplasmic reticulum, and the triad. Dev. Biol. *154*, 245–260.

Flucher, B.E., Phillips, J.L., and Powell, J.A. (1991). Dihydropyridine receptor alpha subunits in normal and dysgenic muscle in vitro: expression of alpha 1 is required for proper targeting and distribution of alpha 2. J. Cell Biol. *115*, 1345–1356.

Folker, E.S., Schulman, V.K., and Baylies, M.K. (2012). Muscle length and myonuclear position are independently regulated by distinct Dynein pathways. Development *139*, 3827–3837.

Fontaine, B., and Changeux, J.P. (1989). Localization of nicotinic acetylcholine receptor alpha-subunit transcripts during myogenesis and motor endplate development in the chick. J. Cell Biol. *108*, 1025–1037.

Forrest, K.M., and Gavis, E.R. (2003). Live imaging of endogenous RNA reveals a diffusion and entrapment mechanism for nanos mRNA localization in Drosophila. Curr. Biol. CB *13*, 1159–1168.

Fritzsche, R., Karra, D., Bennett, K.L., Ang, F. yee, Heraud-Farlow, J.E., Tolino, M., Doyle, M., Bauer, K.E., Thomas, S., Planyavsky, M., et al. (2013). Interactome

of Two Diverse RNA Granules Links mRNA Localization to Translational Repression in Neurons. Cell Rep. *5*, 1749–1762.

Fulton, A.B., and Alftine, C. (1997). Organization of Protein and mRNA for Titin and Other Myofibril Components during Myofibrillogenesis in Cultured Chicken Skeletal Muscle. Cell Struct. Funct. *22*, 51–58.

Fusco, D., Accornero, N., Lavoie, B., Shenoy, S.M., Blanchard, J.-M., Singer, R.H., and Bertrand, E. (2003). Single mRNA molecules demonstrate probabilistic movement in living mammalian cells. Curr. Biol. CB *13*, 161–167.

Gagnon, J.A., and Mowry, K.L. (2011). Molecular motors: directing traffic during RNA localization. Crit. Rev. Biochem. Mol. Biol. *46*, 229–239.

García-Pelagio, K.P., Bloch, R.J., Ortega, A., and González-Serratos, H. (2011). Biomechanics of the sarcolemma and costameres in single skeletal muscle fibers from normal and dystrophin-null mice. J. Muscle Res. Cell Motil. *31*, 323–336.

Gaspar, I., and Ephrussi, A. (2015). Strength in numbers: quantitative single-molecule RNA detection assays. Wiley Interdiscip. Rev. Dev. Biol. *4*, 135–150.

Gáspár, I., Sysoev, V., Komissarov, A., and Ephrussi, A. (2017). An RNA-binding atypical tropomyosin recruits kinesin-1 dynamically to oskar mRNPs. EMBO J. *36*, 319–333.

Gavis, E.R., and Lehmann, R. (1992). Localization of nanos RNA controls embryonic polarity. Cell *71*, 301–313.

Gavis, E.R., Chatterjee, S., Ford, N.R., and Wolff, L.J. (2008). Dispensability of nanos mRNA localization for abdominal patterning but not for germ cell development. Mech. Dev. *125*, 81–90.

Ghosh, S., Marchand, V., Gáspár, I., and Ephrussi, A. (2012). Control of RNP motility and localization by a splicing-dependent structure in *oskar* mRNA. Nat. Struct. Mol. Biol. *19*, 441–449.

Gibbons, I.R., and Rowe, A.J. (1965). Dynein: A Protein with Adenosine Triphosphatase Activity from Cilia. Science *149*, 424–426.

Gill, S.R., Schroer, T.A., Szilak, I., Steuer, E.R., Sheetz, M.P., and Cleveland, D.W. (1991). Dynactin, a conserved, ubiquitously expressed component of an activator of vesicle motility mediated by cytoplasmic dynein. J. Cell Biol. *115*, 1639–1650.

Gimpel, P., Lee, Y.L., Sobota, R.M., Calvi, A., Koullourou, V., Patel, R., Mamchaoui, K., Nédélec, F., Shackleton, S., Schmoranzer, J., et al. (2017). Nesprin-1α-Dependent Microtubule Nucleation from the Nuclear Envelope via Akap450 Is Necessary for Nuclear Positioning in Muscle Cells. Curr. Biol. *27*, 2999-3009.e9.

Goldstein, J.A., and McNally, E.M. (2010). Mechanisms of muscle weakness in muscular dystrophy. J. Gen. Physiol. *136*, 29–34.

González-Reyes, A., Elliott, H., and St Johnston, D. (1995). Polarization of both major body axes in Drosophila by gurken-torpedo signalling. Nature *375*, 654–658.

Grady, R.M., Starr, D.A., Ackerman, G.L., Sanes, J.R., and Han, M. (2005). Syne proteins anchor muscle nuclei at the neuromuscular junction. Proc. Natl. Acad. Sci. U. S. A. *102*, 4359–4364.

Grigoriev, I., Splinter, D., Keijzer, N., Wulf, P.S., Demmers, J., Ohtsuka, T., Modesti, M., Maly, I.V., Grosveld, F., Hoogenraad, C.C., et al. (2007). Rab6 Regulates Transport and Targeting of Exocytotic Carriers. Dev. Cell *13*, 305–314.

Grounds, M.D. (2014). The need to more precisely define aspects of skeletal muscle regeneration. Int. J. Biochem. Cell Biol.

Gu, W., Pan, F., Zhang, H., Bassell, G.J., and Singer, R.H. (2002). A predominantly nuclear protein affecting cytoplasmic localization of beta-actin mRNA in fibroblasts and neurons. J. Cell Biol. *156*, 41–51.

Guichet, A., Peri, F., and Roth, S. (2001). Stable Anterior Anchoring of the Oocyte Nucleus Is Required to Establish Dorsoventral Polarity of the Drosophila Egg. Dev. Biol. *237*, 93–106.

Gundersen, K. (2016). Muscle memory and a new cellular model for muscle atrophy and hypertrophy. J. Exp. Biol. *219*, 235–242.

Gundersen, K., and Bruusgaard, J.C. (2008). Nuclear domains during muscle atrophy: nuclei lost or paradigm lost? J. Physiol. *586*, 2675–2681.

Guo, X., Greene, K., Akanda, N., Smith, A.S.T., Stancescu, M., Lambert, S., Vandenburgh, H., and Hickman, J.J. (2013). In vitro differentiation of functional human skeletal myotubes in a defined system. Biomater. Sci. *2*, 131–138.

Gussoni, E., Blau, H.M., and Kunkel, L.M. (1997). The fate of individual myoblasts after transplantation into muscles of DMD patients. Nat. Med. *3*, 970–977.

Gutierrez, N., Eromobor, I., Petrie, R.J., Vedula, P., Cruz, L., and Rodriguez, A.J. (2014). The β-actin mRNA zipcode regulates epithelial adherens junction assembly but not maintenance. RNA *20*, 689–701.

Hall, Z.W., and Ralston, E. (1989). Nuclear domains in muscle cells. Cell *59*, 771–772.

Hancock, W.O. (2014). Bidirectional cargo transport: moving beyond tug of war. Nat. Rev. Mol. Cell Biol. *15*, 615–628.

Herbert, A.L., Fu, M., Drerup, C.M., Gray, R.S., Harty, B.L., Ackerman, S.D., O'Reilly-Pol, T., Johnson, S.L., Nechiporuk, A.V., Barres, B.A., et al. (2017). Dynein/dynactin is necessary for anterograde transport of Mbp mRNA in oligodendrocytes and for myelination in vivo. Proc. Natl. Acad. Sci. *114*, E9153–E9162.

Hinds, S., Bian, W., Dennis, R.G., and Bursac, N. (2011). The role of extracellular matrix composition in structure and function of bioengineered skeletal muscle. Biomaterials *32*, 3575–3583.

Hippenmeyer, S., Huber, R.M., Ladle, D.R., Murphy, K., and Arber, S. (2007). ETS Transcription Factor Erm Controls Subsynaptic Gene Expression in Skeletal Muscles. Neuron *55*, 726–740.

Hirokawa, N., Noda, Y., Tanaka, Y., and Niwa, S. (2009). Kinesin superfamily motor proteins and intracellular transport. Nat. Rev. Mol. Cell Biol. *10*, 682–696.

Hodges, A.R., Krementsova, E.B., and Trybus, K.M. (2008). She3p Binds to the Rod of Yeast Myosin V and Prevents It from Dimerizing, Forming a Single-headed Motor Complex. J. Biol. Chem. *283*, 6906–6914.

Holt, C.E., and Bullock, S.L. (2009). Subcellular mRNA Localization in Animal Cells and Why It Matters. Science *326*, 1212–1216.

Holzbaur, E.L., and Goldman, Y.E. (2010). Coordination of molecular motors: from in vitro assays to intracellular dynamics. Curr. Opin. Cell Biol. *22*, 4–13.

Hoogenraad, C.C., and Akhmanova, A. (2016). Bicaudal D Family of Motor Adaptors: Linking Dynein Motility to Cargo Binding. Trends Cell Biol. *26*, 327–340.

Huang, D.W., Sherman, B.T., and Lempicki, R.A. (2009a). Bioinformatics enrichment tools: paths toward the comprehensive functional analysis of large gene lists. Nucleic Acids Res. *37*, 1–13.

Huang, D.W., Sherman, B.T., and Lempicki, R.A. (2009b). Systematic and integrative analysis of large gene lists using DAVID bioinformatics resources. Nat. Protoc. *4*, 44–57.

Huang, F., Chotiner, J.K., and Steward, O. (2007). Actin Polymerization and ERK Phosphorylation Are Required for Arc/Arg3.1 mRNA Targeting to Activated Synaptic Sites on Dendrites. J. Neurosci. *27*, 9054–9067.

Hüttelmaier, S., Zenklusen, D., Lederer, M., Dictenberg, J., Lorenz, M., Meng, X., Bassell, G.J., Condeelis, J., and Singer, R.H. (2005). Spatial regulation of β-actin translation by Src-dependent phosphorylation of ZBP1. Nature *438*, 512.

Irion, U., and St Johnston, D. (2007). bicoid RNA localization requires specific binding of an endosomal sorting complex. Nature *445*, 554–558.

Jain, R.A., and Gavis, E.R. (2008). The Drosophila hnRNP M homolog Rumpelstiltskin regulates nanos mRNA localization. Dev. Camb. Engl. *135*, 973–982.

Jaka, O., Casas-Fraile, L., Munain, A.L. de, and Sáenz, A. (2015). Costamere proteins and their involvement in myopathic processes. Expert Rev. Mol. Med. *17*.

Janssen, I., Heymsfield, S.B., Wang, Z., and Ross, R. (2000). Skeletal muscle mass and distribution in 468 men and women aged 18–88 yr. J. Appl. Physiol. *89*, 81–88.

Jeffery, W., Tomlinson, C., and Richard, B. (1983). Localization of actin messenger RNA during early ascidian development. Dev. Biol. *99*, 408–417.

Jha, R., Roostalu, J., Cade, N.I., Trokter, M., and Surrey, T. (2017). Combinatorial regulation of the balance between dynein microtubule end accumulation and initiation of directed motility. EMBO J. e201797077.

Julio, S.S. (2013). Texto atlas de histología: biología celular y tisular.

Jung, H., Yoon, B.C., and Holt, C.E. (2012). Axonal mRNA localization and local protein synthesis in nervous system assembly, maintenance and repair. Nat. Rev. Neurosci. *13*, 308–324.

Jungbluth, H., and Gautel, M. (2014). Pathogenic Mechanisms in Centronuclear Myopathies. Front. Aging Neurosci. *6*.

Kaisto, T., and Metsikkö, K. (2003). Distribution of the endoplasmic reticulum and its relationship with the sarcoplasmic reticulum in skeletal myofibers. Exp. Cell Res. *289*, 47–57.

Kardon, J.R., and Vale, R.D. (2009). Regulators of the cytoplasmic dynein motor. Nat. Rev. Mol. Cell Biol. *10*, 854–865.

Karpati, G., Pouliot, Y., Zubrzycka-Gaarn, E., Carpenter, S., Ray, P.N., Worton, R.G., and Holland, P. (1989). Dystrophin is expressed in mdx skeletal muscle fibers after normal myoblast implantation. Am. J. Pathol. *135*, 27–32.

Katz, Z.B., Wells, A.L., Park, H.Y., Wu, B., Shenoy, S.M., and Singer, R.H. (2012). β-Actin mRNA compartmentalization enhances focal adhesion stability and directs cell migration. Genes Dev. *26*, 1885–1890.

Katz, Z.B., English, B.P., Lionnet, T., Yoon, Y.J., Monnier, N., Ovryn, B., Bathe, M., and Singer, R.H. (2016). Mapping translation “hot-spots” in live cells by tracking single molecules of mRNA and ribosomes. ELife *5*, e10415.

Kerr, J.P., Robison, P., Shi, G., Bogush, A.I., Kempema, A.M., Hexum, J.K., Becerra, N., Harki, D.A., Martin, S.S., Raiteri, R., et al. (2015). Detyrosinated microtubules modulate mechanotransduction in heart and skeletal muscle. Nat. Commun. *6*, 8526.

Khairallah, R.J., Shi, G., Sbrana, F., Prosser, B.L., Borroto, C., Mazaitis, M.J., Hoffman, E.P., Mahurkar, A., Sachs, F., Sun, Y., et al. (2012). Microtubules Underlie Dysfunction in Duchenne Muscular Dystrophy. Sci Signal *5*, ra56–ra56.

King, S.J., Bonilla, M., Rodgers, M.E., and Schroer, T.A. (2002). Subunit organization in cytoplasmic dynein subcomplexes. Protein Sci. Publ. Protein Soc. *11*, 1239–1250.

Kirby, T.J., Patel, R.M., McClintock, T.S., Dupont-Versteegden, E.E., Peterson, C.A., and McCarthy, J.J. (2016). Myonuclear transcription is responsive to mechanical load and DNA content but uncoupled from cell size during hypertrophy. Mol. Biol. Cell *27*, 788–798.

Kislauskis, E.H., Zhu, X., and Singer, R.H. (1994). Sequences responsible for intracellular localization of beta-actin messenger RNA also affect cell phenotype. J. Cell Biol. *127*, 441–451.

Kislauskis, E.H., Zhu, X., and Singer, R.H. (1997). beta-Actin messenger RNA localization and protein synthesis augment cell motility. J. Cell Biol. *136*, 1263–1270.

Knowles, R.B., Sabry, J.H., Martone, M.E., Deerinck, T.J., Ellisman, M.H., Bassell, G.J., and Kosik, K.S. (1996). Translocation of RNA granules in living neurons. J. Neurosci. Off. J. Soc. Neurosci. *16*, 7812–7820.

König, J., Baumann, S., Koepke, J., Pohlmann, T., Zarnack, K., and Feldbrügge, M. (2009). The fungal RNA-binding protein Rrm4 mediates long-distance transport of ubi1 and rho3 mRNAs. EMBO J. *28*, 1855–1866.

Kourtidis, A., Necela, B., Lin, W.-H., Lu, R., Feathers, R.W., Asmann, Y.W., Thompson, E.A., and Anastasiadis, P.Z. (2017). Cadherin complexes recruit mRNAs and RISC to regulate epithelial cell signaling. J Cell Biol jcb.201612125.

Krauss, J., López de Quinto, S., Nüsslein-Volhard, C., and Ephrussi, A. (2009). Myosin-V regulates oskar mRNA localization in the Drosophila oocyte. Curr. Biol. CB *19*, 1058–1063.

Kurebayashi, N., and Ogawa, Y. (2001). Depletion of Ca2+ in the sarcoplasmic reticulum stimulates Ca2+ entry into mouse skeletal muscle fibres. J. Physiol. *533*, 185–199.

Latham, V.M., Yu, E.H.S., Tullio, A.N., Adelstein, R.S., and Singer, R.H. (2001). A Rho-dependent signaling pathway operating through myosin localizes β-actin mRNA in fibroblasts. Curr. Biol. *11*, 1010–1016.

Lawrence, J.B., and Singer, R.H. (1986). Intracellular localization of messenger RNAs for cytoskeletal proteins. Cell *45*, 407–415.

Lécuyer, E., Yoshida, H., Parthasarathy, N., Alm, C., Babak, T., Cerovina, T., Hughes, T.R., Tomancak, P., and Krause, H.M. (2007). Global Analysis of mRNA Localization Reveals a Prominent Role in Organizing Cellular Architecture and Function. Cell *131*, 174–187.

Lei, K., Zhang, X., Ding, X., Guo, X., Chen, M., Zhu, B., Xu, T., Zhuang, Y., Xu, R., and Han, M. (2009). SUN1 and SUN2 play critical but partially redundant roles in anchoring nuclei in skeletal muscle cells in mice. Proc. Natl. Acad. Sci. *106*, 10207–10212.

Lewis, Y.E., Moskovitz, A., Mutlak, M., Heineke, J., Caspi, L.H., and Kehat, I. (2018). Localization of transcripts, translation, and degradation for spatiotemporal sarcomere maintenance. J. Mol. Cell. Cardiol. *116*, 16–28.

Ligon, L.A., Tokito, M., Finklestein, J.M., Grossman, F.E., and Holzbaur, E.L.F. (2004). A Direct Interaction between Cytoplasmic Dynein and Kinesin I May Coordinate Motor Activity. J. Biol. Chem. *279*, 19201–19208.

Liu, G., Grant, W.M., Persky, D., Latham, V.M., Singer, R.H., and Condeelis, J. (2002). Interactions of elongation factor 1alpha with F-actin and beta-actin mRNA: implications for anchoring mRNA in cell protrusions. Mol. Biol. Cell *13*, 579–592.

Liu, J.-X., Höglund, A.-S., Karlsson, P., Lindblad, J., Qaisar, R., Aare, S., Bengtsson, E., and Larsson, L. (2009). Myonuclear domain size and myosin isoform expression in muscle fibres from mammals representing a 100 000-fold difference in body size. Exp. Physiol. *94*, 117–129.

Lovering, R.M., and De Deyne, P.G. (2004). Contractile function, sarcolemma integrity, and the loss of dystrophin after skeletal muscle eccentric contraction-induced injury. Am. J. Physiol. Cell Physiol. *286*, C230–C238.

Lyons, D.A., Naylor, S.G., Scholze, A., and Talbot, W.S. (2009). Kif1b is essential for mRNA localization in oligodendrocytes and development of myelinated axons. Nat. Genet. *41*, 854–858.

Ma, S., and Chisholm, R.L. (2002). Cytoplasmic dynein-associated structures move bidirectionally in vivo. J. Cell Sci. *115*, 1453–1460.

Ma, B., Savas, J.N., Yu, M.-S., Culver, B.P., Chao, M.V., and Tanese, N. (2011). Huntingtin mediates dendritic transport of β-actin mRNA in rat neurons. Sci. Rep. *1*, 140.

Macdonald, P.M., and Kerr, K. (1997). Redundant RNA recognition events in bicoid mRNA localization. RNA *3*, 1413–1420.

Macdonald, P.M., and Struhl, G. (1988). Cis- acting sequences responsible for anterior localization of bicoid mRNA in Drosophila embryos. Nature *336*, 595–598.

Macdonald, P.M., Kerr, K., Smith, J.L., and Leask, A. (1993). RNA regulatory element BLE1 directs the early steps of bicoid mRNA localization. Development *118*, 1233–1243.

Madden, L., Juhas, M., Kraus, W.E., Truskey, G.A., and Bursac, N. (2015). Bioengineered human myobundles mimic clinical responses of skeletal muscle to drugs. ELife *4*, e04885.

Mallik, R., Carter, B.C., Lex, S.A., King, S.J., and Gross, S.P. (2004). Cytoplasmic dynein functions as a gear in response to load. Nature *427*, 649–652.

Manring, H., Abreu, E., Brotto, L., Weisleder, N., and Brotto, M. (2014). Novel excitation-contraction coupling related genes reveal aspects of muscle weakness

beyond atrophy—new hopes for treatment of musculoskeletal diseases. Striated Muscle Physiol. *5*, 37.

Mardakheh, F.K., Paul, A., Kümper, S., Sadok, A., Paterson, H., Mccarthy, A., Yuan, Y., and Marshall, C.J. (2015). Global Analysis of mRNA, Translation, and Protein Localization: Local Translation Is a Key Regulator of Cell Protrusions. Dev. Cell *35*, 344–357.

Marieb, E.N., and Hoehn, K. (2007). Human Anatomy & Physiology (Pearson Education).

McKenney, R.J., Huynh, W., Vale, R.D., and Sirajuddin, M. (2016). Tyrosination of α-tubulin controls the initiation of processive dynein-dynactin motility. EMBO J. *35*, 1175–1185.

Melton, D.A. (1987). Translocation of a localized maternal mRNA to the vegetal pole of Xenopus oocytes. Nature *328*, 80–82.

Meng, H., Janssen, P.M.L., Grange, R.W., Yang, L., Beggs, A.H., Swanson, L.C., Cossette, S.A., Frase, A., Childers, M.K., Granzier, H., et al. (2014). Tissue Triage and Freezing for Models of Skeletal Muscle Disease. J. Vis. Exp.

Mercuri, E., and Muntoni, F. (2013). Muscular dystrophies. The Lancet *381*, 845–860.

Merlie, J.P., and Sanes, J.R. (1985). Concentration of acetylcholine receptor mRNA in synaptic regions of adult muscle fibres. Nature *317*, 66–68.

Messitt, T.J., Gagnon, J.A., Kreiling, J.A., Pratt, C.A., Yoon, Y.J., and Mowry, K.L. (2008). Multiple Kinesin Motors Coordinate Cytoplasmic RNA Transport on a Subpopulation of Microtubules in Xenopus Oocytes. Dev. Cell *15*, 426–436.

Metzger, T., Gache, V., Xu, M., Cadot, B., Folker, E.S., Richardson, B.E., Gomes, E.R., and Baylies, M.K. (2012). MAP and kinesin-dependent nuclear positioning is required for skeletal muscle function. Nature *484*, 120–124.

Meyer, G.A. (2018). Evidence of induced muscle regeneration persists for years in the mouse. Muscle Nerve *0*.

Mihailovska, E., Raith, M., Valencia, R.G., Fischer, I., Banchaabouchi, M.A., Herbst, R., and Wiche, G. (2014). Neuromuscular synapse integrity requires linkage of acetylcholine receptors to postsynaptic intermediate filament networks via rapsyn–plectin 1f complexes. Mol. Biol. Cell *25*, 4130–4149.

Miki, H., Setou, M., Kaneshiro, K., and Hirokawa, N. (2001). All kinesin superfamily protein, KIF, genes in mouse and human. Proc. Natl. Acad. Sci. U. S. A. *98*, 7004–7011.

Mili, S., Moissoglu, K., and Macara, I.G. (2008). Genome-wide screen reveals APC-associated RNAs enriched in cell protrusions. Nature *453*, 115–119.

Milner, D.J., Weitzer, G., Tran, D., Bradley, A., and Capetanaki, Y. (1996). Disruption of muscle architecture and myocardial degeneration in mice lacking desmin. J. Cell Biol. *134*, 1255–1270.

Mingle, L.A., Okuhama, N.N., Shi, J., Singer, R.H., Condeelis, J., and Liu, G. (2005). Localization of all seven messenger RNAs for the actin-polymerization nucleator Arp2/3 complex in the protrusions of fibroblasts. J. Cell Sci. *118*, 2425–2433.

Mische, S., Li, M., Serr, M., Hays, T.S., and Wente, S. (2007). Direct Observation of Regulated Ribonucleoprotein Transport Across the Nurse Cell/Oocyte Boundary. Mol. Biol. Cell *18*, 2254–2263.

Mogessie, B., Roth, D., Rahil, Z., and Straube, A. (2015). A novel isoform of MAP4 organises the paraxial microtubule array required for muscle cell differentiation.

Moor, A.E., Golan, M., Massasa, E.E., Lemze, D., Weizman, T., Shenhav, R., Baydatch, S., Mizrahi, O., Winkler, R., Golani, O., et al. (2017). Global mRNA polarization regulates translation efficiency in the intestinal epithelium. Science *357*, 1299–1303.

Morris, E.J., and Fulton, A.B. (1994). Rearrangement of mRNAs for costamere proteins during costamere development in cultured skeletal muscle from chicken. J. Cell Sci. *107*, 377–386.

Nagaoka, K., Udagawa, T., and Richter, J.D. (2012). CPEB mediated ZO-1 mRNA Localization is Required for Epithelial Tight Junction Assembly and Cell Polarity. Nat. Commun. *3*, 675.

Nazarian, J., Bouri, K., and Hoffman, E.P. (2005). Intracellular expression profiling by laser capture microdissection: three novel components of the neuromuscular junction. Physiol. Genomics *21*, 70–80.

Neuman-Silberberg, F.S., and Schüpbach, T. (1993). The Drosophila dorsoventral patterning gene gurken produces a dorsally localized RNA and encodes a TGF alpha-like protein. Cell *75*, 165–174.

Nevalainen, M., Kaakinen, M., and Metsikkö, K. (2013). Distribution of mRNA transcripts and translation activity in skeletal myofibers. Cell Tissue Res. *353*, 539–548.

Nieuwburg, R., Nashchekin, D., Jakobs, M., Carter, A.P., Trong, P.K., Goldstein, R.E., and Johnston, D.S. (2017). Localised dynactin protects growing microtubules to deliver oskar mRNA to the posterior cortex of the Drosophila oocyte. ELife *6*, e27237.

Nissinen, M., Kaisto, T., Salmela, P., Peltonen, J., and Metsikkö, K. (2005). Restricted Distribution of mRNAs Encoding a Sarcoplasmic Reticulum or Transverse Tubule Protein in Skeletal Myofibers. J. Histochem. Cytochem. *53*, 217–227.

Oddoux, S., Zaal, K.J., Tate, V., Kenea, A., Nandkeolyar, S.A., Reid, E., Liu, W., and Ralston, E. (2013). Microtubules that form the stationary lattice of muscle fibers are dynamic and nucleated at Golgi elements. J. Cell Biol. *203*, 205–213.

Oleynikov, Y., and Singer, R.H. (2003). Real-time visualization of ZBP1 association with beta-actin mRNA during transcription and localization. Curr. Biol. CB *13*, 199–207.

Padovan-Merhar, O., Nair, G.P., Biaesch, A.G., Mayer, A., Scarfone, S., Foley, S.W., Wu, A.R., Churchman, L.S., Singh, A., and Raj, A. (2015). Single Mammalian Cells Compensate for Differences in Cellular Volume and DNA Copy Number through Independent Global Transcriptional Mechanisms. Mol. Cell *58*, 339–352.

Palacios, I.M., and Johnston, D.S. (2002). Kinesin light chain-independent function of the Kinesin heavy chain in cytoplasmic streaming and posterior localisation in the Drosophila oocyte. Development *129*, 5473–5485.

Pan, F., Hüttelmaier, S., Singer, R.H., and Gu, W. (2007). ZBP2 facilitates binding of ZBP1 to beta-actin mRNA during transcription. Mol. Cell. Biol. *27*, 8340–8351.

Park, H.Y., Lim, H., Yoon, Y.J., Follenzi, A., Nwokafor, C., Lopez-Jones, M., Meng, X., and Singer, R.H. (2014a). Visualization of Dynamics of Single Endogenous mRNA Labeled in Live Mouse. Science *343*, 422–424.

Park, Y.-E., Choi, Y.-C., Bae, J.-S., Lee, C.-H., Kim, H.-S., Shin, J.-H., and Kim, D.-S. (2014b). Clinical and Pathological Features of Korean Patients with DNM2-Related Centronuclear Myopathy. J. Clin. Neurol. Seoul Korea *10*, 24–31.

Pasut, A., Jones, A.E., and Rudnicki, M.A. (2013). Isolation and Culture of Individual Myofibers and their Satellite Cells from Adult Skeletal Muscle. J. Vis. Exp.

Pavlath, G.K., Rich, K., Webster, S.G., and Blau, H.M. (1989). Localization of muscle gene products in nuclear domains. Nature *337*, 570–573.

Petkova, M.V., Morales-Gonzales, S., Relizani, K., Gill, E., Seifert, F., Radke, J., Stenzel, W., Garcia, L., Amthor, H., and Schuelke, M. (2016). Characterization of a DmdEGFPreporter mouse as a tool to investigate dystrophin expression. Skelet. Muscle *6*, 25.

Pietrangelo, T., Perni, S., Tano, D., Guglielmo, Fanò-Illic, G., and Franzini-Armstrong, C. (2013). A method for the ultrastructural preservation of tiny percutaneous needle biopsy material from skeletal muscle. Int. J. Mol. Med. *32*, 965–970.

Pimentel, M.R., Falcone, S., Cadot, B., and Gomes, E.R. (2017). In Vitro Differentiation of Mature Myofibers for Live Imaging. J. Vis. Exp. JoVE.

Pohlmann, T., Baumann, S., Haag, C., Albrecht, M., and Feldbrügge, M. (2015). A FYVE zinc finger domain protein specifically links mRNA transport to endosome trafficking.

Poon, M.M., Choi, S.-H., Jamieson, C.A.M., Geschwind, D.H., and Martin, K.C. (2006). Identification of Process-Localized mRNAs from Cultured Rodent Hippocampal Neurons. J. Neurosci. *26*, 13390–13399.

Proske, U., and Morgan, D.L. (2001). Muscle damage from eccentric exercise: mechanism, mechanical signs, adaptation and clinical applications. J. Physiol. *537*, 333–345.

Qaisar, R., and Larsson, L. (2014). What determines myonuclear domain size? Indian J. Physiol. Pharmacol. *58*, 1–12.

Quintyne, N.J., and Schroer, T.A. (2002). Distinct cell cycle-dependent roles for dynactin and dynein at centrosomes. J. Cell Biol. *159*, 245–254.

Raj, A., Bogaard, P. van den, Rifkin, S.A., Oudenaarden, A. van, and Tyagi, S. (2008). Imaging individual mRNA molecules using multiple singly labeled probes. Nat. Methods *5*, nmeth.1253.

Ralston, E., and Hall, Z.W. (1989a). Intracellular and surface distribution of a membrane protein (CD8) derived from a single nucleus in multinucleated myotubes. J. Cell Biol. *109*, 2345–2352.

Ralston, E., and Hall, Z.W. (1989b). Transfer of a protein encoded by a single nucleus to nearby nuclei in multinucleated myotubes. Science *244*, 1066–1069.

Ralston, E., and Hall, Z.W. (1992). Restricted distribution of mRNA produced from a single nucleus in hybrid myotubes. J. Cell Biol. *119*, 1063–1068.

Ralston, E., McLaren, R.S., and Horowitz, J.A. (1997). Nuclear Domains in Skeletal Myotubes: The Localization of Transferrin Receptor mRNA Is Independent of Its Half-Life and Restricted by Binding to Ribosomes. Exp. Cell Res. *236*, 453–462.

Ralston, E., Lu, Z., and Ploug, T. (1999). The Organization of the Golgi Complex and Microtubules in Skeletal Muscle Is Fiber Type-Dependent. J. Neurosci. *19*, 10694–10705.

Ramachandran, B., and Frey, J.U. (2009). Interfering with the Actin Network and Its Effect on Long-Term Potentiation and Synaptic Tagging in Hippocampal CA1 Neurons in Slices In Vitro. J. Neurosci. *29*, 12167–12173.

Roberts, A.J., Kon, T., Knight, P.J., Sutoh, K., and Burgess, S.A. (2013). Functions and mechanics of dynein motor proteins. Nat. Rev. Mol. Cell Biol. *14*, nrm3667.

Roberts, A.J., Goodman, B.S., and Reck-Peterson, S.L. (2014). Reconstitution of dynein transport to the microtubule plus end by kinesin. ELife *3*, e02641.

Rodriguez, A.J., Shenoy, S.M., Singer, R.H., and Condeelis, J. (2006). Visualization of mRNA translation in living cells. J. Cell Biol. *175*, 67–76.

Rogers, S.L., and Gelfand, V.I. (1998). Myosin cooperates with microtubule motors during organelle transport in melanophores. Curr. Biol. CB *8*, 161–164.

Rogers, S.L., Tint, I.S., Fanapour, P.C., and Gelfand, V.I. (1997). Regulated bidirectional motility of melanophore pigment granules along microtubules in vitro. Proc. Natl. Acad. Sci. U. S. A. *94*, 3720–3725.

Roman, W., and Gomes, E.R. (2017). Nuclear positioning in skeletal muscle. Semin. Cell Dev. Biol.

Roman, W., Martins, J.P., Carvalho, F.A., Voituriez, R., Abella, J.V.G., Santos, N.C., Cadot, B., Way, M., and Gomes, E.R. (2017). Myofibril contraction and crosslinking drive nuclear movement to the periphery of skeletal muscle. Nat. Cell Biol. *19*, 1189.

Romero, N.B. (2010). Centronuclear myopathies: A widening concept. Neuromuscul. Disord. *20*, 223–228.

Rongo, C., Gavis, E.R., and Lehmann, R. (1995). Localization of oskar RNA regulates oskar translation and requires Oskar protein. Dev. Camb. Engl. *121*, 2737–2746.

Ross, A.F., Oleynikov, Y., Kislauskis, E.H., Taneja, K.L., and Singer, R.H. (1997). Characterization of a beta-actin mRNA zipcode-binding protein. Mol. Cell. Biol. *17*, 2158–2165.

Ross, J.L., Wallace, K., Shuman, H., Goldman, Y.E., and Holzbaur, E.L.F. (2006). Processive bidirectional motion of dynein–dynactin complexes *in vitro*. Nat. Cell Biol. *8*, 562–570.

Rossi, A.E., and Dirksen, R.T. (2006). Sarcoplasmic reticulum: The dynamic calcium governor of muscle. Muscle Nerve *33*, 715–731.

Roth, S., Shira Neuman-Silberberg, F., Barcelo, G., and Schüpbach, T. (1995). cornichon and the EGF receptor signaling process are necessary for both anterior-posterior and dorsal-ventral pattern formation in Drosophila. Cell *81*, 967–978.

Saitoh, O., Arai, T., and Obinata, T. (1988). Distribution of microtubules and other cytoskeletal filaments during myotube elongation as revealed by fluorescence microscopy. Cell Tissue Res. *252*, 263–273.

Salerno, V.P., Calliari, A., William Provance, D., Sotelo-Silveira, J.R., Sotelo, J.R., and Mercer, J.A. (2008). Myosin-Va Mediates RNA Distribution in Primary Fibroblasts From Multiple Organs. Cell Motil. Cytoskeleton *65*, 422–433.

Saunders, C., and Cohen, R.S. (1999). The Role of Oocyte Transcription, the 5′UTR, and Translation Repression and Derepression in Drosophila gurken mRNA and Protein Localization. Mol. Cell *3*, 43–54.

Schaeffer, L., de Kerchove d'Exaerde, A., and Changeux, J.P. (2001). Targeting transcription to the neuromuscular synapse. Neuron *31*, 15–22.

Schiaffino, S., and Reggiani, C. (2011). Fiber Types in Mammalian Skeletal Muscles. Physiol. Rev. *91*, 1447–1531.

Schlager, M.A., Hoang, H.T., Urnavicius, L., Bullock, S.L., and Carter, A.P. (2014). In vitro reconstitution of a highly processive recombinant human dynein complex. EMBO J. *33*, 1855–1868.

Shestakova, E.A., Singer, R.H., and Condeelis, J. (2001). The physiological significance of β-actin mRNA localization in determining cell polarity and directional motility. Proc. Natl. Acad. Sci. *98*, 7045–7050.

Shi, L., Fu, A.K.Y., and Ip, N.Y. (2012). Molecular mechanisms underlying maturation and maintenance of the vertebrate neuromuscular junction. Trends Neurosci. *35*, 441–453.

Sil, A., and Herskowitz, I. (1996). Identification of an Asymmetrically Localized Determinant, Ash1p, Required for Lineage-Specific Transcription of the Yeast HO Gene. Cell *84*, 711–722.

Sladewski, T.E., Bookwalter, C.S., Hong, M.-S., and Trybus, K.M. (2013). Single-molecule reconstitution of mRNA transport by a class V myosin. Nat. Struct. Mol. Biol. *20*, 952–957.

Song, T., Zheng, Y., Wang, Y., Katz, Z., Liu, X., Chen, S., Singer, R.H., and Gu, W. (2015). Specific interaction of KIF11 with ZBP1 regulates the transport of β-actin mRNA and cell motility. J Cell Sci *128*, 1001–1010.

Song, Y., Forsgren, S., Yu, J., Lorentzon, R., and Stål, P.S. (2012). Effects on Contralateral Muscles after Unilateral Electrical Muscle Stimulation and Exercise. PLOS ONE *7*, e52230.

Soundararajan, H.C., and Bullock, S.L. (2014). The influence of dynein processivity control, MAPs, and microtubule ends on directional movement of a localising mRNA. ELife *3*, e01596.

Sparrow, J.C., and Schöck, F. (2009). The initial steps of myofibril assembly: integrins pave the way. Nat. Rev. Mol. Cell Biol. *10*, 293.

Spaulding, E.L., and Burgess, R.W. (2017). Accumulating Evidence for Axonal Translation in Neuronal Homeostasis. Front. Neurosci. *11*.

Spencer, J.A., Eliazer, S., Ilaria, R.L., Richardson, J.A., and Olson, E.N. (2000). Regulation of Microtubule Dynamics and Myogenic Differentiation by Murf, a Striated Muscle Ring-Finger Protein. J. Cell Biol. *150*, 771–784.

Splinter, D., Razafsky, D.S., Schlager, M.A., Serra-Marques, A., Grigoriev, I., Demmers, J., Keijzer, N., Jiang, K., Poser, I., Hyman, A.A., et al. (2012). BICD2, dynactin, and LIS1 cooperate in regulating dynein recruitment to cellular structures. Mol. Biol. Cell *23*, 4226–4241.

St Johnston, D. (2005). Moving messages: the intracellular localization of mRNAs. Nat. Rev. Mol. Cell Biol. *6*, 363–375.

St Johnston, D., Beuchle, D., and Nüsslein-Volhard, C. (1991). Staufen, a gene required to localize maternal RNAs in the Drosophila egg. Cell *66*, 51–63.

Stroud, M.J., Feng, W., Zhang, J., Veevers, J., Fang, X., Gerace, L., and Chen, J. (2017). Nesprin 1α2 is essential for mouse postnatal viability and nuclear positioning in skeletal muscle. J Cell Biol jcb.201612128.

Sutton, M.A., and Schuman, E.M. (2006). Dendritic Protein Synthesis, Synaptic Plasticity, and Memory. Cell *127*, 49–58.

Tajbakhsh, S. (2009). Skeletal muscle stem cells in developmental versus regenerative myogenesis. J. Intern. Med. *266*, 372–389.

Tanaka, T., Kato, Y., Matsuda, K., Hanyu-Nakamura, K., and Nakamura, A. (2011). Drosophila Mon2 couples Oskar-induced endocytosis with actin remodeling for cortical anchorage of the germ plasm. Dev. Camb. Engl. *138*, 2523–2532.

Tas, R.P., Chazeau, A., Cloin, B.M.C., Lambers, M.L.A., Hoogenraad, C.C., and Kapitein, L.C. (2017). Differentiation between Oppositely Oriented Microtubules Controls Polarized Neuronal Transport. Neuron *96*, 1264-1271.e5.

Tassin, A.M., Maro, B., and Bornens, M. (1985). Fate of microtubule-organizing centers during myogenesis in vitro. J. Cell Biol. *100*, 35–46.

Thomsen, G.H., and Melton, D.A. (1993). Processed Vg1 protein is an axial mesoderm inducer in Xenopus. Cell *74*, 433–441.

Tissot, N., Lepesant, J.-A., Bernard, F., Legent, K., Bosveld, F., Martin, C., Faklaris, O., Bellaïche, Y., Coppey, M., and Guichet, A. (2017). Distinct molecular cues ensure a robust microtubule-dependent nuclear positioning in the *Drosophila* oocyte. Nat. Commun. *8*, 15168.

Trokter, M., Mücke, N., and Surrey, T. (2012). Reconstitution of the human cytoplasmic dynein complex. Proc. Natl. Acad. Sci. *109*, 20895–20900.

Trong, P.K., Doerflinger, H., Dunkel, J., Johnston, D.S., and Goldstein, R.E. (2015). Cortical microtubule nucleation can organise the cytoskeleton of Drosophila oocytes to define the anteroposterior axis. ELife *4*, e06088.

Trovisco, V., Belaya, K., Nashchekin, D., Irion, U., Sirinakis, G., Butler, R., Lee, J.J., Gavis, E.R., and Johnston, D.S. (2016). bicoid mRNA localises to the Drosophila oocyte anterior by random Dynein-mediated transport and anchoring. ELife *5*, e17537.

Tskhovrebova, L., and Trinick, J. (2003). Titin: properties and family relationships. Nat. Rev. Mol. Cell Biol. *4*, 679–689.

Twelvetrees, A.E., Pernigo, S., Sanger, A., Guedes-Dias, P., Schiavo, G., Steiner, R.A., Dodding, M.P., and Holzbaur, E.L.F. (2016). The Dynamic Localization of Cytoplasmic Dynein in Neurons Is Driven by Kinesin-1. Neuron *90*, 1000–1015.

Vale, R.D., Reese, T.S., and Sheetz, M.P. (1985). Identification of a novel force-generating protein, kinesin, involved in microtubule-based motility. Cell *42*, 39–50.

Vanzo, N.F., and Ephrussi, A. (2002). Oskar anchoring restricts pole plasm formation to the posterior of the Drosophila oocyte. Dev. Camb. Engl. *129*, 3705–3714.

Veeranan-Karmegam, R., Boggupalli, D.P., Liu, G., and Gonsalvez, G.B. (2016). A new isoform of Drosophila non-muscle Tropomyosin 1 interacts with Kinesin-1 and functions in oskar mRNA localization. J Cell Sci *129*, 4252–4264.

Vendra, G., Hamilton, R.S., and Davis, I. (2007). Dynactin suppresses the retrograde movement of apically localized mRNA in Drosophila blastoderm embryos. RNA *13*, 1860–1867.

Vilmont, V., Cadot, B., Ouanounou, G., and Gomes, E.R. (2016a). A system to study mechanisms of neuromuscular junction development and maintenance. Development dev.130278.

Vilmont, V., Cadot, B., Vezin, E., Le Grand, F., and Gomes, E.R. (2016b). Dynein disruption perturbs post-synaptic components and contributes to impaired MuSK clustering at the NMJ: implication in ALS. Sci. Rep. *6*, 27804.

Wang, C., and Lehmann, R. (1991). Nanos is the localized posterior determinant in Drosophila. Cell *66*, 637–647.

Wang, T., Hamilla, S., Cam, M., Aranda-Espinoza, H., and Mili, S. (2017). Extracellular matrix stiffness and cell contractility control RNA localization to promote cell migration. Nat. Commun. *8*, 896.

Wang, Z., Cui, J., Wong, W.M., Li, X., Xue, W., Lin, R., Wang, J., Wang, P., Tanner, J.A., Cheah, K.S.E., et al. (2013). Kif5b controls the localization of myofibril components for their assembly and linkage to the myotendinous junctions. Development *140*, 617–626.

Warren, R.H. (1974). Microtubular Organization in Elongating Myogenic Cells. J. Cell Biol. *63*, 550–566.

Weatheritt, R.J., Gibson, T.J., and Babu, M.M. (2014). Asymmetric mRNA localization contributes to fidelity and sensitivity of spatially localized systems. Nat. Struct. Mol. Biol. *21*, 833–839.

Weil, T.T., Forrest, K.M., and Gavis, E.R. (2006). Localization of bicoid mRNA in Late Oocytes Is Maintained by Continual Active Transport. Dev. Cell *11*, 251–262.

Wu, B., Eliscovich, C., Yoon, Y.J., and Singer, R.H. (2016). Translation dynamics of single mRNAs in live cells and neurons. Science *352*, 1430–1435.

Wurth, L., and Gebauer, F. (2015). RNA-binding proteins, multifaceted translational regulators in cancer. Biochim. Biophys. Acta BBA - Gene Regul. Mech. *1849*, 881–886.

Yaffe, D., and Saxel, O. (1977). Serial passaging and differentiation of myogenic cells isolated from dystrophic mouse muscle. Nature *270*, 725–727.

Yamagishi, M., Ishihama, Y., Shirasaki, Y., Kurama, H., and Funatsu, T. (2009). Single-molecule imaging of β-actin mRNAs in the cytoplasm of a living cell. Exp. Cell Res. *315*, 1142–1147.

Ye, Y., Meyer, H.H., and Rapoport, T.A. (2001). The AAA ATPase Cdc48/p97 and its partners transport proteins from the ER into the cytosol. Nature *414*, 652–656.

Yogev, S., Maeder, C.I., Cooper, R., Horowitz, M., Hendricks, A.G., and Shen, K. (2017). Local inhibition of microtubule dynamics by dynein is required for neuronal cargo distribution. Nat. Commun. *8*, 15063.

Zaessinger, S., Busseau, I., and Simonelig, M. (2006). Oskar allows nanos mRNA translation in Drosophila embryos by preventing its deadenylation by Smaug/CCR4. Dev. Camb. Engl. *133*, 4573–4583.

Zhang, F., Wang, L.-P., Brauner, M., Liewald, J.F., Kay, K., Watzke, N., Wood, P.G., Bamberg, E., Nagel, G., Gottschalk, A., et al. (2007a). Multimodal fast optical interrogation of neural circuitry. Nature *446*, 633–639.

Zhang, T., Zaal, K.J.M., Sheridan, J., Mehta, A., Gundersen, G.G., and Ralston, E. (2009). Microtubule plus-end binding protein EB1 is necessary for muscle cell differentiation, elongation and fusion. J. Cell Sci. *122*, 1401–1409.

Zhang, X., Xu, R., Zhu, B., Yang, X., Ding, X., Duan, S., Xu, T., Zhuang, Y., and Han, M. (2007b). Syne-1 and Syne-2 play crucial roles in myonuclear anchorage and motor neuron innervation. Development *134*, 901–908.

Zid, B.M., and O'Shea, E.K. (2014). Promoter sequences direct cytoplasmic localization and translation of mRNAs during starvation in yeast. Nature *514*, 117–121.

Zimyanin, V.L., Belaya, K., Pecreaux, J., Gilchrist, M.J., Clark, A., Davis, I., and St Johnston, D. (2008). In Vivo Imaging of oskar mRNA Transport Reveals the Mechanism of Posterior Localization. Cell *134*, 843–853.